PROTON SCATTERING FROM ^{32}S

by

L. M. SPITZ

The University of Cape Town

A thesis submitted to the
UNIVERSITY OF CAPE TOWN
for the Degree of
DOCTOR OF PHILOSOPHY

Supervisor: Professor F.D. Brooks. October, 1968

The copyright of this thesis vests in the author. No quotation from it or information derived from it is to be published without full acknowledgement of the source. The thesis is to be used for private study or non-commercial research purposes only.

Published by the University of Cape Town (UCT) in terms of the non-exclusive license granted to UCT by the author.

The University of Cape Town

ABSTRACT

The differential proton elastic scattering cross section of ^{32}S was measured at four angles simultaneously in the proton energy range E_p = 2.8 to 5.5 MeV. The measurements were carried out using semiconductor detectors which were placed at 89°, 123°, 139° and 165° with respect to the incident beam direction.

Forty resonances, of which 28 have previously been reported, were observed in the cross section data and these were analysed by means of a phase shift method in order to extract level parameters for the corresponding compound nucleus levels.

In addition the differential cross section for protons inelastically scattered to the 1st excited state of ^{32}S, was measured at 165°. Angular distributions were measured at most of the resonance energies and these were analysed in order to supplement the assignments made in the elastic scattering studies.

Spins and parities were assigned for 21 of the levels observed, and parities and tentative spins were assigned for a further 16. Partial widths for elastic and inelastic scattering were derived and reduced widths were calculated.

The level structure of ^{33}Cl is discussed and a comparison made with neighbouring isobaric nuclei. An attempt is also made to interpret the energy levels of ^{33}Cl in terms of the Nilsson model.

ACKNOWLEDGEMENTS

The author wishes to express sincere thanks to his supervisor, Professor F.D. Brooks, for his guidance and encouragement during the course of this project and for valuable suggestions in the preparation of this manuscript.

Thanks are also due to the following:

Dr. W.R. McMurray and Professor I.J. van Heerden for helpful discussions;

Dr. J. Kritzinger, Mr. E. Blignaut and the operator staff of the Southern Universities Nuclear Institute for efficient running of the accelerator;

Mr. W.B. de V. Smit and Mrs. W. Ensor of the computer centre at U.C.T. for their cooperation;

Messrs. D.T.L. Jones, C.A.R. Bain, J.C. Cornell and A. Bottega for assistance during data acquisition;

Mrs. A. Briscoe for typing a draft copy and Mrs. E.B. Prosser for typing this manuscript; and

The South African Council for Scientific and Industrial Research for financial assistance.

CONTENTS

CHAPTER 1

INTRODUCTION

1.1 Historical Background

Charged particle scattering has long been known to provide a useful and relatively simple means of obtaining spectroscopic information about the level structure of light nuclei.

The elastic scattering of α-particles dates back to the classical work of Rutherford (Ru 06, Ru 11) and Geiger and Marsden (Ge 13). These early studies led directly to the hypothesis of a nuclear atom. Departure from the Rutherford scattering cross sections was first observed by Bieler (Bi 24) in α-scattering experiments on Aluminium and Magnesium. This anomalous behaviour suggested the use of scattering to obtain information about the structure of nuclei.

With the advent of electrostatic accelerators in the early 1930's, experiments using protons became possible. Suggestions were made that protons could be used in the study of nuclear structure (Ha 38). Early experiments in which resonance scattering of protons was studied were those of Bender et al. (Be 48) and Fowler et al. (Fo 49). Since then a large number of experiments of this kind have been undertaken.

The type of spectroscopic data which may be obtained from these studies are level parameters such as spins J, parities π, level energies E, and partial and total widths. These para-

meters are of considerable interest since a detailed knowledge of the level structure of nuclei provides a basis for formulating nuclear models or testing the assumptions of existing models.

1.2 Nuclear Models

In recent years nuclear models have developed along two lines. These are the independent particle type of model and collective models respectively.

The independent particle models have as their starting point the extreme single particle shell model (Ma 49,Ha 49). The basic assumption of this model is that each nucleon within a nucleus moves independently under the influence of an average potential produced by the field of the other nucleons. The most prominent feature of this average potential is the occurrence of a strong spin orbit coupling term. In its simplest form this model has had success in predicting "magic number" effects, as well as many other nuclear properties, notably, in describing the ground state configurations of odd A nuclei. However, it cannot successfully predict the properties of excited states of nuclei, nor does it predict values of magnetic and quadrupole moments which are consistent with experimental values.

An extension to this model is the independent particle

model in which residual interactions between nucleons in unfilled shells are considered. In this model central force terms which favour L-S type coupling are considered in addition to the j-j coupling, resulting in an intermediate coupling scheme. As a result of this the wave function of a given nuclear state may have components of various configurations. With a knowledge of this configuration mixing, it is possible to improve single particle shell model predictions.

If the mixing of configurations were taken to its extreme, the motions of all the particles in the nucleus would have to be taken into account. This forms the basis of the second type of model mentioned above, namely the collective model. The development of the collective model is attributed to Rainwater (Ra 50) and Bohr and Mottelson (Bo 53). The model assumes separation of the individual motion of nucleons outside the core and motion of the core itself. The shape of the core is assumed to be deformed. This leads to modes of excitation which are classified as vibrational and rotational.

The unified model of Nilsson (Ni 55) embodies aspects of both the shell model and the collective model. The nuclear wave functions are constructed by filling the lowest available state in a self consistent deformed potential. The single particle wave functions (Nilsson Orbitals) are obtained by solving the Schrödinger equation with an axially symmetric oscillator potential with spin-orbit coupling. This model

has had considerable success in predicting energy levels, magnetic and dipole moments and transition probabilities in many nuclei. (See for example Li 58 and Bh 62)

The levels amenable to interpretation in terms of these nuclear models are those at low excitation energies in the nucleus. In a reaction such as elastic proton scattering, the levels excited are often at high energies and are thus not usually directly amenable to interpretation. However the determination of spectroscopic properties of low lying states such as energies, spins, parities and branching ratios often proceed via levels at higher excitation energies. An example is the determination of spins and parities of low lying levels by means of $(p,\gamma\gamma)$ angular correlation measurements. A knowledge of the properties of levels at relatively high excitation energies may thus serve as an intermediate step in obtaining information regarding low lying states which are often of more interest in model applications.

1.3 Analogue states

Recently much attention has been focussed on proton elastic scattering since it provides the kind of information of interest in analogue state studies. Analogue states are assigned an isospin quantum number T. The isospin formalism can be used to express the fact that several nuclear isobars

can have similar states belonging to an isospin multiplet; the number of isobaric nuclei in which the level of given T occurs being equal to 2T + 1. These states are of great interest for a number of reasons. (See for example review articles by Morrison (Mo 67), Endt (En 67) and Temmer (Te 67)). Coulomb energy differences arising from the interchanging of protons and neutrons, may be calculated by accurately measuring the excitation energies of analogue states. The coulomb energy differences in turn can give information about the charge distribution and charge radius of nuclei (Ja 66) and may also be of interest in theories relating to charge dependence of nuclear forces (He 66).

A further important interest in analogue states is in their value as a spectroscopic tool. In general they are high energy states which have structures very similar to those of low lying states in the isobaric nucleus. Their structures or configurations, in other words, are generally simpler than those of neighbouring states at the same high excitation. The existence of such simple states at high excitation energies is useful in the study of lower lying states to which they decay.

In the case of a proton which is ascribed an isospin $T = \frac{1}{2}$, being scattered from a nucleus with ground state spin $T = 0$, the excitation and decay of an analogue state with isospin $T = 3/2$ is forbidden by isospin selection rules.

This is shown schematically in fig. 1.1. These states, if observed, are intrinsically extremely sharp since their particle widths arise solely from isospin mixing. Observation of such states may therefore be useful in extracting information regarding the nature of this mixing.

1.4 Choice of Nucleus

The nucleus ^{32}S was chosen as a target in this project for a number of reasons. From the point of view of obtaining detailed spectroscopic information this nucleus, which in the ground state constitutes a $2S_{1/2}$ subshell, has the advantage of having a relatively low proton binding energy (E_b = 2.29 MeV). This low binding energy results in relatively low energies of states excited in the ^{33}Cl compound nucleus, which in turn allows spectroscopic information to be extracted in a relatively simple way. In most other light nuclei, the proton binding energies are considerably higher ($\sim$ 7 MeV); levels excited in the compound nuclei are thus at high excitation energies and therefore relatively closely spaced. This often precludes simple analysis, such as a single level phase shift analysis which is applied in the present case. The fact that ^{32}S is an even-even (zero ground state spin) nucleus is a further advantage since this simplifies the

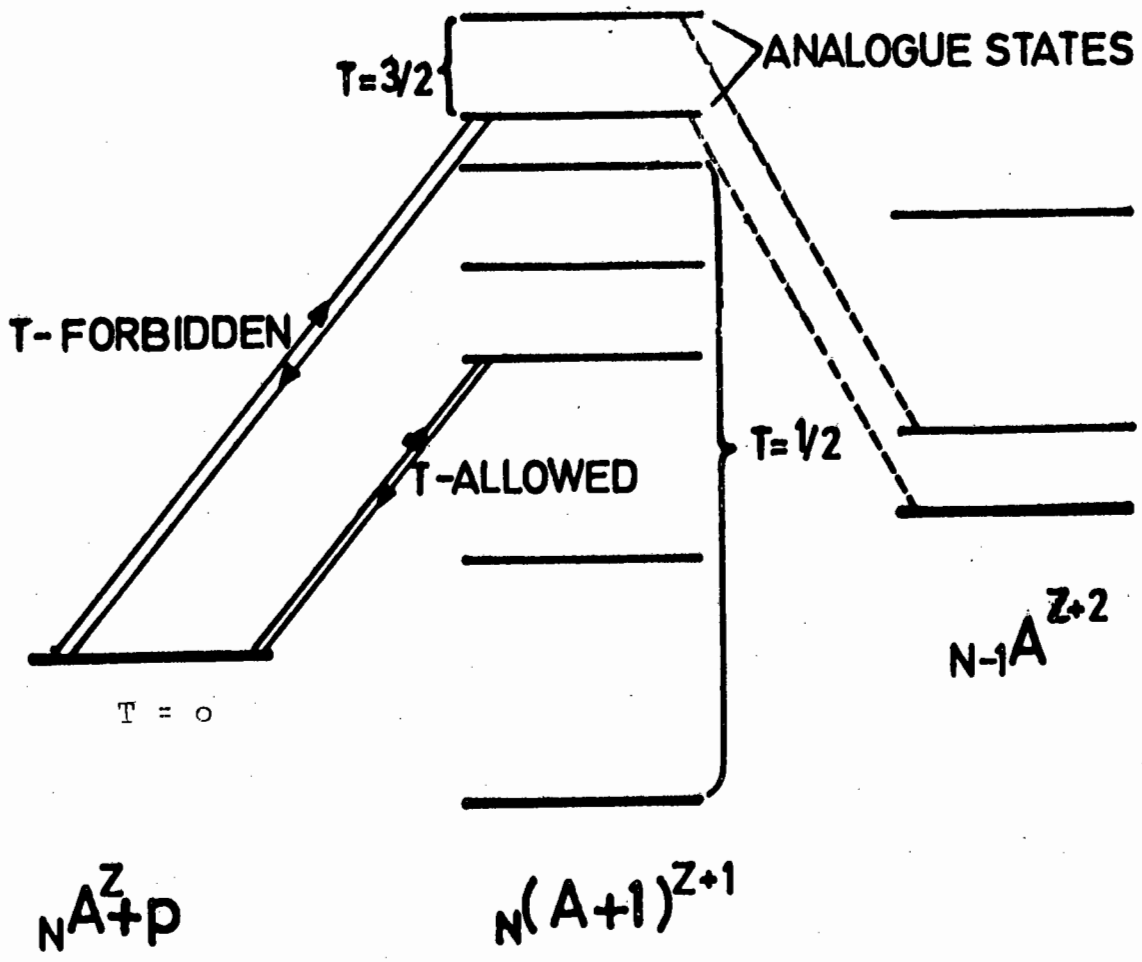

Figure 1.1. Schematic Diagram showing excitation of states of isospin T = 1/2 and T = 3/2 by proton elastic scattering

extraction of level parameters.

The ^{33}Cl compound nucleus is of interest since it lies in a region in which there is a distinct lack of spectroscopic information. The level structure of ^{33}Cl has recently been reviewed by Endt and van der Leun (En 67(a)). Fig. 1.2 shows the energy level diagram adapted from this review.

Two bound states have been reported; the level at 0.806 MeV with spin-parity $1/2^+$ and the level at 1.97 MeV. (Va 58, Su 59, Va 59).

The low lying virtual states between 2.5 and 4.8 MeV have been investigated by means of $^{32}S(p,\gamma)^{33}Cl$ angular distribution and polarisation measurements and by $^{32}S(d,n)^{33}Cl$ stripping reactions. Twelve levels have been reported in this region of excitation. Spins and parities have been assigned to four of these: $5/2^+$, $3/2^-$, $3/2^-$ and $1/2^-$ to the levels at 2.85, 2.86, 4.13 and 4.53 MeV respectively.

Levels in the 4.13 to 5.89 MeV region have been studied by means of proton scattering by Olness et al. (Ol 58). These authors report 14 levels to which they have assigned spins (12), parities (all) and partial widths.

Recently two levels have been reported (Ha 65, Ha 66) at 5.55 and 7.75 MeV. These levels were excited by the beta decay of the isobar ^{33}A. The level at 5.55 has been identified as the isobaric analogue of the ground state of ^{33}A and is thus the lowest $T = 3/2$ state in ^{33}Cl.

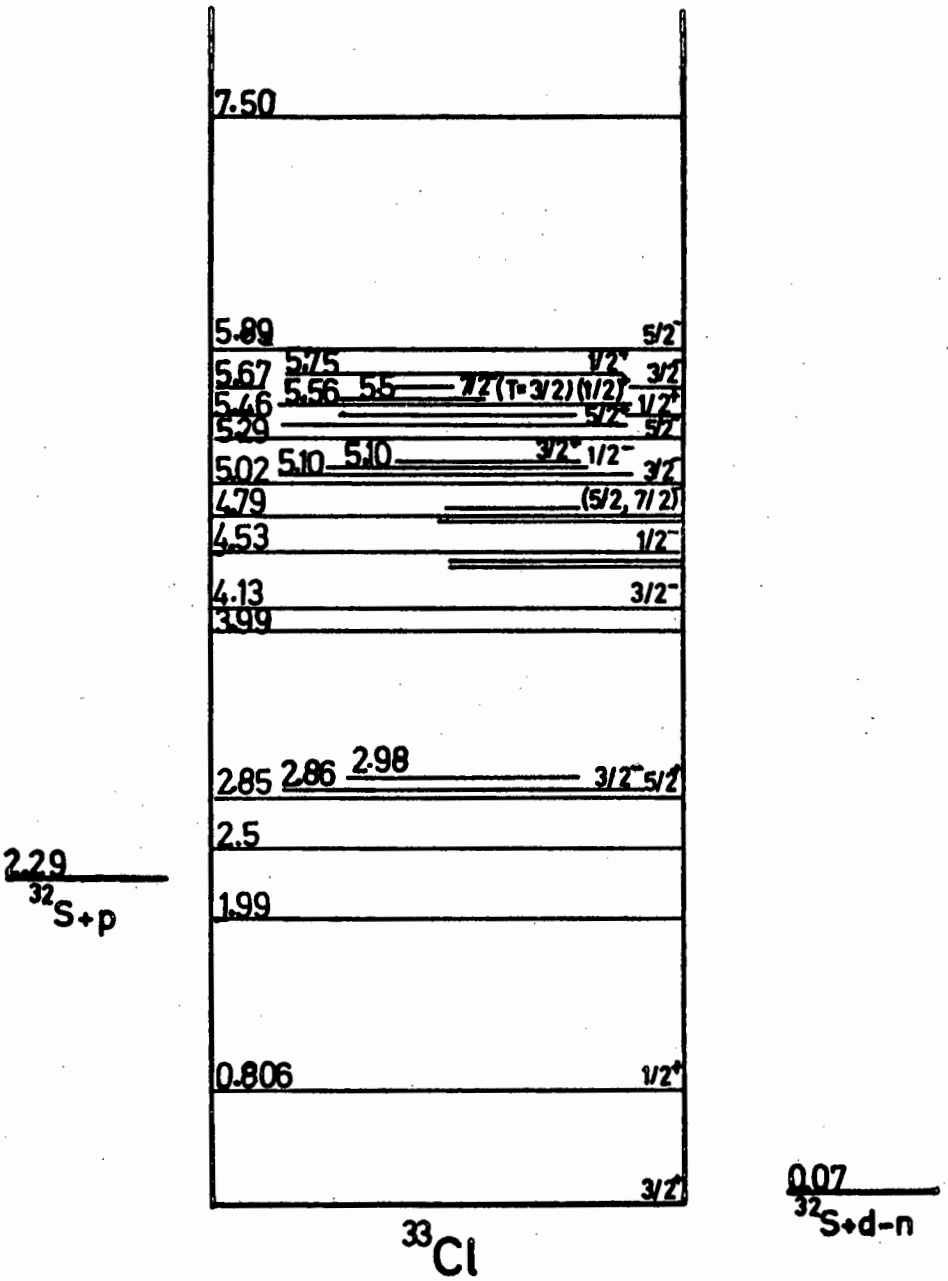

Figure 1.2. Energy level diagram adapted from the review article of Endt and Van der Leun (En 67(a))

It is thus seen that there is virtually no information about the structure of the ^{33}Cl nucleus above 5.9 MeV. There is also a lack of information about the structure in the intermediate 2 to 4 MeV region.

There has been recent interest (We 68, Ta 66) in the application of the unified model in predicting level properties in nuclei with N (number of neutrons) or Z (number of protons) equal to 17. It would be useful to have a more complete knowledge of ^{33}Cl (N = 16, Z = 17) in order to further test these predictions.

A further motivation for the choice of nucleus was the interest in the T = 3/2 analogues of low lying states of ^{33}A and ^{33}P. The analogue of the ground state of these nuclides is expected to be at an excitation energy of 5.55 MeV in ^{33}Cl. However besides the direct interest in this state it is still important to have a detailed knowledge of the background T = 1/2 states.

Finally, the choice of nucleus was influenced by the available facilities at the Southern Universities Nuclear Institute. Protons up to 5.5 MeV were available thus setting an upper limit to the region of excitation which could be studied. The spread in the beam energy of about 1 keV limited the resolution with which the experiment could be performed.

1.5 Proton elastic scattering

In order to study the energy levels of the nucleus ^{33}Cl by means of a proton scattering reaction, it is necessary in the first instance to measure the differential cross section for elastic scattering of protons from ^{32}S as a function of energy. The differential cross section in general has the following components:

1) A slowly varying component due to Rutherford scattering which is a result of the charge carried by the proton and nucleus;

2) a slowly varying component due to "hard sphere" or potential scattering; and

3) a resonance component which is due to protons that enter the nucleus and excite it to a compound state. This state in turn decays by emitting a proton, leaving the nucleus in its initial state. Thus structure observed in the cross section data may be related to excited levels in the compound nucleus.

The analysis of these resonances is facilitated by the presence of interference between the Rutherford and resonance components of the scattering cross section. This interference results in distinctive shapes of the resonances observed at various laboratory angles for various spins and parities of the corresponding compound nucleus levels. An example of this is shown in fig. 1.3, where it is seen that a spin-parity $3/2^+$ results in a dip at 89° and a peak at 165° while a spin

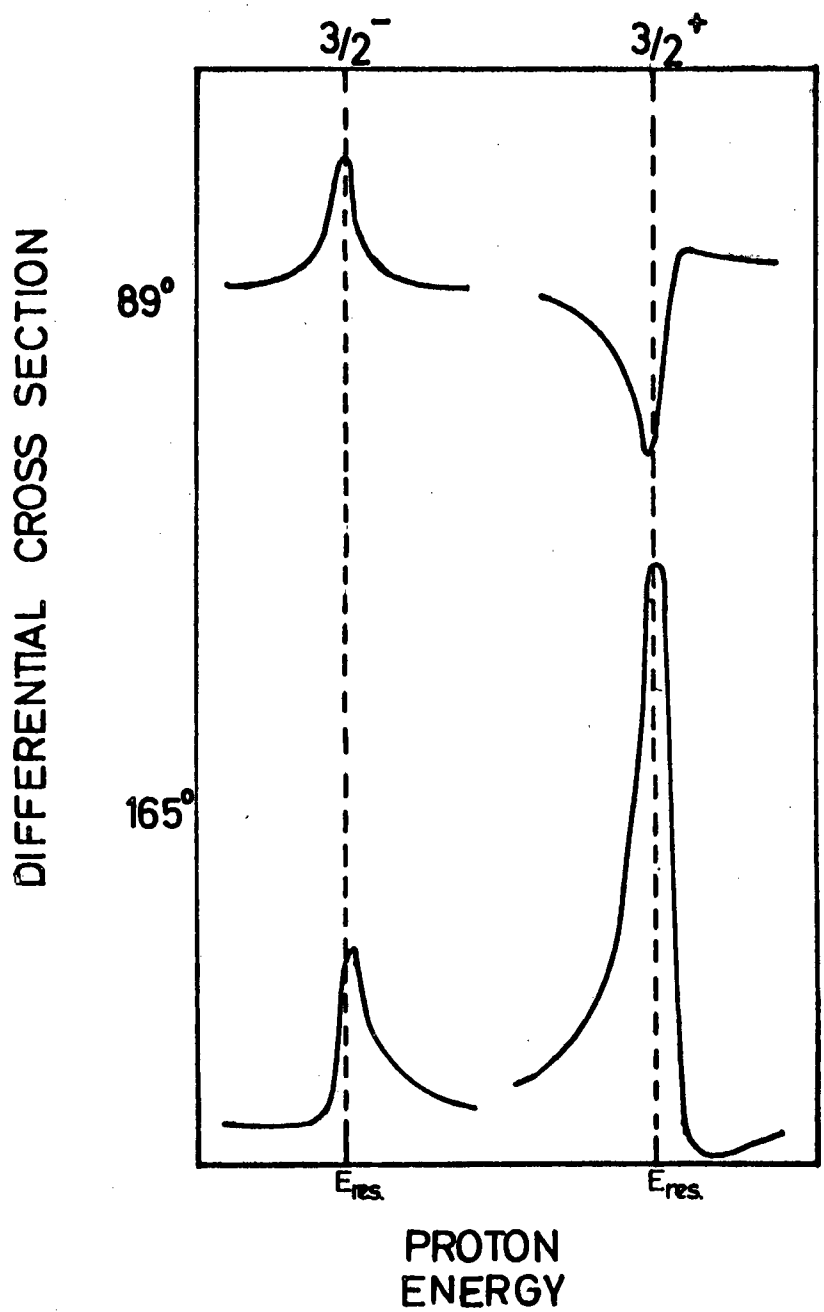

Figure 1.3. Theoretical proton scattering cross sections in the region of resonances with $J^{\pi} = 3/2^{-}$ and $3/2^{+}$ calculated at 89° and 165°

parity $3/2^-$ results in a peak at both 89° and 165°. The relative peak cross sections at 165° also vary for different spins. It is thus often possible to determine the value of the orbital angular momentum ℓ and in some cases the spin, merely by inspection of the resonance shapes at a number of angles. In the present experiment measurements were carried out at the four angles 89°, 123°, 139° and 165°.

In order to derive spins and parities more rigorously and also to extract values of the energies and partial widths of the levels a phase-shift analysis was carried out. This method is well known (Ol 58, La 51, Bl 52) and in practice it amounts to generating a cross section versus energy curve using parameters obtained by inspection of the data, and then varying these parameters until the best fit of the curve to the data is obtained.

In the present case, decisions as to the quality of the fits were made by visual inspection since computer facilities available were not adequate to carry out a least squares fitting.

The total width Γ of the level is a sum of partial widths Γ_a ; where $\Gamma_{a/\Gamma}$ is the probability of the level decaying via the channel designated by a. This decay probability is a function of effects which are external to the nucleus such as the Coulomb barrier and also effects which are related to the actual nuclear configuration. The

partial width is thus written as a product of a penetrability factor, P_ℓ which relates to the external effects, and the reduced widths, i.e.

$$\Gamma_{a\ell} = 2 P_\ell \gamma^2_{a\ell} \qquad 1.1$$

The penetrability factors are calculated at the interaction radius of the nucleus involved and they are functions of the regular and irregular solutions of the Schrödinger equation for the interaction of a proton with a nuclear plus a Coulomb potential. They are sensitive functions of energy and of orbital angular momentum ℓ.

The reduced widths are usually given units of the Wigner single particle limit (Te 52) γ^2_W :

$$\theta^2_p = \frac{\gamma^2_p}{\gamma^2_W} \qquad 1.2$$

These quantities correspond to the spectroscopic factors determined in stripping reactions. Since they are related to the nuclear configuration, they are often of importance in testing the predictions of nuclear models.

To conclude therefore, the work to be described in the remainder of this thesis may be summarised as follows: The sections which follow immediately deal with the experimental measurements of the differential cross sections for proton elastic scattering from ^{32}S in the energy range 2.8 to 5.5 MeV.

The results are then analysed so as to extract information about the excited states of the compound nucleus ^{33}Cl. Special attention is given to obtain parameters such as level energies, reduced widths, spins and parities which are of interest to nuclear model theories. An attempt is also made to interpret the level structure of ^{33}Cl in terms of the unified model of Nilsson (Ni 55). Finally an investigation of the level structure of neighbouring isobaric nuclei is undertaken with a view to identifying analogue states.

CHAPTER 2

EXPERIMENTAL PROCEDURE

2.1 Apparatus

2.1.1 Accelerator

The protons for this experiment were supplied by the 5.5 MeV van de Graaff accelerator† at the Southern Universities Nuclear Institute. The proton beam on emerging from the electrostatic accelerator is deflected through 90° by a vertical plane analysing magnet. (see fig. 2.1(a)) The field of this magnet is set so as to allow particles of the chosen energy to pass through the slits B. This magnetic field in turn is monitored by a nuclear magnetic resonance (N.M.R.) device. The current falling on the two plates of the exit slits of the magnet feeds a correction signal to the corona discharge device in the terminal of the accelerator. A finite energy spread is introduced due to the width of the entrance and exit slits of the analysing magnet and fluctuations in the magnetic field. This energy spread was $\sim$ 1 keV for 4 MeV protons.

On emerging from the analysing magnet the beam enters a switching magnet where it is deflected into the required

---

† Type CN supplied by HVEC Burlington, Massachusetts, U.S.A.

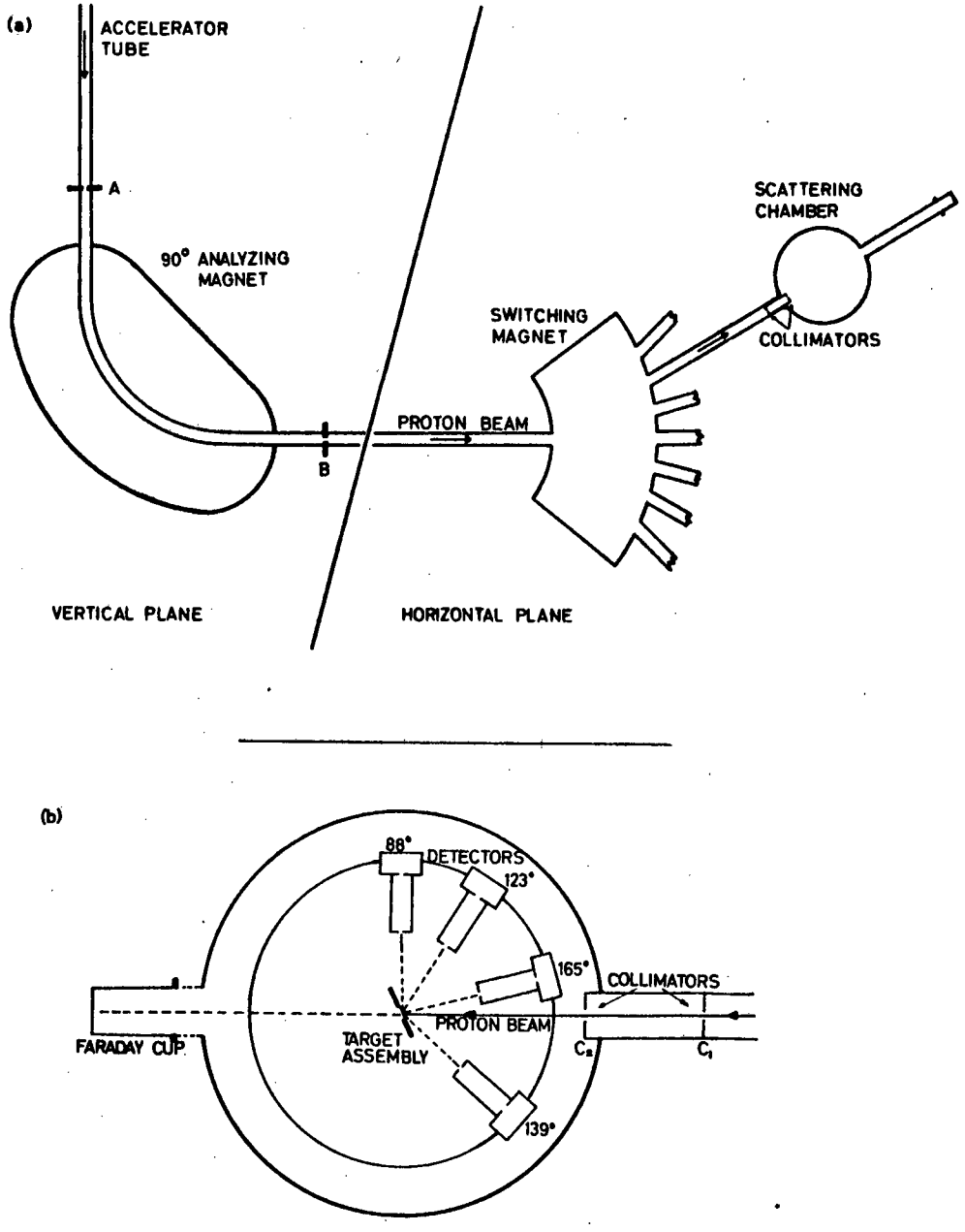

Figure 2.1 (a) The beam collimation and deflection system of the S.U.N.I. Van de Graaff accelerator
(b) The scattering chamber used for proton scattering measurements showing relative positions of 4 detectors and target assembly

flight tube where it is again collimated before entering the scattering chamber.

2.1.2 Scattering Chamber

The scattering chamber is shown diagramatically in fig. 2.1(b). The first collimator C_1 defines a parallel beam and the second collimator C_2 of aperture larger than C_1, intercepts protons which may have straggled from the beam. In this way it was hoped to eliminate protons striking the target holder assembly.

The four detectors were mounted in stainless steel holders which were in turn mounted in aluminium supports. Collimators of diameter 3 mm. were placed 4 to 6 cm in front of the detectors.

Protons passing through the target were collected in a Faraday cup assembly after traversing a further one meter of flight tube. This extra length of flight tube was introduced to reduce the probability of backscattered protons from reaching the detectors. The Faraday cup was insulated from the rest of the scattering chamber by means of a 1 cm perspex spacer.

2.1.3 Detectors

Partially depleted surface barrier detectors were used to detect the scattered protons. Most of the runs were carried out using detectors which were constructed at the Southern Universities Nuclear Institute. In later runs Ortec detectors (type SBDJ025-300) were introduced.

The locally constructed detectors were made using a technique communicated by Dearnaley (De 63) and others. The procedure was briefly as follows:

A silicon slice (supplied by Wacker-Chemie, Germany) was cleaned in concentrated HNO_3. It was then etched in a solution made up of 1 part HCl, 3 parts HNO_3 and 1 part HF. The etching process resulted in one side of the slice being very smooth whilst the reverse side remained relatively rough. After etching the slice was washed repeatedly in deionised water. This was continued until water in which the slice had been swirled was found to have a resistivity > 10^6 Ωcm. The slice was then allowed to dry in a normal atmosphere for 24 hours.

Gold and aluminium electrodes were then vacuum evaporated onto the smooth and reverse sides of the silicon slice respectively. A thin gold foil contact was glued to the gold electrode using a p-type epoxy paste; the other end of this contact was attached to a feedthrough connector in the detector holder. The aluminium electrode was attached to the

base of the detector holder by means of an n-type epoxy paste. After drying in a 60°C oven for 1-2 hours, the detectors were ready for use.

These detectors had an active area of 28 mm^2 and depletion depth of about 300 microns. The resolution for 2 MeV protons was 25 to 35 keV.

2.1.4 Electronics

A block diagram of the electronics is shown in figure 2.2. The detectors were connected to charge sensitive preamplifiers and the outputs from these amplifiers were fed to biased amplifiers which were set to give output pulses in the range 0 to 8 volts. Often the pulses were amplified considerably and a back bias was applied to improve the dispersion of the peaks in the pulse height spectrum. The outputs from the four biased amplifiers were analysed simultaneously using a 400 channel analyser.

2.2 Data Collection

Typical pulse height spectra recorded at 165° and 89° for proton energies E_p = 3.095 and 3.099 MeV are shown in fig. 2.3. The four major peaks are attributed to protons scattered from carbon, oxygen, sulphur and antimony

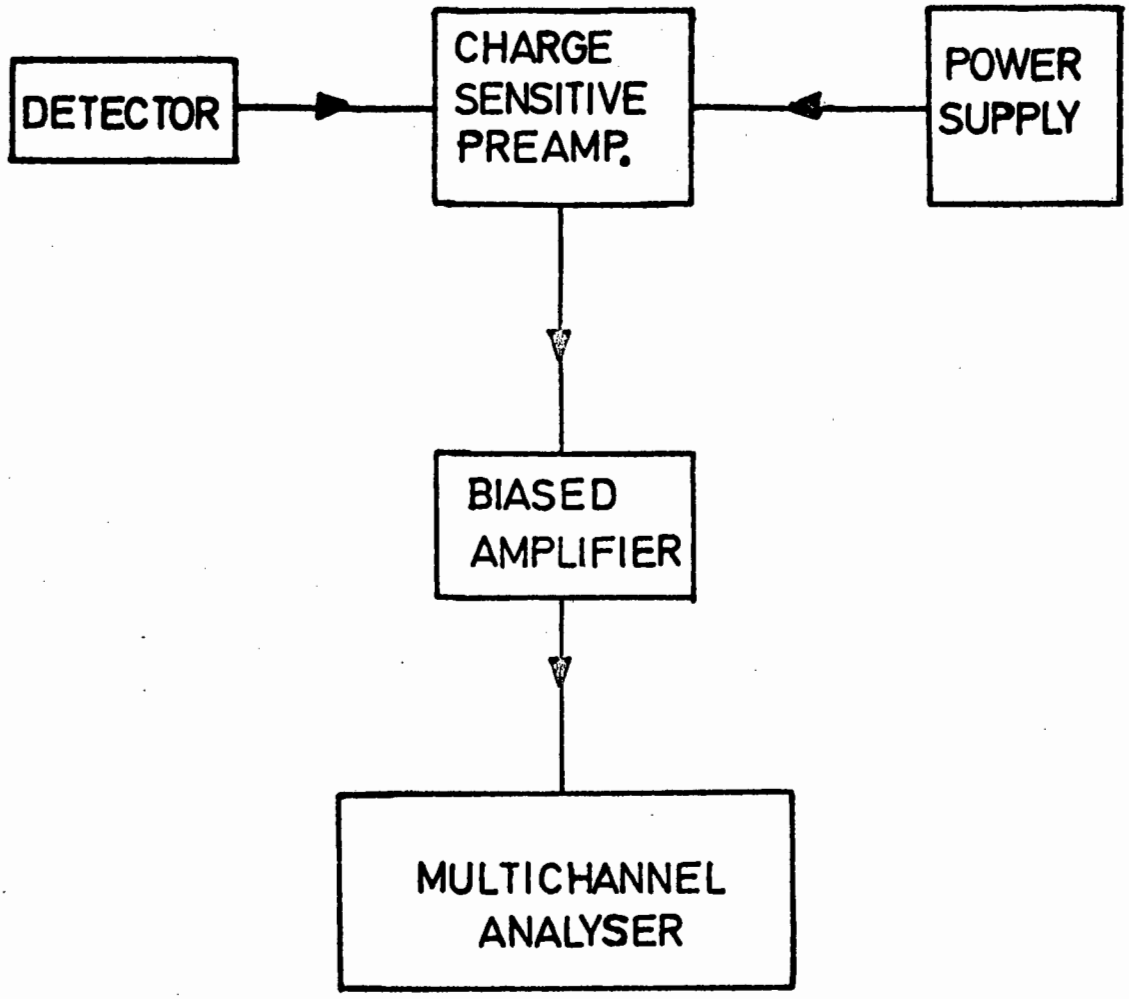

Figure 2.2. Block diagram of the electronics associated with each semi-conductor detector in this experiment

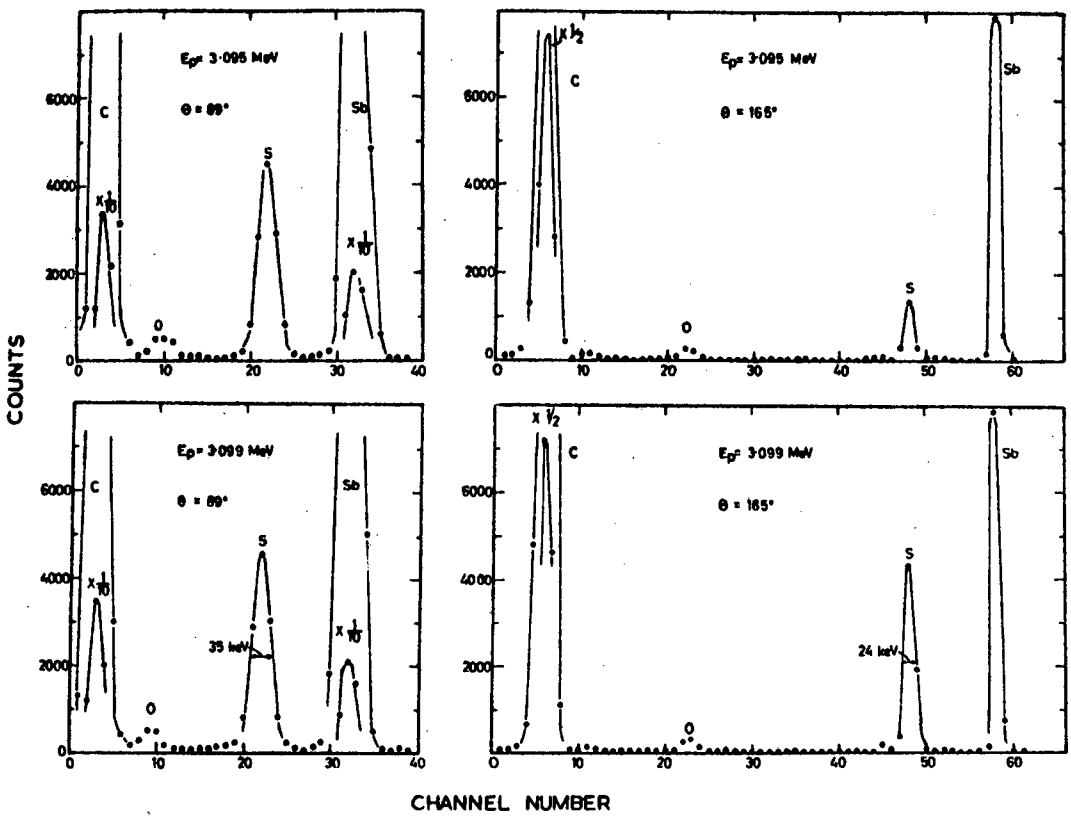

Figure 2.3. Pulse height spectra recorded for protons scattered from an Sb_2S_3 target on carbon backing. Spectra were measured at $\theta = 89^{\circ}$ and 165° for protons of incident energy 3.095 and 3.099 MeV

respectively. The small peak on the left of the sulphur peak is due to silicon contamination of the target. This will be discussed in section 2.3.3.

The proton beam energy was varied in steps of 0.3 to 2.5 keV. At each energy pulse height spectra were recorded for a fixed integrated proton flux for each of the four detectors.

The time taken to record each set of spectra in the multichannel analyser was usually about 1 to 2 minutes. The method of recording the complete spectra had the advantage that background levels could be reliably estimated from the counting rate between elastic scattering peaks. This was particularly important at 89^{o} and to a lesser extent at 123^{o} where the background was higher and the sulphur peak was not separated from the silicon contaminant peak. An alternative procedure to recording the full pulse height spectrum would be to set a single channel analyser "gate" on the sulphur peak and count the pulses selected by this gate by means of a scaler. Although less time consuming this method would not be amenable to such a convenient means of background subtraction.

By suitable arrangement of electronics and pulse height amplification it proved possible to record the spectra from the four detectors simultaneously over a total of 200 channels thus reducing the time to read out a set of spectra from the

analyser to 40 seconds.

Before and after a series of runs over each energy region a short run was carried out over the resonance at E_p = 3.099 MeV. This was to serve as an energy calibration point. (see section 3.2). During each series of runs a run was carried out in the energy region of 4.4 MeV. These runs were used as an efficiency monitor (see section 3.3).

2.3 Targets

The targets used in this work consisted of vacuum evaporated antimony sulphide (Sb_2S_3) on thin carbon backings. Cadmuim sulphide was also considered as a target material but it was found that the preparation of targets was easier with Sb_2S_3. Experiments showed that the two compounds were equally suitable as ^{32}S targets. Gas targets such as H_2S were also considered but were not actively pursued in view of the beam energy spread that would be introduced.

2.3.1 Preparation

Carbon backings were prepared in the following way: Glass microscope slides 2.5 cm × 10 cm × 2 mm were thoroughly cleaned. A thin layer of Teepol (soap solution) was spread evenly over the surface and allowed to dry. The surface was

then wiped with a soft dry cloth until it appeared to be clean. This allowed a thin even layer of Teepol to remain on the slide. A number of slides prepared in this way were then placed facing carbon rods in a vacuum evaporator. The carbon arc was struck in short bursts of about 3 to 5 second duration. About 20 seconds was allowed between bursts to allow the vacuum to restore and to prevent overheating. This was continued until a thin, light brown film of carbon was deposited on the glass slides.

The carbon film was removed by floating it off in warm water, in sections of about 2.5 cm square. The sections were then lifted out on aluminium holders with a 1 cm diameter hole.

An alternative method was also used in the preliminary experiments. In this method BaCl instead of Teepol was first evaporated onto the slides. The use of BaCl, which is very soluble in water makes the floating off procedure much easier. This method was later rejected however due to the possibility of Cl contamination.

A carbon backing, after being allowed to dry for at least 3 hours, was placed in the vacuum evaporator facing a tungsten boat containing about 100 mg, of natural Sb_2S_3. The Sb_2S_3 was then evaporated onto the backings by heating the boat electrically under vacuum. The thickness of the Sb_2S_3 layer could not be controlled in a quantitative way and an approximate method of controlling the evaporation was thus

used. This consisted of observing the light transmission through a thin mica film placed alongside the target in the vacuum chamber.

2.3.2 Thickness Measurements

It was necessary to know the thickness of a number of the targets used in the experiment since this was required in the analysis of narrow levels (see section 4.3.2). An attempt was made to measure the target thickness by weighing but this proved unsatisfactory due to the small weight involved ($\sim$ 50 μg). The following method was therefore devised for measuring the thickness with reasonable accuracy.

It was assumed that the observed width (full width at half maximum) of a narrow ($\lesssim$ 1 keV), symmetrical resonance in the proton scattering excitation curve is approximated by

$$W = \sqrt{\Gamma^2 + T^2 + (\Delta E)^2} \qquad 2.1$$

where Γ = true full width at half maximum (FWHM) of the resonance in the excitation function.

T = spread (FWHM) introduced by finite target thickness.

ΔE = spread (FWHM) in incident beam energy.

The excitation function was measured in the region of a narrow resonance using two targets of different thickness. In addition the yield was determined in an "off-resonance"

region for each target.

From eq. 2.1 it follows that for the measurement on the resonance

$$W_1^2 = \Gamma^2 + T_1^2 + (\Delta E)^2 \qquad 2.2$$

$$W_2^2 = \Gamma^2 + T_2^2 + (\Delta E)^2 \qquad 2.3$$

For the measurements in the off-resonance region we may assume that the scattering yield Y is proportional to the target thickness T so that

$$\frac{Y_1}{Y_2} = \frac{T_1}{T_2} \qquad 2.4$$

where the subscripts 1 and 2 refer to targets 1 and 2 respectively.

The target thickness T_1 and T_2 may thus be obtained by solving the equations 2.2, 2.3 and 2.4 for the three unknown quantities T_1, T_2 and $(\Gamma^2 + (\Delta E)^2)$. Their solution gives

$$T_1 = \{(W_1^2 - W_2^2)/[\,1 - (Y_2/Y_1)^2]\,\}^{1/2}$$

and

$$T_2 = \{(W_2^2 - W_1^2)/[\,1 - (Y_1/Y_2)^2]\,\}^{1/2}$$

Furthermore if the resonance width is known, the beam energy spread may be determined from:

$$\Delta E = [W_1^2 - T_1^2 - \Gamma^2\,]^{1/2}$$

The error in the target thickness δT_1 resulting from a

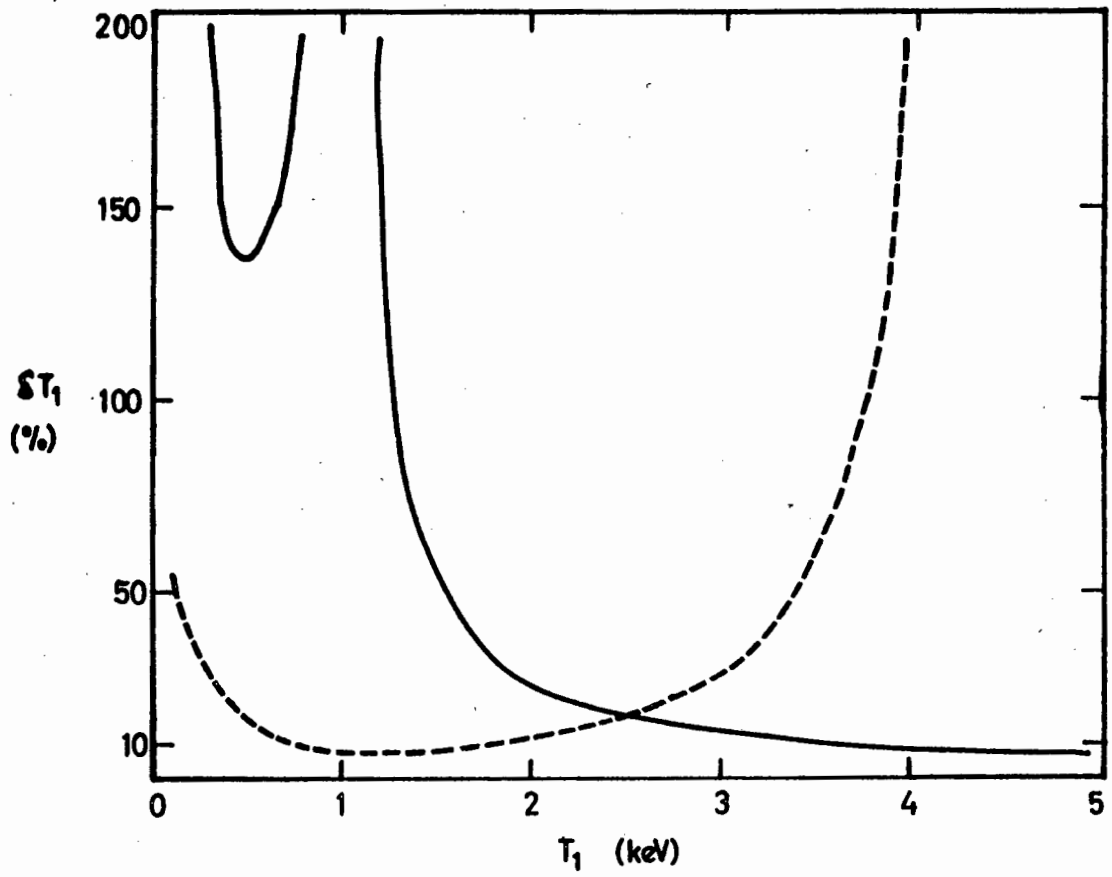

Figure 2.4. Relative error δT_1 in target thickness T_1 as a function of T_1. The solid curves were calculated for a second target thickness T_2 = 1 keV, and the error in the yield measurement ΔY = 5%. The dashed curve is calculated for T_2 = 4 keV

measurement such as this is shown as a function of target thickness T_1 in fig. 2.4. The solid curve has been calculated assuming that target 2 has a thickness T_2 = 1 keV, that the uncertainty in measurement of W is 0.2 keV and that the relative uncertainty in Y is 5%. The dashed curve is calculated assuming that T_2 = 4 keV, the uncertainties in the other quantities remaining the same. Thus it is seen that by suitable choice of targets the thickness of any target may be measured with tolerable accuracy.

The following is an example of such a target thickness measurement: The resonance numbered 5 in fig. 3.2 (E_p = 3.099 MeV) was observed to have a width 2.28 and 1.06 keV and the off-resonance yield was 2980 and 699 counts for the two targets respectively. The target thicknesses in this case were 2.08 ± 0.39 keV and 0.49 ± 0.12 keV respectively.

2.3.3 Si contamination

A peak on the low energy side of the sulphur was often observed in the pulse height spectra. A typical example of this is shown in fig. 2.5. Kinematic considerations showed that this peak was due to Mg, Al, Si or P. The peak was found to increase in intensity during long runs and since it was known that silicon oil was used in the diffusion pump attached to the beam tube as well as in the pump attached to

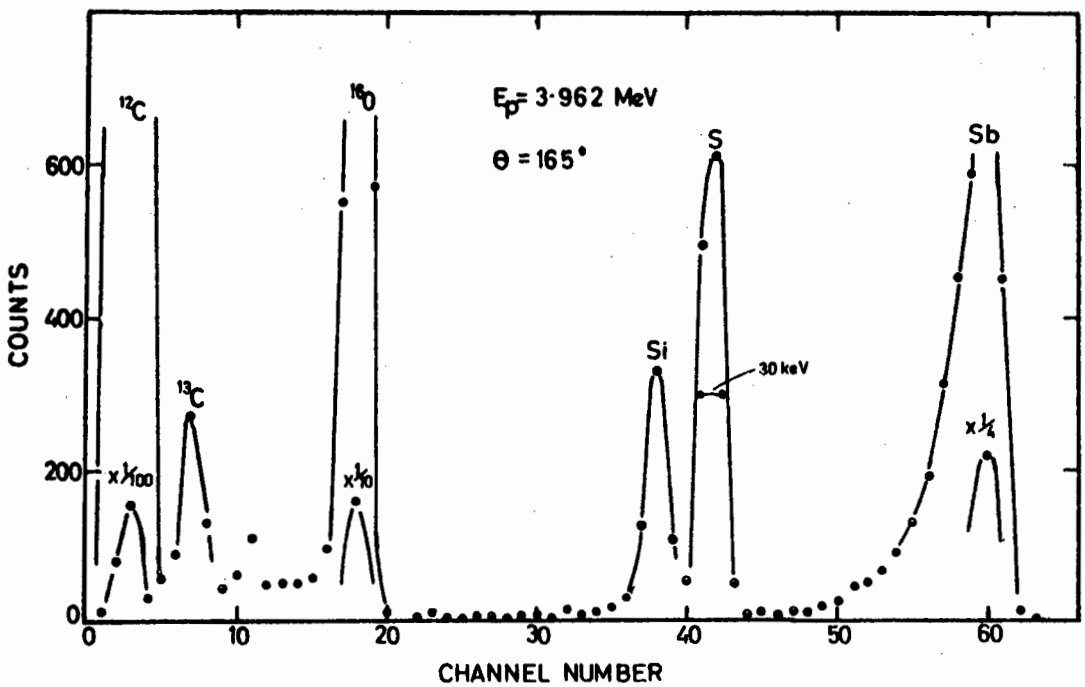

Figure 2.5. Pulse height spectrum for protons scattered from a target which contains silicon contamination

the evaporating chamber used for target preparation, it appeared that this contamination was in fact due to Si. This was confirmed by measuring an excitation function in the 4.6 to 4.9 MeV region where a narrow resonance appears, previously observed by Belote et al. (Be 61).

The silicon-based oil in the two diffusion pumps mentioned was replaced by Apiezon (grade B) high vacuum oil which has a carbon base. This reduced the build-up of silicon on targets during long runs but did not entirely eliminate it.

For the detector at 165° the Si peak was completely separated in the energy region studied. The peaks were also resolved at 139° for proton energies greater than $\sim$ 4 MeV. In the case of the other two detectors this was not possible. An estimate was made of the counts in the sulphur peak due to silicon and this was subtracted with the general background. This procedure probably led to an error in the relative cross sections at 90° and 123° of about 15%.

CHAPTER 3

REDUCTION OF CROSS SECTION DATA

In this section the procedure followed in reducing the raw data to cross sections is described. The yield of protons scattered from sulphur into the detectors at the four angles is obtained at each energy. These data are then reduced to a relative cross section scale. Finally the relative scale is normalised, in the region of pure Rutherford scattering, to the calculated Rutherford cross sections.

3.1 Background subtraction

In the pulse height spectra recorded it was found that the backgrounds observed in the region of the sulphur peak varied from a negligible $\lesssim$1% for spectra recorded at 165° using suitable targets, to approximately 10% for some spectra at 89°. The spectra were also complicated by the silicon contamination peaks which were not resolved at 89° and 123°. (see section 2.3.3). The assumption was made that the background varied uniformly over the region of the sulphur peak. A straight line was drawn through the wings of the peak and the counts above this were summed. It is estimated that the probable error introduced in this way was

about 3 to 8% for 89°, 123° and 139° yields but negligible, relative to the statistical error of counting, at 165°.

3.2 Calibration of proton energy scale

The energy of the proton beam is selected by means of an analysing magnet as described in section 2.1. The field of the magnet is monitored by means of a nuclear magnetic resonance device, and the resonance frequency ν is related to the proton energy by

$$E_p = K\nu^2 \qquad 3.1$$

where K is a proportionality constant.

Since K varied by about 0.2% from one series of runs to the next it was necessary to calibrate the energy for each series of runs. For this purpose a calibration point of known energy was needed. The calibration energy decided on for this work was the well known $^{7}Li(p,n)^{7}Be$ threshold.

A thin Li target was prepared and placed at the end of the faraday cup assembly (fig. 2.1(a)). The neutron threshold was measured in terms of the frequency ν and since the threshold energy is known to be 1.8806 MeV (Ma 63) the constant K was determined. The Sb_2S_3 target was now replaced and the excitation function over a narrow (<1 keV) resonance in $^{32}S(p,p)^{32}S$ was measured. Using the constant K just

determined, the energy of this resonance was found to be 3.099 ± 0.0005 MeV. This energy was then used as a secondary standard for the experiment. Each series of runs was preceded or followed by an excitation function measurement over the resonance and the frequency ν on resonance was then used to determine the value of K for that series of runs.

3.3 Relative cross sections

The proton elastic scattering data were collected over several series of runs carried out at different times using different targets and detector systems. Naturally the yield measured at a particular energy varied from one series of runs to another owing to variations in target thickness and detector geometry. To obtain a relative cross section curve over the entire energy range a reliable quantitative method of combining runs was required.

The method used was as follows: In each series of runs yield measurements were carried out in the 4.4 MeV region. This region is lacking in structure and is thus independent of resolution. The data obtained at the other energies were thus expressed relative to the yield in the 4.4 MeV region. This was done separately and independently for the data at each angle.

In the early stages of the experiment, i.e. in the

energy region 2.8 to 3.4 MeV, measurements were not carried out in the 4.4 MeV region. In these cases the procedure followed was to simply overlap the various runs in regions where there was no structure in the yield curve. This was again done independently at the four angles. A separate measurement was later made of the yield at 3 MeV relative to that at 4.4 MeV thus relating the yield data in the 2.8 to 3.4 MeV region to the relative cross section scale at 4.4 MeV.

The data were thus reduced to four sets of relative cross section data, one set at each angle. To reduce these data to a common cross section scale one detector was used to measure the yield at each of the angles in turn. The proton energy for this measurement was 4.4 MeV. The yields were corrected in the usual way for background and a centre of mass solid angle correction was included. As a check on possible geometric errors in the measurements, the angular distribution of 1 MeV α-particles elastically scattered from gold was measured. This was found to obey the Rutherford scattering angular distribution expected, thus confirming the absence of any systematic geometric errors in the relative yield measurement at the four angles.

3.4 Calibration of the cross section scale

The relative cross section scale in terms of which all the data were now expressed, was calibrated as follows:

The yield of scattered protons at 165° was measured using identical target and detector geometry in the proton energy region 0.9 to 1.4 MeV and then in the 4.4 MeV region. The yields in the Rutherford region (0.9 to 1.4 MeV) were thus expressed on the same relative cross section scale as the rest of the data. This relative cross section scale was then normalised to the Rutherford cross sections calculated in the 0.9 to 1.4 MeV region. It would have been interesting to normalise each set of data at the other angles in the same way. However this was not possible since in the Rutherford region the detector resolution was not sufficient to separate the peaks attributed to protons scattered from S and Sb, in the pulse height spectrum.

Corrections had to be applied to the yield measured in the 1 MeV region due to the fact that the protons scattered from the Si contaminant in the target could not be separated from those scattered from sulphur. The correction was determined in the following way: (The regions of Rutherford scattering and E_p = 4.4 MeV will be referred to as the E_R and the E_N regions respectively in this discussion). In the E_N region the S and Si peaks were completely resolved and the

yield of protons scattered from Si in this region could thus be obtained. The differential cross section of ^{28}Si (Natural isotopic abundance 92.3%) at this energy and angle, $d\sigma_{Si}(E_N,\theta)$ was measured by Belote, Kashy and Risser. (Be 61). From this value and the calculated silicon Rutherford cross sections, $d\sigma_{Si}(E_R,\theta)$, we determine the yield of silicon scattered protons in the E_R region ($Y_{Si}(E_R,\theta)$ from:

$$Y_{Si}(E_R,\theta) = Y_{Si}(E_N,\theta)d\sigma_{Si}(E_R,\theta)/d\sigma_{Si}(E_N,\theta) \qquad 3.2$$

The error in the absolute value of $d\sigma_{Si}(E_N,\theta)$ is estimated by Belote et al. to be ±10%. The error in $Y_{Si}(E_N,\theta)$ is estimated to be not more than 15%. The error in $Y_{Si}(E_R,\theta)$ is thus ∿18%.

The yield of protons scattered from sulphur at E_R could now be determined by subtracting the contribution from Si and the background. In the targets chosen for these measurements the Si contribution was found to be about 10% of the total yield in the sulphur peak. The error in the sulphur yield due to the error in Si contribution was thus only about ∿2%.

Another correction that had to be considered was due to the fact that the targets used consisted of natural Sb_2S_3. The natural isotopic abundance of ^{32}S is 95.0%. The contributions in the E_R region due to ^{33}S and ^{34}S were subtracted from the suplhur yield. The contribution from these isotopes in the E_N region was assumed to be due to Rutherford

scattering only. The yield relative to the ^{32}S yield was thus negligible ($\lesssim$ 1%). In fact this assumption is probably not valid owing to structure in ^{33}S and ^{34}S yields and is likely to lead to errors in the off-resonance cross sections of $\lesssim$ 5%.

To check the validity of the assumption that in the 0.9 to 1.4 MeV region we have pure Rutherford scattering, the corrected yield of protons scattered from ^{32}S was plotted against $1/E^2$. This plot is shown in figure 3.1. For pure Rutherford scattering one expects the points to be on a straight line through the origin. This is seen to be the case. The standard deviation from the straight line is $\lesssim$ 2%.

3.5 The cross section data

The differential proton elastic scattering cross section data are shown as a function of energy in fig. 3.2. Open and solid circles are used to represent different series of runs. Most energy regions were covered at least twice. The solid curves show theoretical fits to the data. These will be discussed in chapter 6. The lower set of data are due to inelastically scattered protons and these will be discussed in section 5.1.

The various sources of error introduced in arriving at the cross sections shown in the figures have already been

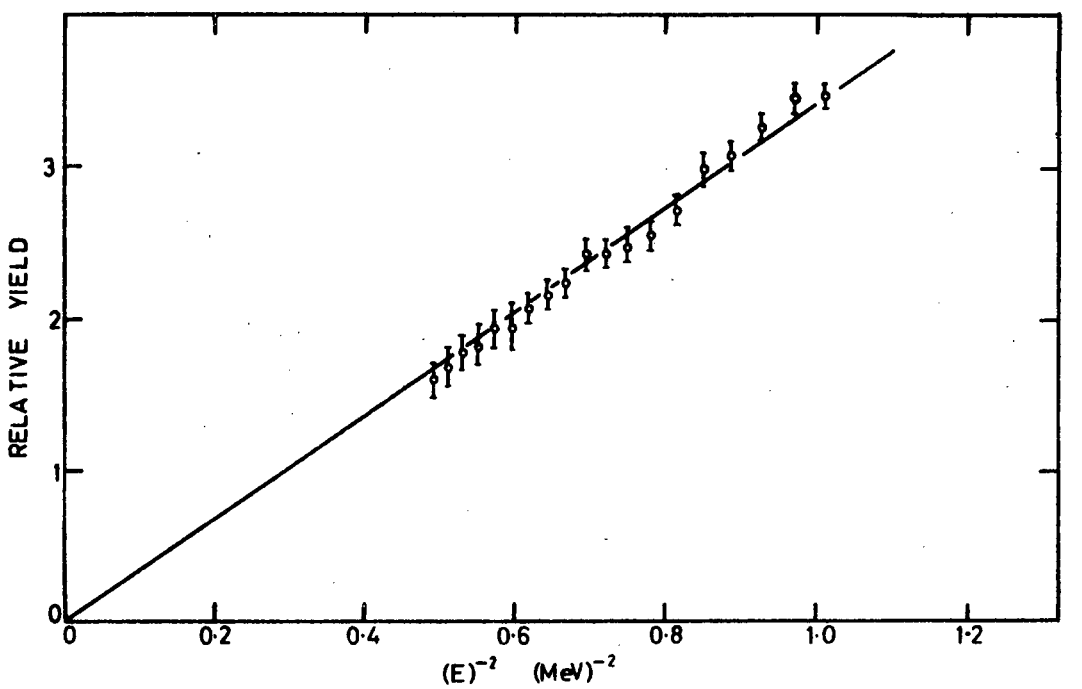

Figure 3.1. Relative cross section in the 0.9 to 1.2 MeV region plotted as a function of $1/E^2$. Straight line indicates Rutherford scattering

discussed in the previous sections. It remains to estimate the error in the final results.

Relative cross sections of adjoining data are believed to be in error by not more than 5% to 10%. Together with the uncertainty of normalisation this results in an uncertainty in the absolute cross section values of not more than 7% at 165°, 10% at 139°, 15% at 123° and 20% at 89°. The larger error in the latter case is due to the larger background and uncertainty in the silicon contribution to the yield.

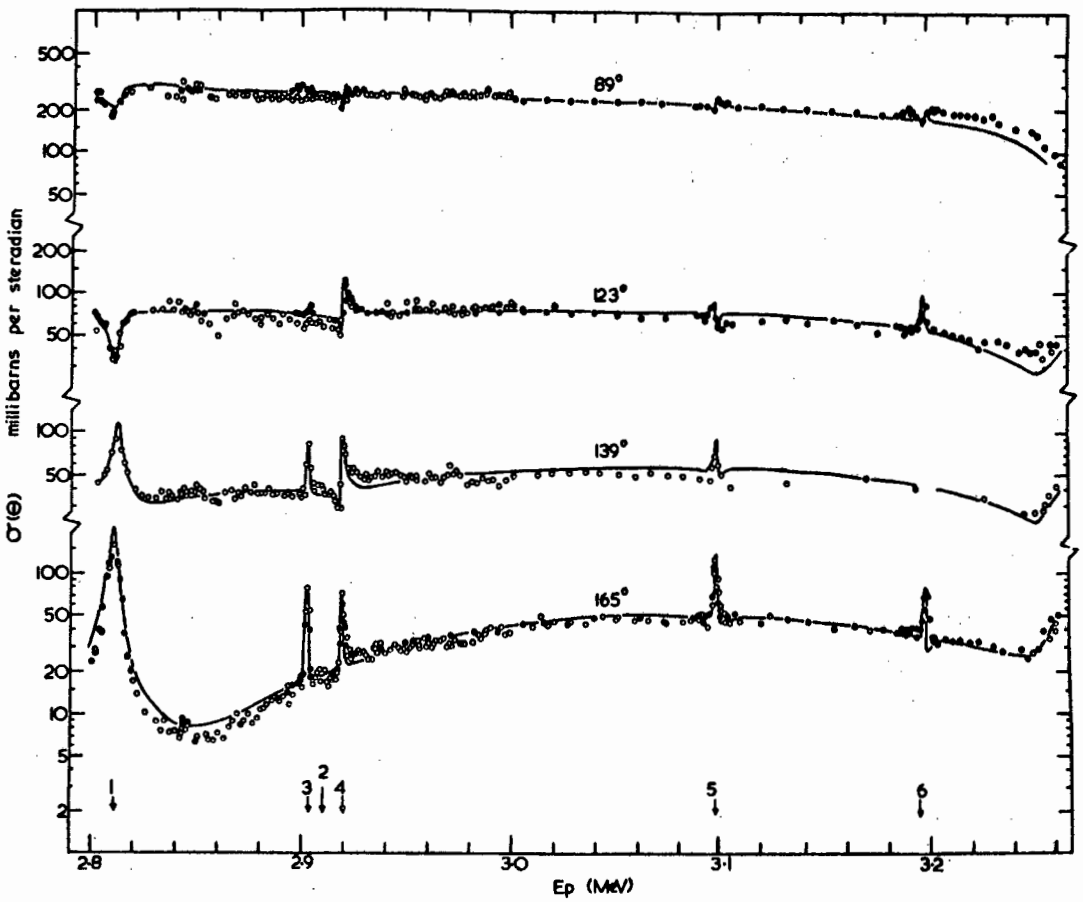

Figure 3.2 (a) Differential proton elastic scattering cross sections in the energy range E_p = 2.80 to 3.26 MeV.

Open and solid circles represent data obtained in different series of runs. Solid curves are theoretical fits to the data (see sections 4.3 and 6.1) calculated using the parameters in table 6.1.

Note: The data shown in this figure are collected together with the data of figs. 3.2.(b) to 3.2.(f) in a foldout on inside of back cover.

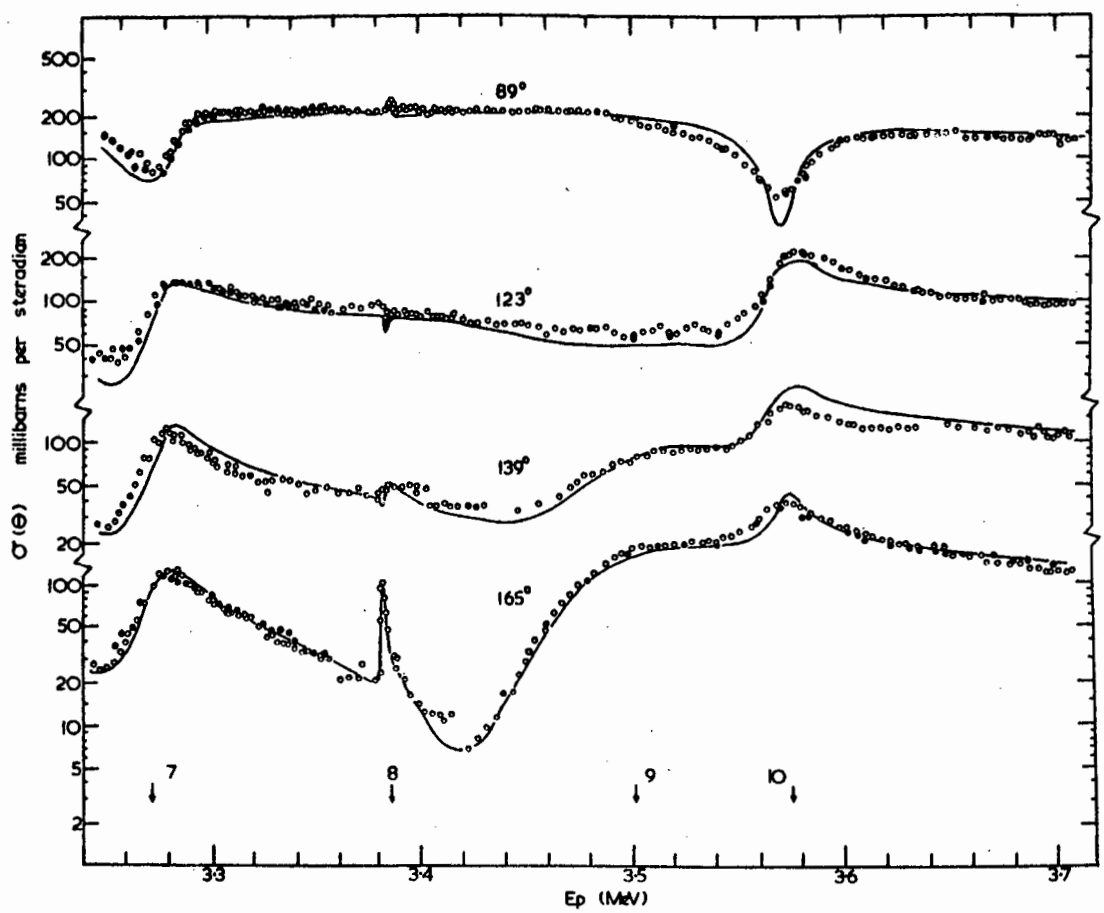

Figure 3.2 (b) Differential proton elastic scattering cross sections in the energy range E_p = 3.25 to 3.70 MeV.

For details see caption to fig. 3.2 (a)

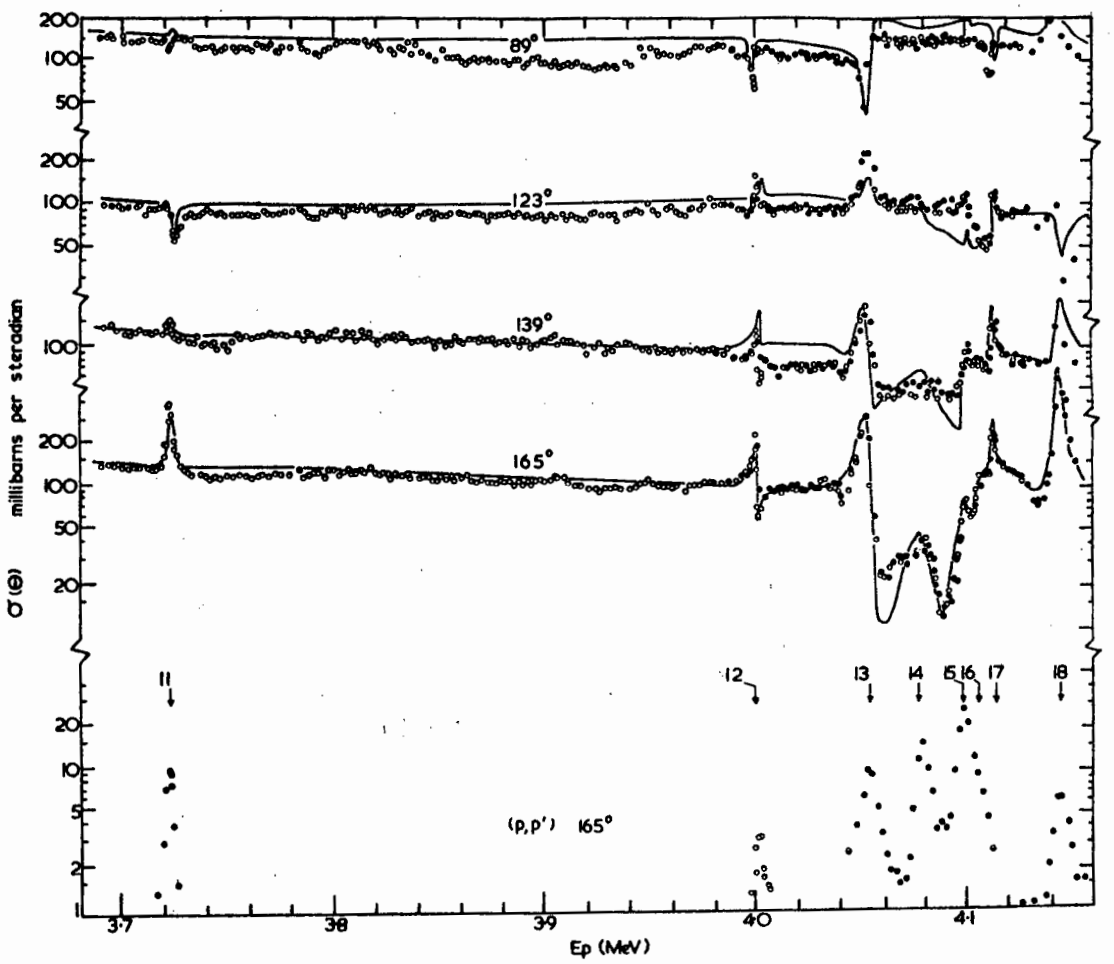

Figure 3.2 (c) Differential proton elastic scattering cross sections in the energy range E_p = 3.69 to 4.15 MeV

For details see caption to fig. 3.2(a)

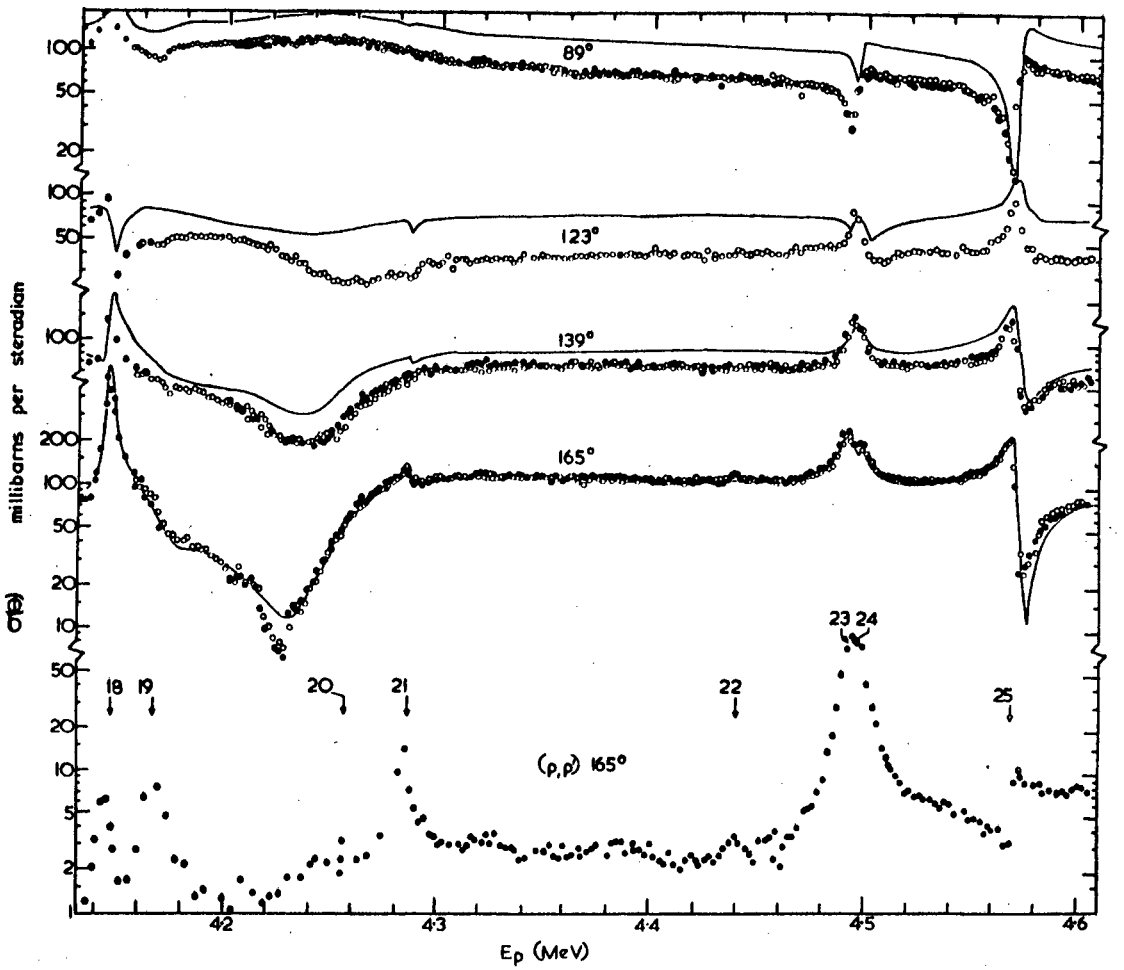

Figure 3.2 (d) Differential proton elastic scattering cross sections in the energy range

E_p = 4.14 to 4.60 MeV

For details see caption to fig. 3.2(a)

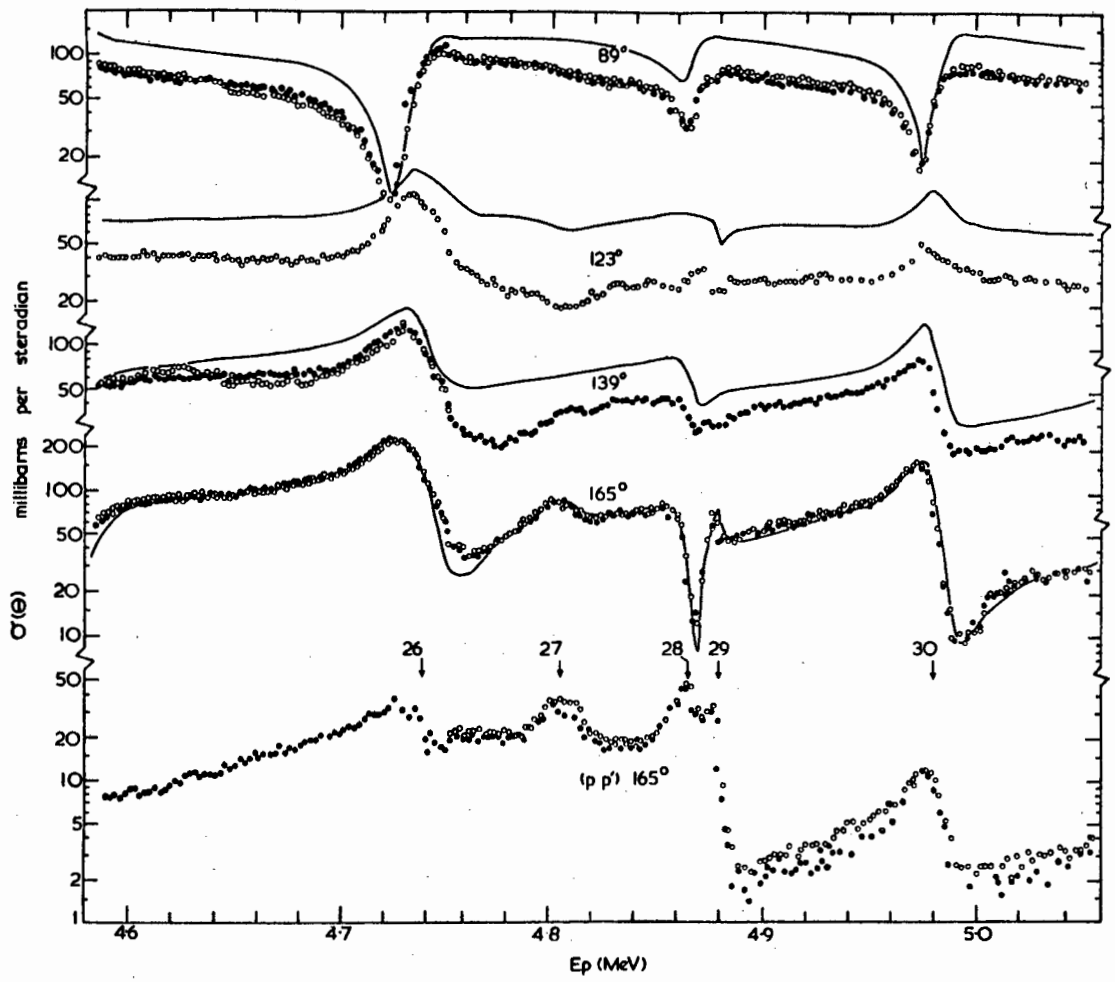

Figure 3.2 (e) Differential proton elastic scattering cross sections in the energy range

E_p = 4.59 to 5.05 MeV

For details see caption to fig. 3.2(a)

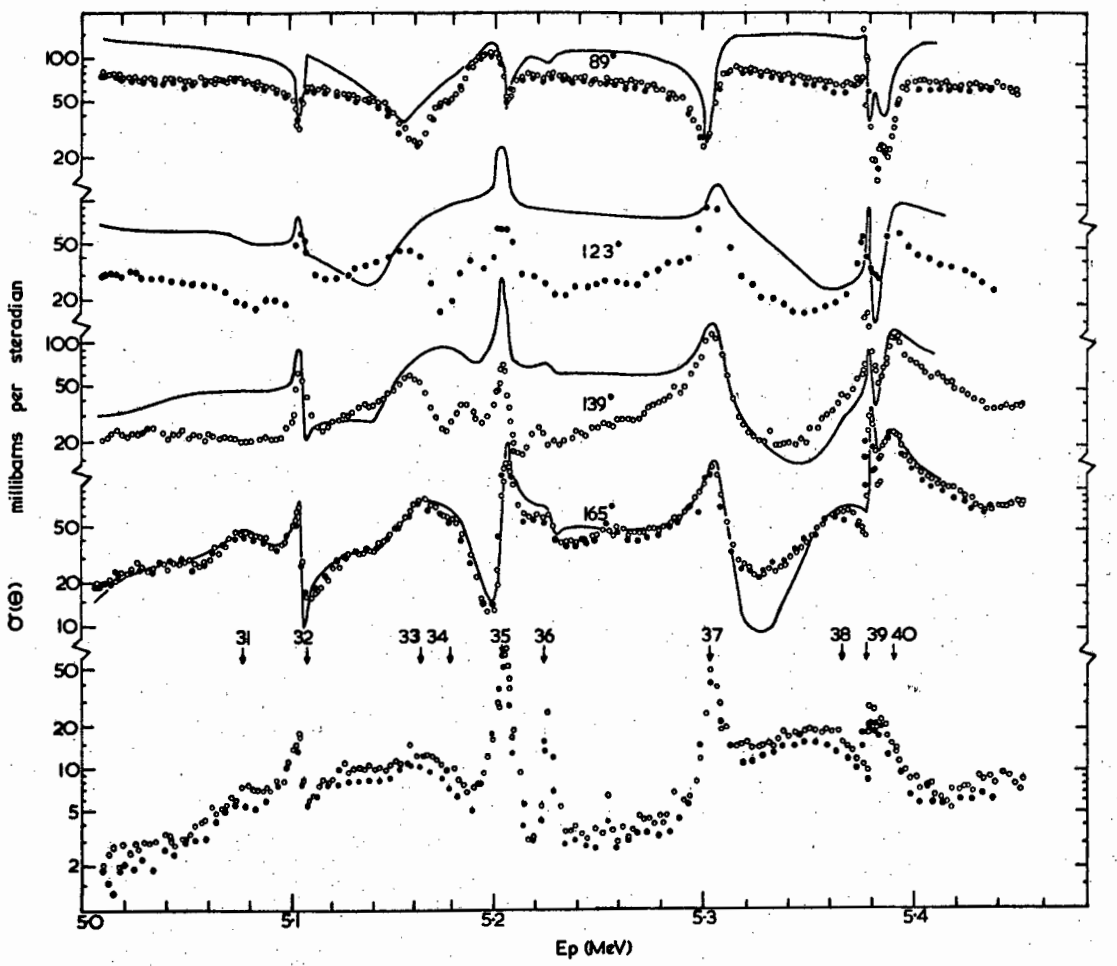

Figure 3.2 (f) Differential proton elastic scattering cross sections in the energy range

E_p = 5.01 to 5.46 MeV

For details see caption to fig. 3.2(a)

CHAPTER 4

ANALYSIS OF THE ELASTIC SCATTERING DATA

The measured cross section data shows a considerable amount of resonance structure. In the compound nucleus theory these resonances are associated with energy levels of the compound nucleus. An analysis of the data is undertaken in order to extract spectroscopic information from the observed resonances regarding the energy levels of the ^{33}Cl nucleus. The analysis is carried out by calculating the differential proton elastic scattering cross section as a function of energy using various parameters such as energies, spins, parities and widths. The calculated cross sections are compared with the observed data and the parameters are adjusted in order to obtain a good visual fit of the calculated cross section to the data.

The theory of elastic scattering, leading to a cross section equation, is presented in the next section. The calculation of this cross section and the method of analysis are then discussed.

4.1 Theory of elastic scattering

The differential cross section for a particle scattered by a central potential is given by (Ro 67, Bl 52, Me 61).

$$d\sigma(\theta) = |f(\theta)|^2 d\Omega \qquad 4.1$$

where $f(\theta)$ is the scattering amplitude. If the reaction cross section is negligible then $f(\theta)$ can be expressed as follows:

$$f(\theta) = \lambda\!\!\!^{-} \sum_{\ell} (2\ell + 1)\, e^{2i\delta_\ell} \sin \delta_\ell \; P_\ell(\cos \theta) \qquad 4.2$$

where $\lambda\!\!\!^{-}$ is the particle wavelength, δ_ℓ is the phase shift for the partial wave representing particles of orbital angular momentum ℓ and $P_\ell(\cos \theta)$ is the Legendre polynomial. In the case of scattering of a zero-spin charged particle incident on a zero-spin nucleus, the Coulomb as well as the nuclear potential must be taken into account. The scattering amplitude thus becomes: (Bl 56)

$$f(\theta) = f_c(\theta) + f_N(\theta) \qquad 4.3$$

where

$$f_c(\theta) = -\eta/2\lambda\!\!\!^{-} \csc^2 (\theta/2) \exp [i\eta \ln(\csc^2(\theta/2))] \qquad 4.4$$

and

$$f_N(\theta) = \lambda\!\!\!^{-} \sum_{\ell=0}^{\infty} (2\ell + 1) \sin \delta_\ell \exp [i(\delta_\ell + \alpha_\ell)] \; P_\ell(\cos\theta) \qquad 4.5$$

where $\eta = \dfrac{zz'e^2}{\hbar v}$, ze and z'e are the charges of target nucleus and protons respectively and v is their relative velocity. α_ℓ is the Coulomb phase shift:

$$\alpha_\ell = 2 \sum_{s=1}^{\ell} \arctan (\eta/s) \quad \text{for } \ell > 0$$

$$\alpha_0 = 0$$

In the present experiment protons (spin-$\frac{1}{2}$) are scattered from a zero-spin nucleus. The modifications to eq. 4.3 required for spin=$\frac{1}{2}$ particles have been derived by Critchfield and Dodder (Cr 49) and are given in convenient form by Laubenstein and Laubenstein (La 51). The partial wave which represents particles with orbital angular momentum ℓ is separated into two components corresponding to the two possible orientations of spin with respect to orbital angular momentum. The phase shift for the component of the ℓth partial wave with channel spin $j = \ell+\frac{1}{2}$ is denoted by δ_ℓ^+, and the phase shift of the component which forms the compound state with $j = \ell-\frac{1}{2}$ is given by δ_ℓ^-. Equations 4.1, 4.3, 4.4 and 4.5 thus reduce to (La 51):

$$d\sigma(\theta) = \lambda^2 \left[|A + B|^2 + |C|^2 \right] d\Omega \qquad 4.6$$

where

$$A = f_c(\theta) \qquad \text{(eq. 4.4)}$$

$$B = \sum_{\ell=0}^{\infty} (\ell+1) \exp\left[i(\alpha_\ell+\delta_\ell^+)\right] \sin \delta_\ell^+ P_\ell(\cos\theta) + \sum_{\ell=1}^{\infty} \ell \exp\left[i(\alpha_\ell+\delta_\ell^-)\right] \times \sin \delta_\ell^- P_\ell(\cos\theta) \qquad 4.7$$

$$\text{and } C = \sin\theta \sum_{\ell=1}^{\infty} \exp\left[i\,\alpha_\ell(\sin\ \delta_\ell^- e^{i\delta_\ell^-} - \sin\ \delta_\ell^+ e^{i\delta_\ell^+})\right] \times P'_\ell(\cos\theta) \quad 4.8$$

$$\text{where } P'_\ell(\cos\theta) = \frac{dP_\ell(\cos\theta)}{d(\cos\theta)}$$

In eq. 4.6, A represents the Coulomb (Rutherford) scattering amplitude and B and C represent the coherent and incoherent nuclear scattering amplitudes respectively. The "incoherent term", C, is introduced in order to account for the reversal of the intrinsic spin along the Z-axis due to the fact that the beam is unpolarized.

The phase shifts δ_ℓ^+ and δ_ℓ^- may each be written as the sum of two components:

$$\delta_\ell^\pm = \beta_\ell^\pm + \phi_\ell$$

where ϕ_ℓ the slowly varying off-resonant contribution is usually taken to be that for a charged hard sphere.

$$\text{i.e. } \phi = -\arctan\,(F_\ell/G_\ell)_{r=a}$$

where F_ℓ and G_ℓ are the regular and irregular solutions of the Schrödinger equation for the interaction of a proton with a nuclear plus Coulomb potential.

All the nuclear information is contained in the resonant phase shift $\beta_\ell^\pm$. The R-matrix theory of Wigner and Eisenbud (Wi 47) leads to the following expression for $\beta_\ell^\pm$:

$$\tan \beta_\ell^{\pm} = \frac{P_\ell}{1/R_\ell^{\pm} - S_\ell} \qquad 4.10$$

where the quantities P_ℓ and S_ℓ may be expressed in terms of F_ℓ and G_ℓ. The boundary conditions of Wigner and Eisenbud (Wi 47) give the penetrability,

$$P_\ell = \frac{k}{A_\ell^2(ka)}, \quad \text{where } A_\ell^2 = F_\ell^2 + G_\ell^2$$

and

$$S_\ell = \frac{k(F_\ell F_\ell' + G_\ell G_\ell')}{A_\ell^2} = \frac{1}{2}\,\frac{ka}{A_\ell^2}\,(A_\ell^2)' \qquad 4.11$$

where

$$(A_\ell^2)' = \frac{d}{d(kr)}\,[A_\ell^2(kr)]_{r=a}$$

The nuclear information is now contained in the R-functions,

$$R_\ell^{\pm} = \sum_\lambda \frac{\gamma_{\lambda\ell}}{E_{\lambda\ell} - E} \qquad 4.12$$

where $E_{\lambda\ell}$ is related to the energy of the resonance λ and $\gamma_{\lambda\ell}^2$, the reduced widths of the levels λ, are energy independent quantities which are related to the observed resonance width Γ_λ through the following relation:

$$\frac{\Gamma_{\lambda\ell}}{2} = \gamma_{\lambda\ell}^2 P_\ell \qquad 4.13$$

If we now substitute the expressions for P_ℓ and S_ℓ (eq. 4.11) in 4.10 we get

$$\tan \beta_\ell^\pm = \left[\frac{1}{R_\ell^\pm} - \left(\frac{A_\ell^2}{2} \right)' \right]^{-1} \qquad 4.14$$

$$\text{with } R_\ell^\pm = \sum_\lambda \Gamma_{\lambda/2} / (E_\lambda - E)$$

For a single isolated resonance this expression reduces to the single level dispersion relation

$$\beta_\ell = \arctan \left[\frac{E_\lambda - E}{\Gamma_{\lambda/2}} - \left(\frac{A_\ell^2}{2} \right)' \right]^{-1} \qquad 4.15$$

$$= \arctan \frac{\Gamma_{\lambda/2}}{E_\lambda - E + \Delta_{\lambda\ell}}$$

where $\Delta_\lambda = - \left(\frac{A_\ell^2}{2} \right)' \frac{\Gamma_\lambda}{2}$ is the level shift parameter.

In the above discussion it was assumed that the only channel available for the decay of a given compound nucleus level was that corresponding to proton elastic scattering. However, this assumption was not valid in the present studies since inelastic scattering was also possible. To take account of the availibility of other open channels eq. 4.6. is modified by reducing the resonant part of the elastic scattering amplitude by a factor $\frac{\Gamma_{p\lambda}}{\Gamma_\lambda}$; where $\Gamma_{p\lambda}$ and Γ_λ are the elastic scattering width and total width of a given level λ. The expressions for B and C (eqs. 4.7 and 4.8) thus become (Ol 58):

$$B = \sum_{\ell=0}^{\infty} (\ell+1) P_\ell(\cos\theta) e^{i\alpha_\ell} \{\sin\phi_\ell \, e^{i\phi_\ell} + \frac{\Gamma_{p\lambda}}{\Gamma_\lambda} \sin\beta_\ell^+ \, e^{i(\beta_\ell^+ + 2\phi_\ell)}\}$$

$$+ \sum_{\ell=1}^{\infty} \ell \; P_\ell(\cos\theta) e^{i\alpha_\ell} \{\sin\phi_\ell \, e^{i\phi_\ell} + \frac{\Gamma_{p\lambda}}{\Gamma_\lambda} \sin\beta_\ell^- . e^{i(\beta_\ell^- + 2\phi_\ell)}\} \qquad 4.16$$

$$\text{and } C = \sin\theta \sum_{\ell=0}^{\infty} P'_\ell(\cos\theta) e^{i\alpha_\ell} \{\frac{\Gamma_{p\lambda}}{\Gamma_\lambda} \sin\beta_\ell^- \cdot e^{i(\beta_\ell^- + 2\phi_\ell)}$$

$$- \sum_{\ell=1}^{\infty} P'_\ell(\cos\theta) e^{i\alpha_\ell} \{\frac{\Gamma_{p\lambda}}{\Gamma_\lambda} \sin\beta_\ell^+ \cdot e^{i(\beta_\ell^+ + 2\phi_\ell)}\} \qquad 4.17$$

In addition the expression for Γ_λ (eq. 4.13) and Δ_λ must be modified as follows:

$$\Gamma_\lambda = \sum_s \Gamma_{\lambda s} = 2 \sum_s P_\ell \, \gamma_{\lambda s}^2 \qquad 4.18$$

$$\Delta_\lambda = \sum_s \Delta_{\lambda s} = - \sum_s \left(\frac{A_\ell^2}{2}\right)' \frac{\Gamma_{\lambda s}}{2} \qquad 4.19$$

where the subscipts λ_s denote the different channels available for the decay of the compound level λ. The expression for Δ_λ used in the present case is that given by Sachs (Sa 53):

$$\Delta_\lambda = \sum_s \left\{\frac{F_{\ell(\rho_s)}}{G_{\ell(\rho_s)}}\right\} \frac{\Gamma_{\lambda s}}{2}$$

The coefficient of $\Gamma_{\lambda s}$ in this expression is simply the tangent of the potential scattering phase shift for channel s, ϕ_s. According to Olness et al. (Ol 58) the difference in Δ_λ calculated from these two expressions is negligible.

The equations used in the calculation of the differential elastic scattering cross section for purposes of this analysis were eqs. 4.6, 4.4, 4.16 and 4.17. When the quantity $|A + B|$ is squared, three terms result. The first term A corresponds to Rutherford scattering and the second term B to specifically nuclear scattering. The third term is given by twice the real part of A and B (2ReAB) and therefore depends on the relative phase between A and B. This term represents interference between the two amplitudes and it often dominates in determining the shape of the cross section as a function of energy. Since B is a sum over various spin states the nuclear cross section consists of components due to various levels and interference terms between these components. However the phase shift β for distant levels will be close to either o or π so that the components of the cross section are usually small for these levels.

In using the expression for β_ℓ in eq. 4.15 the assumption is made that the levels are isolated. Also in this expression no account is taken of the energy dependence of Γ_λ. This simplification could lead to errors for very broad levels

where the penetrability P_ℓ changes significantly within one resonance width.

4.2 Calculation of cross sections

A computer programme (see appendix A) was written in Manchester Autocode to compute $d\sigma$ from the epxressions given above. (Eqs. 4.6, 4.4, 4.16 and 4.17). In order to facilitate programming these expressions were written as follows:

$$\frac{d\sigma(\theta)}{d\Omega} = \lambda^2 \left\{ D^2 + \sum_{\ell=0}^{4} \sum_{k=1}^{4} \left[U_R U_{k\ell} + V_R V_{k\ell} + \sum_{\ell'=0}^{4} \sum_{k'=0}^{4} (U_{k\ell} U_{k'\ell'} + V_{k\ell} V_{k'\ell'}) \right] + \sum_{\ell,\ell'=0}^{4} \sum_{k,k'=0}^{2'} \left[U'_{k\ell} U'_{k'\ell'} + V'_{k\ell} V'_{k'\ell'} \right] \right\} \qquad 4.20$$

where $D^2 = \eta^2/4 \ \mathrm{cosec}^4 (\theta/2)$

$U_R = \mathrm{Re}(A) = -\eta/2 \ \mathrm{cosec}^2 (\theta/2) \cos [\eta_\ell n \ \mathrm{cosec}^2 (\theta/2)]$

$V_R = \mathrm{Im}(A) = -\eta/2 \ \mathrm{cosec}^2 (\theta/2) \sin [\eta_\ell n \ \mathrm{cosec}^2 (\theta/2)]$

$U_{k\ell} = X_{k\ell} \cos \psi_{k\ell}$

$V_{k\ell} = X_{k\ell} \sin \psi_{k\ell}$

$U'_{k\ell} = Y_{k\ell} \cos \psi'_{k\ell}$

$V'_{k\ell} = Y_{k\ell} \sin \psi'_{k\ell}$

$$\text{and } X_{1\ell} = (\ell+1)P_\ell(\cos\theta)\sin\phi_\ell \qquad \psi_{1\ell} = \phi_\ell + \alpha_\ell$$

$$X_{2\ell} = (\ell+1)P_\ell(\cos\theta)\sin\beta_\ell^+ \cdot \frac{\Gamma_{\lambda p}}{\Gamma_\lambda} \qquad \psi_{2\ell} = \beta_\ell^+ + \alpha_\ell + 2\phi_\ell$$

$$X_{3\ell} = \ell P_\ell(\cos\theta)\sin\phi_\ell \qquad \psi_{3\ell} = \psi_{1\ell}$$

$$X_{4\ell} = \ell P_\ell(\cos\theta)\sin\beta_\ell^- \quad \frac{\Gamma_{\lambda p}}{\Gamma} \qquad \psi_{4\ell} = \alpha_\ell + 2\phi_\ell + \beta_\ell^-$$

$$Y_{1\ell} = \sin\theta \quad \frac{\Gamma_{\lambda p}}{\Gamma_\lambda} P_\ell'(\cos\theta)\sin\beta_\ell^- \qquad \psi'_{1\ell} = \beta_\ell^- + 2\phi_\ell + \alpha_\ell$$

$$Y_{2\ell} = -\sin\theta \frac{\Gamma_{\lambda p}}{\Gamma_\lambda} P_\ell'(\cos\theta)\sin\beta_\ell^+ \qquad \psi'_{2\ell} = \beta_\ell^+ + 2\phi_\ell + \alpha_\ell$$

A few approximations were made in the programme. Provision was made for a maximum of twenty levels with orbital angular momentum in the range $\ell = 0$ to 4. For levels of the same spin and parity it was assumed that the total resonance phase shift, was the sum of the tangents of the individual resonance phase shifts, i.e.:

$$\tan\beta_\ell = \tan\beta_{\ell_1} + \tan\beta_{\ell_2}$$

According to Olness et al. this procedure is satisfactory as long as the resonances are not within a few widths of each other. However if $\frac{\Gamma_{p\lambda}}{\Gamma} \nsim 1$, then the equations are such that all levels of the same spin and parity are reduced by the same factor. This limitation is again less important if these levels are far apart.

The values of the potential scattering phase shift, ϕ, were taken from the tables of Block et al. (Bl 51). The interaction radius was assumed to be $r = 1.4\ (A^{1/3} + 1)$ fm.

The actual values of ϕ used are plotted in figure 4.1.

Other numerical values used in the calculations were

$$\lambda\!\!\!^{-2} = \frac{0.2075}{E} \qquad \lambda\!\!\!^{-2} \text{ in barns}, \quad E \text{ in keV}$$

and

$$\eta = 2.5656\ E^{-\frac{1}{2}}$$

The level shift parameter was included for elastic scattering but neglected for the inelastic channel. This might lead to errors in the determination of E_λ , Γ_λ and $\Gamma_{p\lambda}$ in energy regions where the inelastic cross section is large.

Accurate assignments in cases where levels of the same spin and parity are close to each other are not possible but the results may still be approximately true.

An additional subroutine was added to the programme to facilitate the fitting of the calculated cross section to the experimental data. The function of this subroutine was to convolute the calculated cross section with an energy spread corresponding to that introduced by the experiment. The shape of the energy resolution function was assumed to be Gaussian and its width S was determined by the target thickness T, and beam energy spread ΔE.

$$\text{i.e.} \quad S = \sqrt{T^2 + \Delta E^2}\ .$$

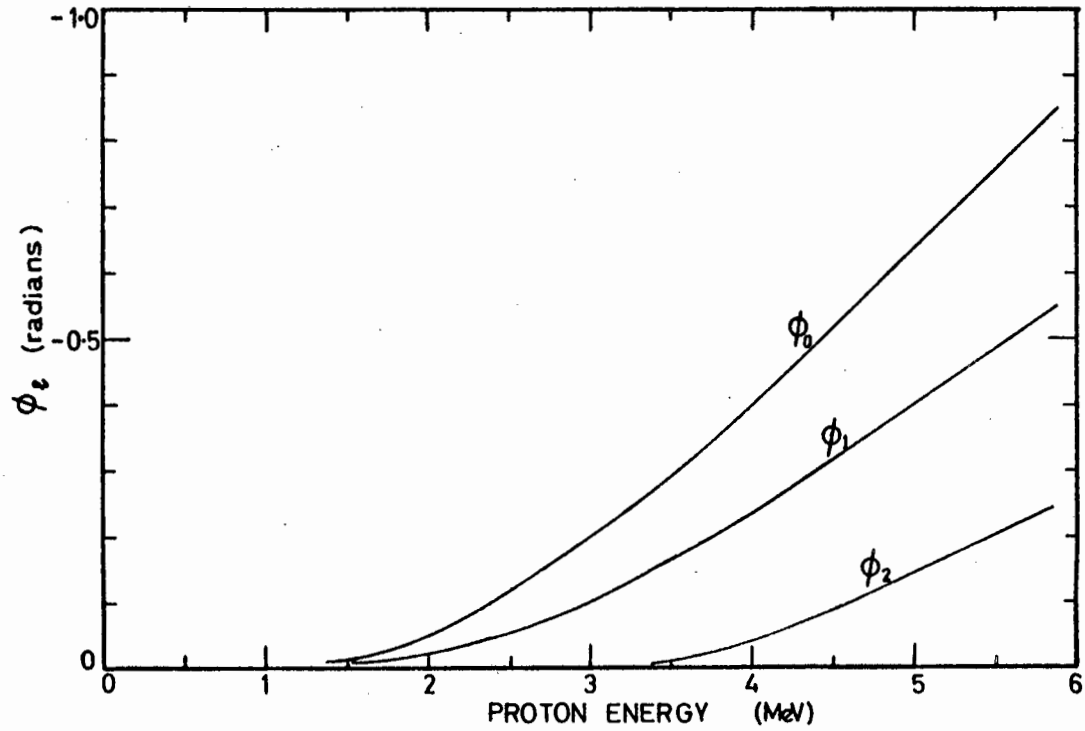

Figure 4.1 Potential scattering phase shift ϕ as a function of energy

4.3 Method of Analysis

4.3.1 General Procedure

The following method was used in extracting level parameters J, π, E, Γ and Γ_p/Γ from the data:

A set of hypothetical resonances was calculated for the proton energy 4 MeV at the four angles used in the experiment. The cross sections were calculated for all values of orbital angular momentum ℓ, up to $\ell = 4$ and, within each ℓ-value, for all allowed values of total angular momentum of the compound nucleus levels. The resonances were assumed to be isolated, ϕ was assumed zero and Γ_p/Γ equal to unity. The results of this calculation are shown in fig. 4.2.

In the first stage of the analysis each resonance observed in the data was compared with the reference set. From this comparison it was usually possible to assign the orbital angular momentum and in some cases, the spin to the level in question. Initial values of the resonance energies E_λ and total widths Γ_λ were estimated by inspection of the elastic and inelastic cross section data. This was done for a number of levels in a given energy region. These parameters were then inserted in eq. 4.20 and a cross section curve was generated over this energy region. The parameters

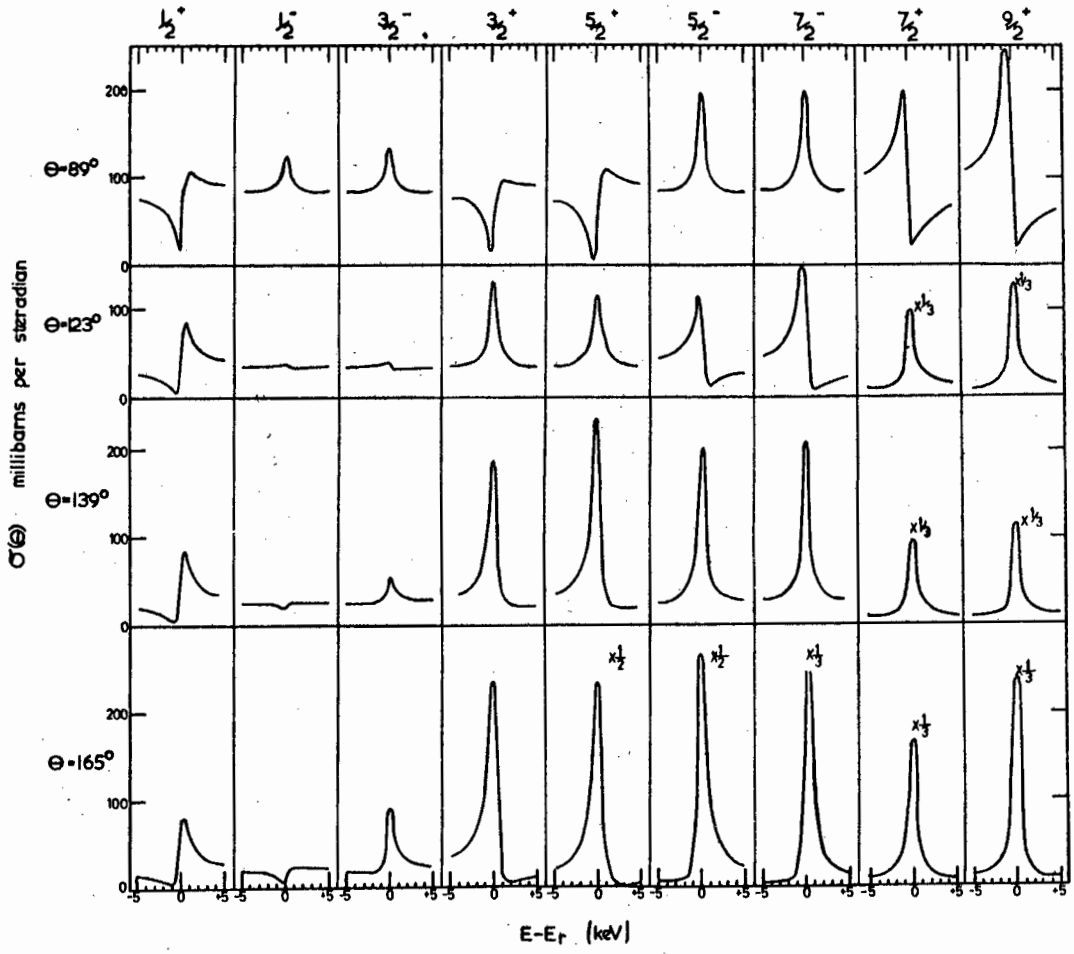

Figure 4.2 Set of theoretical proton elastic scattering cross sections at four angles for an isolated resonance at E_p = 4 MeV with width $\Gamma = \Gamma_p$ = 1 keV

were then adjusted to give the best visual fit to the data at 165° and at the same time to give a qualitative fit to the data at the other angles. The fitting was carried out at 165° since the resonance structure is more clearly defined at this angle and also since the uncertainty in the measured cross section is less at this angle. (see section 3.5). Although most of the resonances were analysed by the method outlined above, there were a number of resonances for which this method proved to be unsuitable. These resonances, numbered 3, 4, 5, 6, 8, 11 and 12 in fig. 3.2, are very narrow ($\lesssim$ 1 keV); their observed widths being largely due to the energy spread in the beam and target thickness. The analysis of these resonances can be carried out by considering the area under the resonances in the elastic as well as inelastic data. However since the inelastic scattering cross sections are relatively low, the statistical errors were found to be relatively large in the present work and thus assignments of widths by this method have large uncertainties. An alternative method of analysis involving only the more accurately measured elastic scattering data was therefore used to analyse the narrow resonances observed in this work. An area analysis on a few of the resonances was, however, carried out as a check on the method and will be discussed in some detail later.

4.3.2 Analysis of Narrow resonances

4.3.2(a) Method A

In this method of analysis the aim is to determine a unique set of parameters (J^{π}, Γ and Γ_p/Γ) for each resonance analysed, in terms of which the cross sections observed at the resonance energy at all four angles can be described. The experimentally observed cross section data are affected by the finite thickness of the target and by fluctuations in the incident beam energy. The calculated cross sections are therefore broadened or convoluted with a Gaussian resolution function before a comparison is made with the experimental data. The full width at half maximum of the resolution function, S is assumed to be given by:

$$S = \sqrt{(\Delta E)^2 + T^2} \qquad 4.21$$

where ΔE is the spread in beam energy and T is the target thickness.

For the purpose of the analysis we ignore the slowly varying "background" component of the cross section (contributed by distant levels, Rutherford scattering and hard sphere scattering) and focus our attention on the component contributed by the resonance under consideration.

For convenience we now introduce three parameters, $\sigma_{T\lambda}$, $\sigma_{R\lambda}$, $\sigma_{R'\lambda}$ which are defined so that after subtraction of the "background" cross section:

1) $\sigma_{T\lambda}$ represents the unbroadened cross section at the resonance energy E_λ, assuming $\Gamma_p/\Gamma = 1$;

2) $\sigma_{R\lambda}$ represents the unbroadened cross section at E_λ, allowing for $\Gamma_p/\Gamma < 1$;

3) $\sigma_{R'\lambda}$ represents the broadened cross section at E_λ , i.e. the value of $\sigma_{R\lambda}$ after convolution with the resolution function (of F.W.H.M., S).

From eqs. 4.6, 4.16 and 4.17 it is seen that for a single isolated level the expressions for the unbroadened cross section $\sigma_{R\lambda}$ has the form:

$$\sigma_{R\lambda} = (\Gamma_p/\Gamma)\ f_1 + (\frac{\Gamma_p}{\Gamma})\ f_2 + f_3 \qquad 4.22$$

where f_1, f_2 and f_3 are all functions of J^π, E_λ and θ.

It is noted that $\sigma_{R\lambda}$ is dependent on Γ only through the ratio Γ_p/Γ . The reason for this is as follows: The dependence of the differential cross section on Γ is introduced through the resonance phase shift β which is given in eq. 4.15 as:

$$\beta = \arctan \frac{\Gamma/2}{E_\lambda - E + \Delta\lambda}$$

If the level shift parameter Δ_λ is assumed to be zero, which appears to be a valid assumption for narrow levels (01 58), then by definition of $\sigma_{R\lambda}$ and $\sigma_{T\lambda}$,

$$\beta = \pi/2$$

Thus $\sigma_{R\lambda}$ and $\sigma_{T\lambda}$ are dependent on Γ only via Γ_p/Γ. We may thus define a factor $R_1 = \frac{\sigma_{R\lambda}}{\sigma_{T\lambda}}$ which is dependent only on Γ_p/Γ and θ for a given E_λ and J^π.

We now introduce a second ratio R_2 defined by $R_2 = \sigma_{R'_\lambda}/\sigma_{R\lambda}$. For given values of S and Γ it is clear that R_2 will be independent of $\sigma_{R\lambda}$. Thus for a fixed value of S, R depends only on Γ.

We may thus write

$$\frac{\sigma_{R'\lambda}}{\sigma_{T\lambda}} = R_1 . R_2 \qquad 4.23$$

where R_1 and R_2 are independent parameters which depend on (Γ_p/Γ, θ) and Γ respectively.

The analysis is now carried out as follows:

(a) Assuming J^π, $\sigma_{T\lambda}(\theta)$ is calculated (eq. 4.20)

(b) From experimental data $\sigma_{o\lambda}$ is obtained. $\sigma_{o\lambda}$ and $\sigma_{R'\lambda}$ are equated; hence $R(\theta) = R_1 . R_2$ is obtained.

(c) From eq. 4.20 R_1 is calculated as a function of Γ_p/Γ for the different angles θ.

(d) Using the convolution subroutine, R_2 is calculated as a function of Γ.

(e) For each value of θ a plot is now constructed of Γ_p/Γ versus Γ as follows:

For a given Γ, R_2 is obtained from (d) and from the value of $R(\theta)$ (b), R_1 is calculated. The value of

Γ_p/Γ corresponding to this value of R_1 is then found from (c).

Thus in general four curves are obtained corresponding to the four angles θ. If the choice of J^π is correct then the curves are concurrent at a point $(\Gamma, \Gamma_p/\Gamma)$ thus completing the solution.

The method may be illustrated with reference to the analysis of resonance number 12 (see fig. 3.2(b) and fig. 4.3) at 4.002 MeV.

From the shape of the resonance at the four angles it is clear that the orbital angular momentum of the protons involved is $\ell = 2$. The initial inspection does not favour either one or the other of the two possible spin values. We assume that $J^\pi = 3/2^+$. The resonance energy is found to be 4.0020 ± 0.0005 MeV.

Using these parameters R_2 was calculated for a series of values of $\Gamma \leq 1$ keV. The results are shown in fig. 4.4(a). Similarly R_1 was calculated (c) at each angle for various values of Γ_p/Γ. These are plotted in fig. 4.4(b). In this particular example the curves corresponding to $\theta = 165^\circ$, 139° and 123° happen to coincide.

The values of $\sigma_{o\lambda}/\sigma_{T\lambda}$ obtained from the data of fig. 4.3 are given in table 4.1. The errors include an uncertainty in the resonance energy. The plots of Γ_p/Γ versus Γ (e) are given in fig. 4.4(c). The shaded areas correspond to errors

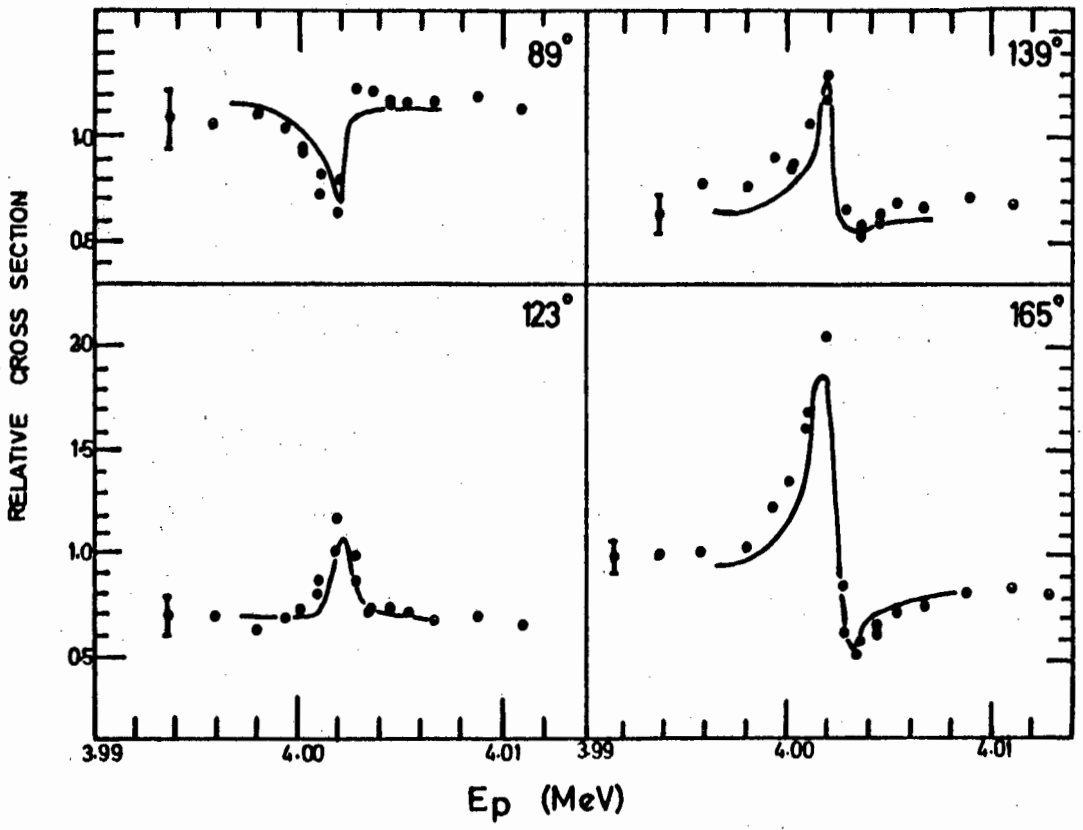

Figure 4.3 Differential proton elastic scattering cross section for resonance 12. Solid curves show cross sections calculated using the parameters determined from analysis by method A

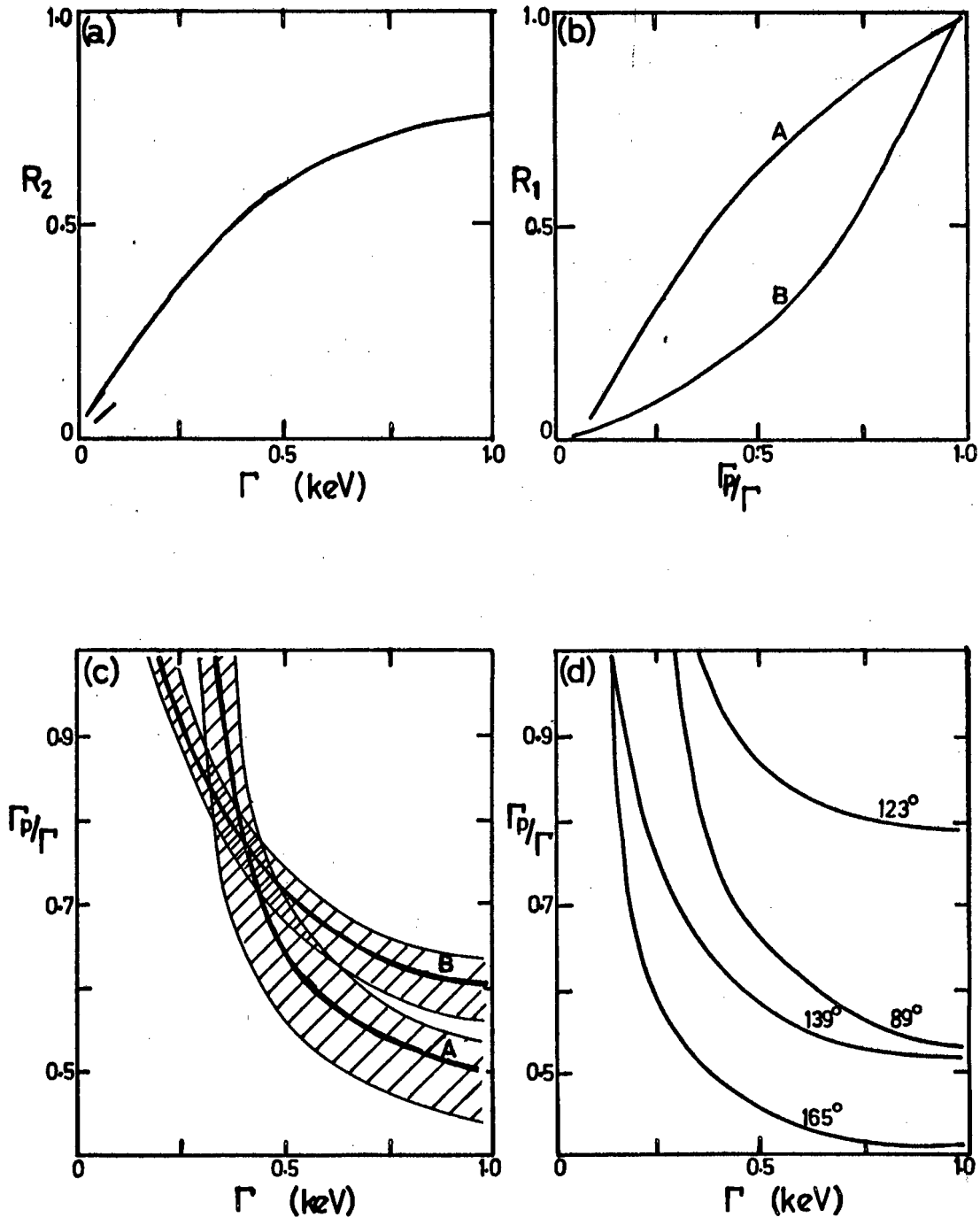

Figure 4.4 Narrow resonance analysis by method A applied to resonance 12. A and B in 4.4(b) and (c) are based on measurements at $\theta = 89^{\circ}$ and $\theta = 123^{\circ}$, 139° and 165° (coinciding) respectively

TABLE 4.1

$\sigma_{o\lambda}/\sigma_{T\lambda}$ observed for resonance 12 (Method A)

θ	89°	123°	139°	165°
$\frac{\sigma_{o\lambda}}{\sigma_{T\lambda}}$	0.44±0.06	0.32±0.04	0.27±0.03	0.32±0.07

TABLE 4.2

Widths for narrow resonance 12 (Method B)

J^π	θ	Γ keV	Γ_p/Γ
$3/2^+$	165°	0.34±0.2	0.65±0.25
	123°	0.29±0.2	0.60±0.18
$5/2^+$	165°	0.32±0.2	0.46±0.21
	123°	0.40±0.25	0.76±0.32

in $\sigma_{o\lambda}$. The value of $\Gamma_{p/\Gamma}$ and Γ at the point of intersection of the curves are:

$$\Gamma = 0.4 \pm 0.15 \text{ keV}$$

and $$\Gamma_{p/\Gamma} = 0.75 \pm 0.14.$$

Figure 4.4(d) shows a corresponding plot if J^{π} is assumed to be $5/2^{+}$. Clearly there are no values of Γ_{p} and $\Gamma_{p/\Gamma}$ which would satisfy the conditions of a unique set of parameters at all four angles.

The parameters determined in the above manner were used to calculate the solid curves in fig. 4.3 The curves are seen to agree reasonably well with the data.

4.3.2(b) Method B (Area analysis).

As a check on the validity of the assignments arrived at by the above method, an area analysis was carried out. The method used has been outlined by Olness et al. (Ol 58). Two independent expressions are derived which contain Γ and $\Gamma_{p/\Gamma}$ explicitly. For a resonance with a symmetric shape, these expressions are:

$$A_{p}(\theta) = \pi\lambda^{2} \left[(ab + b^{2} \Gamma_{p/\Gamma})\Gamma_{p/\Gamma}\right] . \Gamma \qquad 4.24$$

and

$$A'_p = (J + 1/2)4\pi\lambda\!\!\!^{-2}(1 - \Gamma_p/\Gamma)\Gamma_p/\Gamma \quad . \qquad 4.25$$

where $A_p(\theta)$ is the area under the elastic scattering resonance:

$$A_p(\theta) = \int \{\sigma(E,\theta) - \sigma_{NR}(\theta)\}\, d_E \qquad 4.26$$

$\sigma(E,\theta)$ is the observed elastic cross section

and $\sigma_{NR}(\theta)$ is the nonresonance cross section (background)

$\lambda\!\!\!^{-2}a^2$ is the differential cross section off resonance at angle θ.

$\lambda\!\!\!^{-2}(a^2 + b^2)$ is the true (unbroadened) peak differential cross section for $\Gamma_p/\Gamma = 1$ at angle θ.

A'_p is the area under the total inelastic cross section resonance.

Solving eqs. 4.24 and 4.25 we get:

$$\Gamma_p/\Gamma = \frac{4H - ab}{b^2 + 4H} \qquad 4.27$$

where

$$H = (J + 1/2)\frac{A_p(\theta)}{A'_p} \qquad 4.28$$

For the resonance discussed above (res. 12) the area A'_p was obtained from the differential inelastic cross section and the angular distribution of the inelastically scattered protons taken on resonance.

From the equations above values are obtained for Γ and Γ_p/Γ. These are given in table 4.2. From the table

it is seen that the results for $J^{\pi} = 3/2^{+}$ are in reasonable agreement with those found by method A. The results for a $5/2^{+}$ assignment indicate a large difference in the values for different angles and thus that this assignment is inconsistent with the data. These results thus confirm the assignments made by method A.

The resonance assignments for all the observed resonances using the methods discussed in this chapter are discussed in chapter 6. Chapter 5 deals with inelastic scattering studies which were carried out to supplement the elastic scattering assignments.

CHAPTER 5

INELASTIC SCATTERING

Parameters of compound nucleus levels could often be assigned with confidence from the elastic scattering studies. However there were cases where assignments were not possible or ambiguities exist. It was therefore considered worthwhile to undertake some alternative studies of the compound nucleus levels by observing proton inelastic scattering.

Inelastic scattering studies are characterised by a number of useful features. The energy profiles of resonances in the differential inelastic scattering cross section for example are often symmetric since, unlike the elastic scattering case, there is no interference of the resonance and Rutherford term in the scattering amplitude (eq. 4.6). This simplifies the determination of resonance energies and widths. Angular distributions of inelastically scattered protons can be analysed to obtain information about the angular momenta and parities J^{π} of compound nucleus states. Although such an analysis seldom leads directly to unique assignments the results obtained may often be usefully combined with results obtained from the elastic measurements. In this way it may sometimes be possible to confirm, or to remove ambiguities from, assignments based on the elastic data. Information regarding the orbital angular momentum ℓ',

and the channel spin s'†, of the inelastic protons may also be derived from the angular distribution data.

Inelastic scattering studies may be useful in locating analogue states. For example if the target nucleus has a T = o ground state and protons are inelastically scattered to a T = 1 excited state, then elastic scattering from a T = 3/2 analogue state is doubly forbidden by isospin selection rules (see fig. 1.1) whilst the inelastic scattering is only forbidden in the entrance channel. The analogue state should thus be easier to observe in the inelastic scattering reaction. However in the present case this does not apply since the ground state as well as the low lying excited states have T = o. The inelastic scattering work was undertaken solely to supplement the elastic scattering analysis.

5.1 Measurement of inelastic cross sections

The first two excited states of ^{32}S are at 2.237 and 3.78 MeV. In the present work only protons inelastically scattered to the 2.237 MeV state were considered. In the

---

† Channel spin s' refers to Blatt and Biedenharn notation: s' = I ± i where I is the ground state spin of the target nucleus and i the spin of the bombarding particle. This should not be confused with the notation used in chapter 4.

energy region studied, i.e. up to 5.5 MeV, inelastic scattering to the second level will be restricted due to the high penetrabilities and they were thus not considered. This may lead to errors in the inelastic proton partial widths but the elastic scattering partial width will not be affected.

The yield of inelastically scattered protons was measured simultaneously with the elastic scattering yield at 165° in the energy range E_p = 4.0 to 5.5 MeV. In the energy region E_p = 2.8 to 4.0 MeV the yield of inelastically scattered protons was measured only in the region of resonances already determined by the elastic scattering experiment.

The reason for this was that in this region the cross section for inelastic scattering is very low relative to that of elastic scattering and it was thus time-consuming to carry out simultaneous measurements.

The inelastic data were recorded, as in the case of the elastic data, in a multichannel analyser. In early runs pulses in the inelastic peak were selected by a single channel analyser and scaled. Later however, as in the elastic measurements, recording a complete pulse height spectrum over the region of the inelastic peak was preferred since it provided a means of background subtraction. A pulse height spectrum showing the peak due to inelastically scattered protons is shown in figure 5.1.

The yield data were reduced to relative cross sections

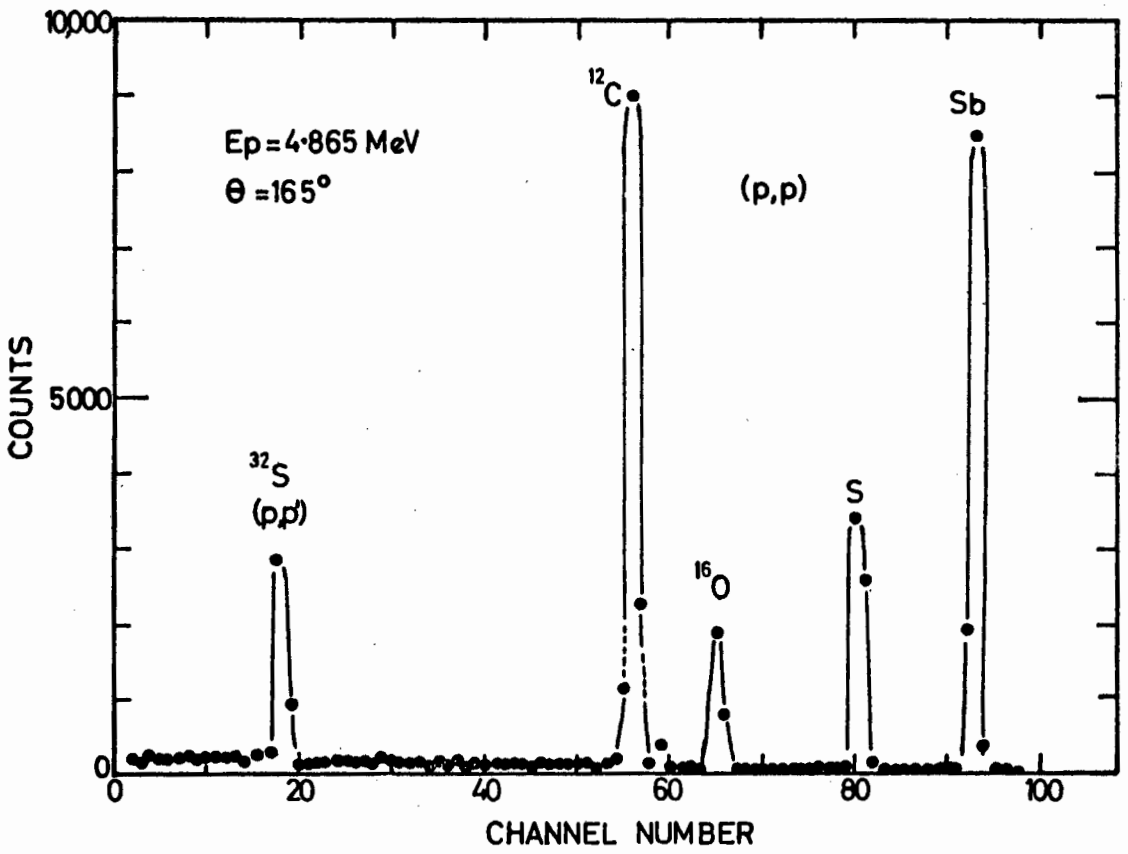

Figure 5.1 Pulse height spectrum showing peak attributed to protons inelastically scattered from ^{32}S

in the same way as described for the elastic scattering data. The intensity of the peak in the pulse height spectrum due to protons inelastically scattered from ^{32}S was typically an order of magnitude lower than that of the elastic peak. Statistical accuracy was consequently much poorer, typically 10 to 20% compared with 0.5 to 5% for the elastic scattering data.

The cross section scale was calibrated using the absolute efficiency of the detector as determined by the normalization of the elastic scattering data. The inelastic scattering differential cross section data at 165° are shown together with the elastic scattering results in figure 3.2.

5.2 Angular distributions

5.2.1 Experimental Procedure

The angular distributions of inelastically scattered protons were measured at incident proton energies corresponding to the resonance maxima in the inelastic cross section data. For this purpose a modified scattering chamber was used. Two detectors were attached to a disc which could be rotated (from outside the chamber) about an axis perpendicular to the beam direction. The centre of the target holder was aligned with the axis and the detectors were placed at an angle of 30° relative to one another with respect to the axis. The second detector was used to check that the angular distribution was

not dependent on some geometrical systematic error which might have arisen due to inaccurate alignment of the detector collimators.

The data were collected in steps of 15° from 60° to 165°. It was not possible to measure the yield at angles less than 60° since the background due to the elastically scattered protons (particularly from the carbon backing) became excessive at forward angles.

Targets used for these measurements were $\sim$ 3-5 keV thick. These thicker targets were used in order to increase the yield and to obtain better counting statistics.

5.2.2 Data Reduction

The data reduction was carried out in the same way as for the elastic scattering data. The background correction was determined by interpolating the background on either side of the peak through the region of the peak and subtracting. The dead-time corrections in these measurements were significant ($\sim$ 2 to 10%) owing to the high count rates of the elastic protons at angles forward of 90° to the beam direction.

The angular distributions were converted to the centre-of-mass system by applying a solid angle intensity correction (Ma 60)

$$\frac{\sigma(\theta)}{\sigma(\psi)} = \frac{\sin^2 \psi}{\sin^2 \theta} \cos(\theta - \psi) \qquad 5.1$$

where ψ and θ refer to angles in the laboratory and centre-of-mass systems respectively.

The centre-of-mass angle, θ, was calculated from

$$\sin \theta = \left[\frac{E_3/(E_1 + Q)}{D} \right]^2 \sin \psi \qquad 5.2$$

where E_3 is the energy of the outgoing proton.

E_1 is the incoming particle and

Q, the energy liberated in the reaction.

$$D = \frac{M_2 M_3}{(M_1 + M_2)(M_3 + M_4)} \left[1 - \frac{M_1}{M_2} \frac{Q}{(E_1 + Q)} \right]$$

and M_1, M_2, M_3 and M_4 refer to the masses of incident particle, target nucleus, scattered particle and final nucleus respectively.

5.2.3 Results

The results of the inelastic scattering angular distribution measurements are shown in figure 5.2. The error bars quoted for the data were determined by the statistical counting errors and the uncertainties introduced by the background subtraction. The results were plotted on a relative scale chosen so that the coefficient of the zero

order Legendre polynomial was ∿1. In order to obtain cross section data, the relative cross section data at 165° should be compared with the peak cross sections of the corresponding inelastic resonances in fig. 3.2.

In order to describe the angular distribution as a sum of Legendre polynomials a least squares fit to the data was carried out using the expression

$$\sigma_p'(\theta) = \sum_L A_L P_L (\cos\theta) \qquad 5.3$$

where $P_L(\cos\theta)$ is the ordinary Legendre Polynomial and A_L are coefficients.

The maximum value of L was limited to $L_{max} = 6$. These fits are shown as solid curves in figure 5.2.

5.2.4 Analysis

Analysis of the data was undertaken in order to determine possible spins and parities of the levels. To achieve this it is necessary to obtain a theoretical expression for the angular distributions in terms of Legendre polynomials. The coefficients may then be compared with the experimental values.

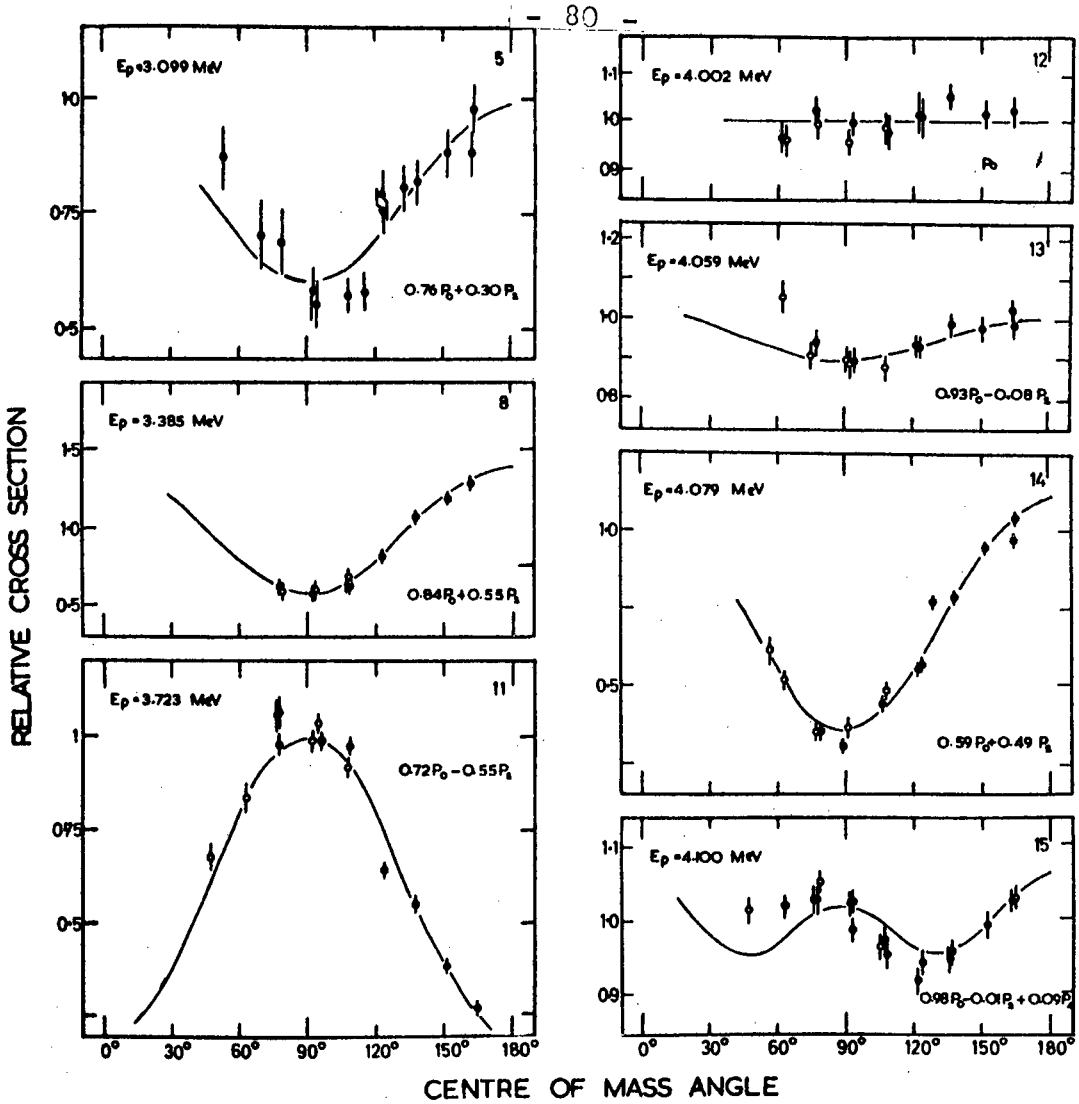

Figure 5.2(a) Inelastic scattering angular distributions measured at various resonance maxima in the cross section data.

Open and closed circles denote measurements made using different detectors.

Solid curves indicate least squares Legendre polynomial fits to the data. The numbers on the right hand side correspond to resonance numbers in fig. 3.2. The coefficients of the Legendre polynomials are given.

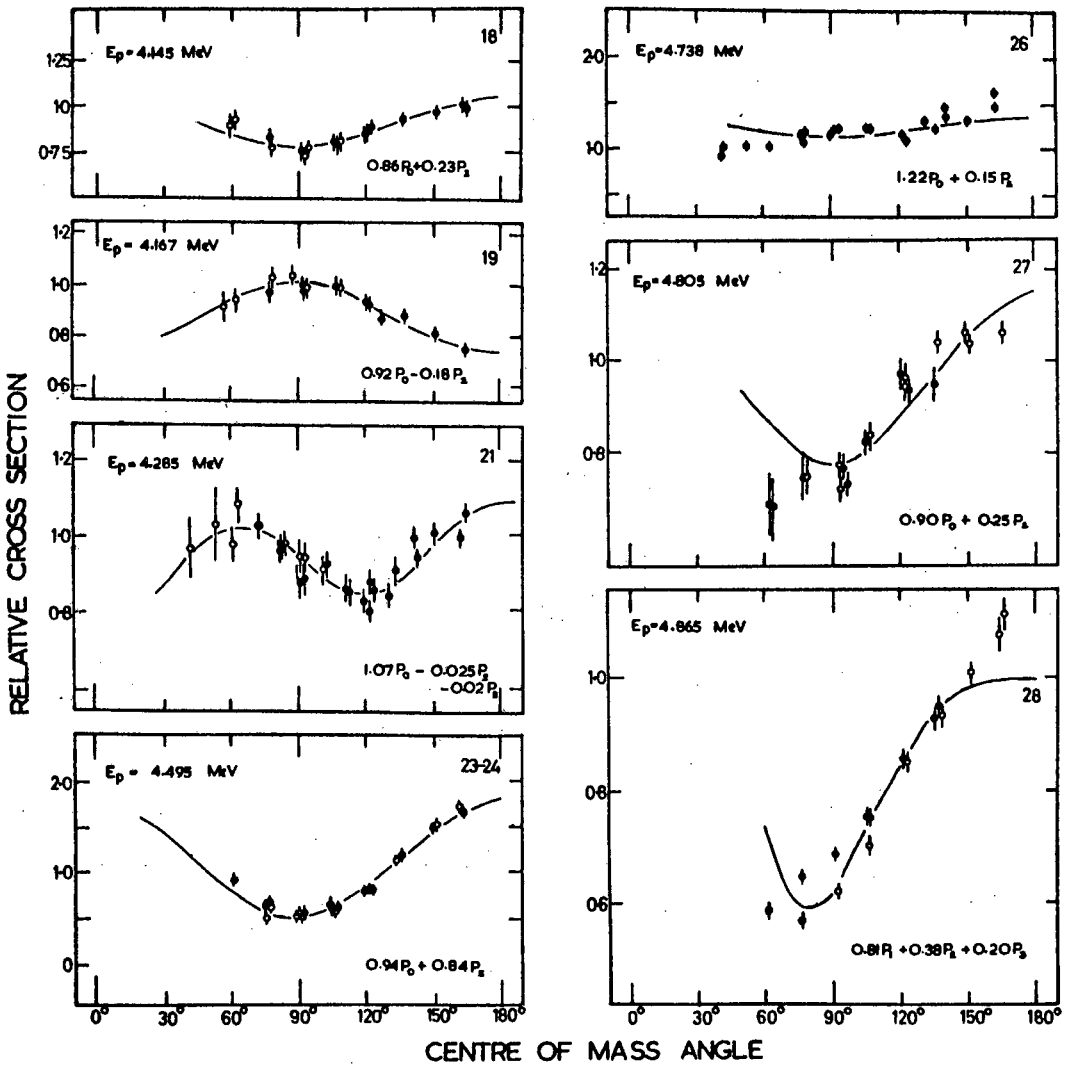

Figure 5.2 (b) Inelastic scattering angular distributions. For details see caption to fig. 5.2(a)

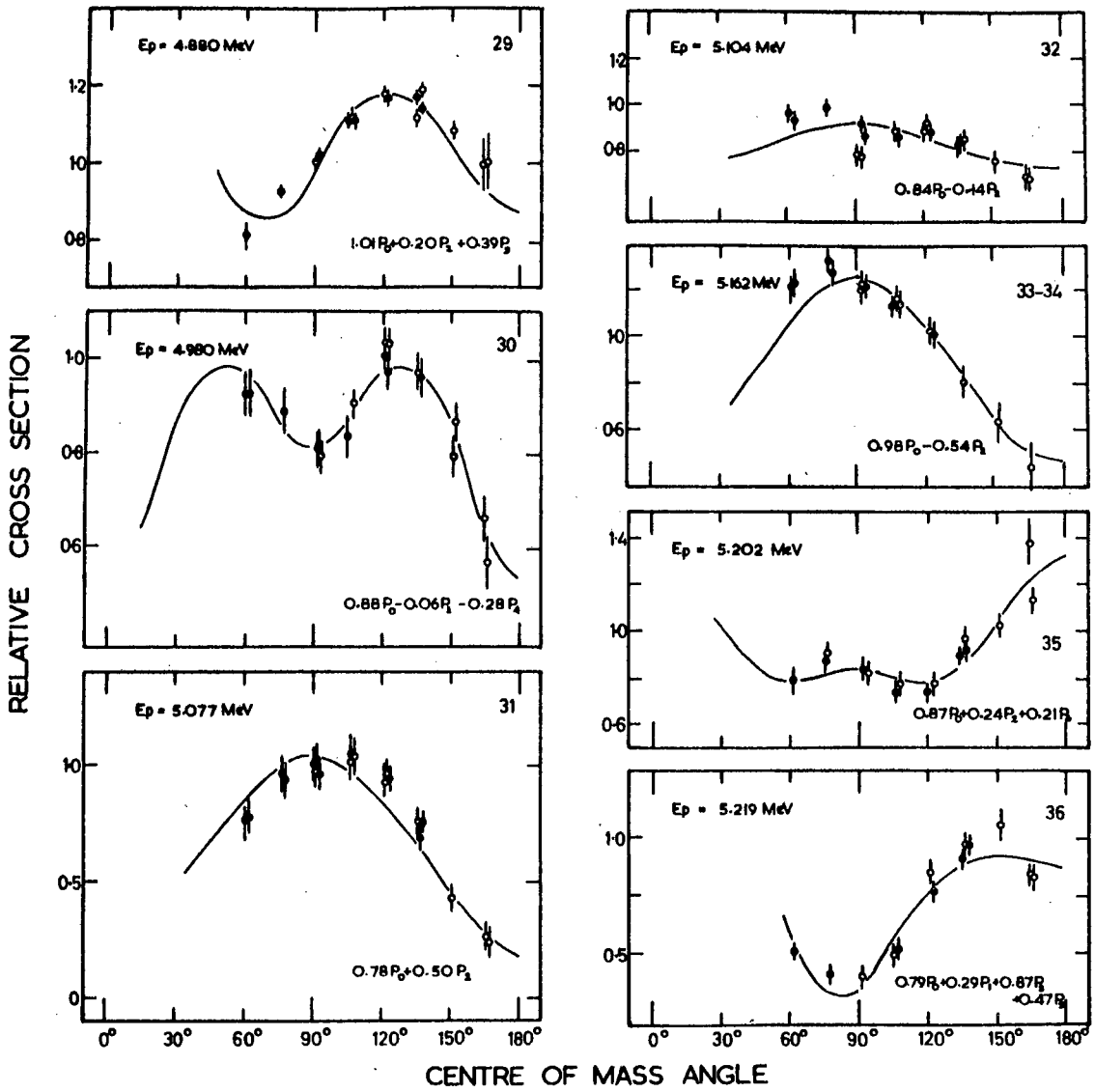

Figure 5.2 (c) Inelastic scattering angular distributions.
For details see caption to fig. 5.2 (a)

5.2.4(a) Theory of inelastic scattering

The theoretical angular distribution is derived from the general form given by Blatt and Biedenharn (Bl 52):

$$d\sigma_{\alpha',\alpha} = \sum_{s=|I-i|}^{I+i} \sum_{s'=|I'-i'|}^{I'+i'} \frac{2s+1}{(2I+1)(2i+1)} d_{\alpha's';\alpha s} \qquad 5.4$$

where

$$d_{\alpha's';\alpha s} = \frac{\lambda^2}{2s+1} \sum_{L=0}^{\infty} B_L(\alpha's',\alpha s) P_L(\cos\theta) d\Omega \qquad 5.5$$

and

$$B_L(\alpha's',\alpha s) = \frac{(-1)^{s'-s}}{4} \sum_{J_1} \sum_{J_2} \sum_{\ell_1} \sum_{\ell_2} \sum_{\ell_1'} \sum_{\ell_2'} C \times Z(\ell_1 J_1 \ell_2 J_2, sL) Z(\ell_1' J_1 \ell_2' J_2, s'L) \qquad 5.6$$

The notation is that of Blatt and Biedenharn.

$Z(\ell J \ell J, sL)$ are the quantities defined by Biedenharn, Blatt and Rose (Bi 52). They contain the products of Racah and Clebsch-Gordon coefficients.

$$C = R.P.\Big[(\delta_{\alpha'\alpha}\delta_{s's}\delta_{\ell_1'\ell_1} - S^{J_1}_{\alpha's'\ell_1,\alpha s\ell_1})(\delta_{\alpha'\alpha}\delta_{s's}\delta_{\ell_2'\ell_2} - S^{J^{2*}}_{\alpha's'\ell_2,\alpha s\ell_2})\Big| \qquad 5.7$$

where $\delta_{\mu\ \mu}$ represent phase shifts

and $S_{\alpha' s' \ell', \alpha \ell s}^{\ J}$ is the scattering matrix.

An expression for C in terms of phase shifts is given by Kashy et al. (Ka 60):

$$C = \frac{\cos(\sigma_{\ell_1}+\phi_{\ell_1}+\sigma_{\ell_1'}+\phi_{\ell_1'}+\beta_1 - \sigma_{\ell_2}-\phi_{\ell_2}-\sigma_{\ell_2'}-\phi_{\ell_2'}-\beta_2)}{\{[(E_1-E)/\Gamma_1/2]^2 + 1\}^{1/2}\{[(E_2-E)/\Gamma_1/2]^2 + 1\}^{1/2}} \qquad 5.8$$

$$\frac{(\Gamma_{\ell_1})^{1/2}(\Gamma_{\ell_1'})^{1/2}(\Gamma_{\ell_2})^{1/2}(\Gamma_{\ell_2'})^{1/2}}{\Gamma_1\ \Gamma_2}$$

where $\sigma_\ell - \sigma_o = \alpha_\ell = \sum_{s=1}^{\ell} \arctan(\eta/s)$

and ϕ_ℓ and β_ℓ are defined as in eqs. 4.9 and 4.15 respectively.

In the special case of inelastic scattering of protons from a spin zero target to a level of known spin a number of simplifications can be made:

1) Since the target spin is zero, the entrance channel spin s can have only one value: $s = \frac{1}{2}$.

2) The spin of the first excited state of ^{32}S is known to be 2^+ (Ol 58).

Thus the exit channel spin can assume only two values:

$$s' = 3/2 \text{ or } s' = 5/2.$$

The barrier penetrability associated with the emission of inelastic protons of orbital angular momentum $\ell' > \ell'_{min}$, the lowest allowed orbital angular momentum, is at least an

order of magnitude higher than for ℓ'_{min} . The assumption is thus made that only ℓ'_{min} contributes to a given resonance scattering process. This assumption is probably not valid for higher energies.

Using these simplifications it is thus seen that the angular distribution for a single isolated resonance, λ, is completely defined by ℓ_λ, J_λ and the mixing parameter, $M_{\lambda s'}$, for the two channel spins s'.

The mixing parameters are defined by

$$M_{\lambda s'} = \frac{\Gamma_{\ell' s'}}{\Gamma_{\lambda p'}} \qquad 5.9$$

where $\Gamma_{\lambda p'}$ is the partial width for decay of the level by inelastic scattering via both s' channels and $\Gamma_{\ell s'}$ is the partial width for decay via channel s', with orbital angular momentum ℓ'.

Rewriting equations 5.4 to 5.8 in terms of the above assumptions, we obtain the following

$$\frac{d\sigma}{d\Omega} = \sum_{s'=3/2}^{5/2} (-1)^{s'-s}\, \pi^2/2 \sum_{L=o}^{L_{max}} \sum_{\lambda} \sum_{\mu} Z(\ell_\lambda J_\lambda \ell_\mu J_\mu ; sL) Z(\ell'_\lambda J_\lambda \ell'_\mu J_\mu ; s'L)$$

$$\times\ C\ P_L(\cos\theta) \qquad 5.10$$

$$\text{where } C = \frac{\cos(\alpha_{\ell\lambda}+\alpha_{\ell\lambda'}-\alpha_{\ell\mu}-\alpha_{\ell\mu'}+\phi_{\ell\lambda}+\phi_{\ell\lambda'}-\phi_{\ell\mu}-\phi_{\ell\mu'}+\beta_\lambda-\beta_\mu)}{\left[\left(\frac{E_\lambda-E}{\Gamma_{\lambda/2}}\right)^2+1\right]^{1/2}\left[\left(\frac{E_\mu-E}{\Gamma_{\mu/2}}\right)^2+1\right]^{1/2}}$$

$$\left[M_{s'\lambda}\cdot M_{s'\mu}\cdot\frac{\Gamma_{\lambda p}\Gamma_{\lambda p'}}{\Gamma_\lambda^2}\cdot\frac{\Gamma_{\mu p}\Gamma_{\mu p'}}{\Gamma_\mu^2}\right]^{1/2} \qquad 5.11$$

where $\lambda, \mu = 1,2\ldots\ldots\ldots$,

and $L_{max} = 2\ \min(l,l',J)$

For a single isolated level λ, μ , the angular distribution on resonance reduces to:

$$\frac{d\sigma}{d\Omega} = \pi^2\frac{\Gamma_p\Gamma_{p'}}{\Gamma^2}\sum_{s'}\sum_{L}(-1)^{s'-s}M_{s'\lambda}Z(\ell J\ell J,sL)Z(\ell' J\ell' J,s'L)P_L(\cos\theta) \qquad 5.12$$

This is the form given by Belote et al. (Be 61).

A programme (see appendix B) was written to compute $\frac{d\sigma}{d\Omega}$ from eqs. 5.10 and 5.11. The number of levels simultaneously handled by the programme was limited to four and special subroutines (Wi 67) were used to calculate the Racah and Clebsch-Gordon coefficients included in the Z-functions.

5.2.4(b) Method of analysis

Using equation 5.12 the theoretical angular distribution for isolated levels with all possible J^π values compatible

with $\ell = 0,1,..4$ were calculated. These are shown in fig. 5.3 for the channel spins s' associated with the lowest allowed ℓ' value. Where the two channel spins s' = 3/2 and 5/2 have the same ℓ', both angular distributions are shown.

The experimental angular distributions for those cases where the contribution from neighbouring levels was small were then compared with the theoretical distributions. In most cases this was done by comparing the ratio of the Legendre polynomial coefficients $\frac{A_2}{A_0}$ for the observed distribution with the calculated values. In cases where both channel spins are allowed, the channel spin mixtures were determined. A unique spin assignment was often not possible as a number of different spin values give the same angular distributions. For example a number of J^π values give an isotropic distribution (see fig. 5.3). However, taken together with the elastic scattering results the possible assignments from the angular distributions may determine a unique spin and parity.

Where interference between resonances was present the possible level parameters assigned by the elastic scattering analysis were used to generate angular distributions for inelastic scattering using eqs. 5.10 and 5.11. Different combinations of channel spin mixtures were tried in an attempt to reproduce the experimental distributions. This was done in an attempt to check that the level parameters assigned from the elastic data were compatible with the inelastic angular

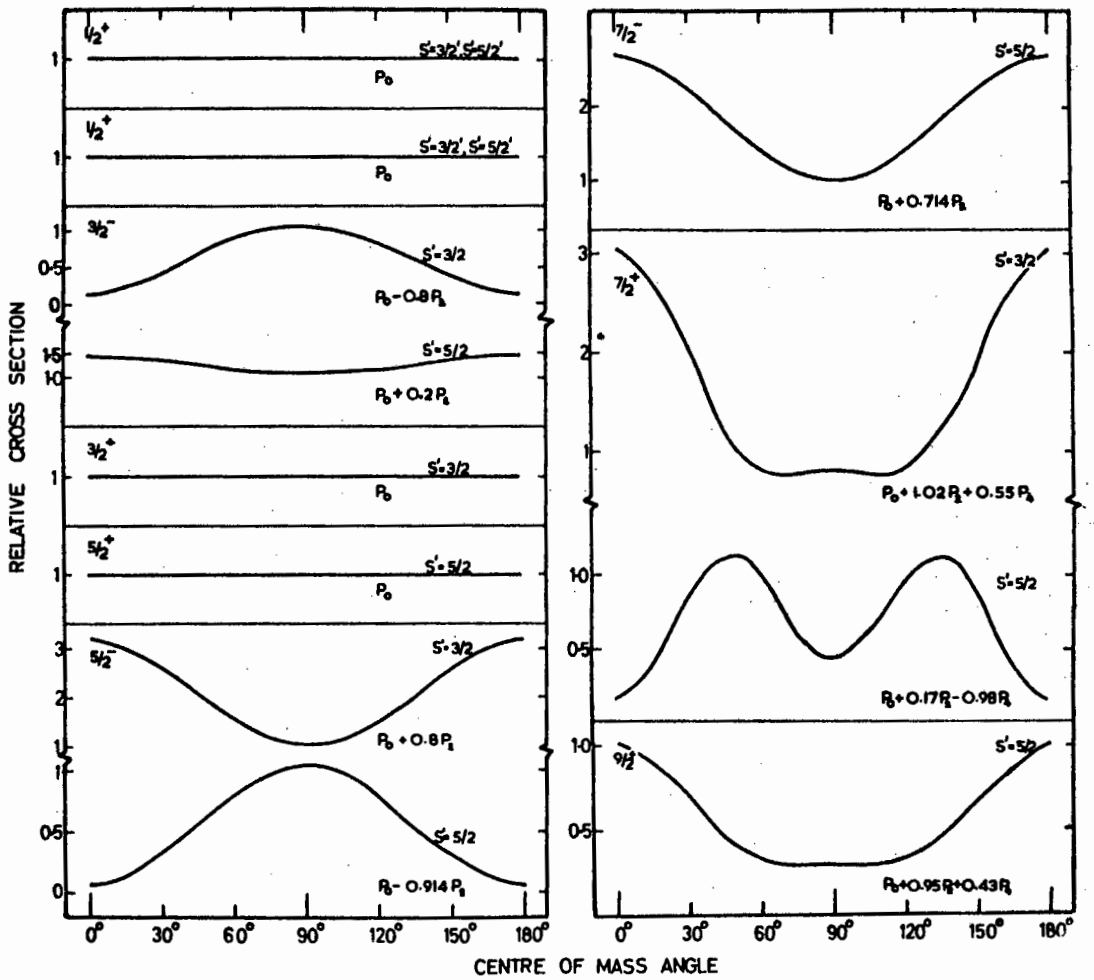

Figure 5.3 Theoretical inelastic scattering angular distributions calculated from eq5.12 for each value of J^{π} for $\ell < 4$ and for channel spin s' compatible with the lowest allowed value of ℓ'

distributions.

The resonance assignments to individual levels are discussed in detail in chapter 6.

5.3 Determination of Γ_p/Γ from inelastic scattering data

Values of Γ_p/Γ obtained in the elastic scattering analysis may be confirmed using inelastic scattering data. The method devised in order to do this is the following:

For an isolated resonance in the excitation function for protons inelastically scattered from ^{32}S the total inelastic cross section is given by the well known Breit-Wigner single level equation:

$$\sigma_{p'} = \frac{\pi\lambda^2}{2} (2J + 1) \frac{\Gamma_p\Gamma_{p'}}{(E - E_\lambda)^2 + (\Gamma/2)^2} \qquad 5.13$$

The total inelastic cross section on resonance thus reduces to

$$\sigma_{p'} = 2\pi\lambda^2 (2J + 1) \frac{\Gamma_p\Gamma_{p'}}{\Gamma^2} \qquad 5.14$$

The total inelastic cross section may be obtained from the differential cross section on resonance and the known angular distribution:

$$\sigma_{p'} = 2\pi \int_0^\pi \sigma(\theta) \sin(\theta)\, d\theta \qquad 5.15$$

If the angular distribution is written in terms of a sum of Legendre polynomials

$$\sigma(\theta) = \sum_{\ell=0}^{4} A_\ell P_\ell (\cos \theta) \qquad 5.16$$

then it is found that eq. 5.15 reduces to:

$$\sigma_{p'} = 4\pi(A_o + A_2) \qquad 5.17$$

From eqs. 5.17 and 5.14 the following is thus obtained:

$$\frac{\Gamma_p \Gamma_{p'}}{\Gamma^2} = \frac{2(A_o + A_2)}{\lambda^2(2J + 1)} \qquad 5.18$$

If, in addition, the assumption is made that the only open channels are those of elastic and inelastic scattering, i.e. that

$$\Gamma = \Gamma_p + \Gamma_{p'} \qquad 5.19$$

then

$$\Gamma_{p/\Gamma} = 0.5 \pm \left(0.5 - \frac{2\Gamma_p \Gamma_{p'}}{\Gamma^2}\right)^{1/2} \qquad 5.20$$

The value of $\Gamma_{p/\Gamma}$ was calculated using eqs. 5.18 and 5.20 for a number of "isolated" resonances. Two possible values are determined by eq. 5.20. The one closest to the result of the elastic scattering analysis was chosen.

A typical example is that of resonance 18 at 4.145 MeV.

The spin assigned was $J = 5/2^-$. The values of the Legendre polynomial coefficients were $A_o = 0.84$. $A_2 = 0.23$. Using eq. 5.20 the values of Γ_p/Γ are found to be 0.89 and 0.11. From the elastic scattering the value of Γ_p/Γ was found to be: 0.75. If the value 0.11 is discarded then the other, 0.89 is seen to be in fair agreement with the elastic data.

The values of Γ_p/Γ from both elastic and inelastic scattering measurements are given together with the other assignments in table 6.1. The values of Γ_p/Γ determined by the two methods are seen to agree to within about 20% in most cases.

CHAPTER 6

RESULTS OF RESONANCE ANALYSIS

The methods of analysis described in chapters 4 and 5 have been used to assign level parameters to the resonances observed in the cross section data. The results of the analysis (i.e. the assignments of spins, parities, energies and widths) are summarised in table 6.1. The cross sections calculated using these parameters are shown as solid curves in fig. 3.2 This chapter is devoted to discussion and commentary concerning the individual resonance analysis. In the discussion the resonances are referred to by the numbers assigned to them in fig. 3.2† as well as their resonance energies.

In the lower energy region a number of broad resonances were observed. Since the assignments to the narrow levels in this region depend on the assignments to the broad levels, the broad levels (i.e. resonances 2, 9 and 10) are discussed first. The remaining resonances are then discussed in order of increasing energy.

---

† See also foldout inside back cover.

TABLE 6.1 RESULTS OF ANALYSIS OF RESONANCES FOR PROTON SCATTERING FROM ^{32}S

Resonance Number	E_λ (MeV)	$E_x(^{33}Cl)$ (MeV)	ℓ	J^π	Γ (keV)	Γ_p/Γ from $^{32}(p,p)$	Γ_p/Γ from $^{32}(p,p')$	$\theta^2_{p_2}$ $\times 10^2$	$\theta^2_{p'}$ $\times 10^2$
1	2.811±0.002	5.016	1	$3/2^-$	6.00±1.0	1		0.72	∿50
2	2.910±0.020	5.112	1	$1/2^-$	400±40	∿1		47.8	
3	2.904±0.002	5.106	3	$(5/2)^-$	<.10	∿1		0.24	
4	2.920±0.002	5.112	2	$3/2^+$	0.25±0.10	∿1		0.076	
5	3.099±0.001	5.295	3	$5/2^-$	0.32±0.15	0.48±0.12		0.21	9.49
6	3.200±0.002	5.393	2	$5/2^+$	0.20±0.10	0.75±0.2		0.035	0.36
7	3.273±0.003	5.464	0	$1/2^+$	25±4	1		1.30	
8	3.385±0.002	5.572	3	$7/2^-$	1.5±0.2	0.25±0.15		0.45	3.63
9	3.500±0.010	5.684	1	$3/2^-$	125±15	1		7.90	
10	3.575±0.005	5.757	0	$1/2^+$	20±5	1		0.88	
11	3.723±0.002	5.900	3	$5/2^-$	1.4±0.02	0.35±0.10		0.31	2.54
12	4.002±0.002	6.170	2	$3/2^+$	0.4±0.15	0.77±0.12		0.034	0.025
13	4.054±0.002	6.221	2	$(5/2)^+$	4.5±1.0	0.8	0.65	0.40	0.25
14	4.079±0.002	6.245	3		12±3	0.22		1.03	7.50
15	4.100±0.002	6.266	3	$(5/2)^-$	≤2.0	0.2		0.16	1.44
16	4.106±0.004	6.271	1	$3/2^-$	26±4	0.9		0.92	2.15
17	4.112±0.002	6.277	0	$1/2^+$	1.0±0.3	1		0.031	-
18	4.145±0.002	6.309	3	$5/2^-$	4±1	0.75	0.89	1.08	0.56
19	4.167±0.004	6.331	(2)	$(3/2^+)$	16±2	0.15±0.1	0.25	0.17	2.29
20	4.259±0.010	6.420	1	$(1/2)^-$	65±10	1		2.33	-
21	4.285±0.002	6.445	(3)		≤2.0	0.2±0.15	0.2	0.13	0.46
22	4.440±0.003	6.595							
23	4.495±0.002	6.649	2	$(3/2)^+$	4.0±1.0	0.5		0.14	0.24
24	4.496±0.002	6.650	3	$(7/2)^-$	12±2	0.3		1.01	1.78
25	4.570±0.002	6.721	2	$(5/2)^+$	7±1	0.9		0.45	0.08
26	4.738±0.004	6.884	2	$(5/2)^+$	25±3	0.95		1.62	0.088
27	4.805±0.005	6.949	3	$(7/2)^-$	22±4	0.09		0.42	3.19
28	4.865±0.003	7.008	2	$5/2^+$	14±2	0.35		0.32	0.73
29	4.879±0.003	7.021	3	$(7/2)^-$	6±1	0.15		0.17	0.65
30	4.980±0.004	7.119	2	$5/2^+$	15±2	0.8	0.83	0.77	0.23
31	5.077±0.004	7.213	3	$5/2^-$	16±2	0.1		0.26	1.37
32	5.104±0.002	7.239	2	$(3/2^+)$	2±0.5	0.8	0.65	0.09	0.25
33	(5.170±0.015)	7.303	(0)	$(1/2^+)$	(45)	0.5			
34	(5.185±0.015)	7.318	(2)	$(3/2^+)$	(10)	0.2			
35	5.201±0.003	7.334	4	$9/2^+$	3±1.0	0.6		1.58	0.43
36	5.224±0.004	7.356	2	$(3/2)^+$	4±2	0.15		0.033	0.203
37	5.304±0.003	7.433	2	$(5/2)^+$	10±3	0.75		0.39	0.129
38	5.367±0.008	7.494	1	$3/2^-$	60±10	0.6		0.092	0.191
39	5.376±0.003	7.503	4	$9/2^+$	1.5±5	0.5		0.54	0.183
40	5.390±0.005	7.517	0	$1/2^+$	12±4	0.85		0.22	0.86

6.1 Discussion of assignments

Resonance 2. $E_\lambda = 2.910 \pm 0.020$ MeV

This resonance is observed in the data at 165° extending from 2.9 to 3.1 MeV. The broad peak preceded by a strong dip at 165° indicates that the orbital angular momentum involved is $\ell = 1$ (see fig. 4.2)

Two spin assignments are possible since $J = \ell \pm 1/2$, i.e. $J = 1/2$ or $3/2$. Of these only $1/2^-$ is compatible with the data since the cross sections calculated for $3/2^-$ are too high. An initial estimate gave the width as 350 keV and the energy $E_p = 2.890$ MeV. These parameters were inserted in eq. 4.20 and cross section curves were generated in the region of the resonance. The parameters were then adjusted to give the best fit to the data at 165°. The final values of the parameters found in this way are listed in table 6.1.

Additional evidence in support of the assignments for this resonance was obtained when the narrow resonances 3, 4, 5 and 6 were analysed. Resonance 2, being very broad, overlaps all of these narrow resonances and their shapes are strongly affected by interference with resonance 2. The good fits achieved for these resonances were not possible if the assignments to resonance 2 were altered significantly.

Resonances 9 and 10 E_λ = 3.500, 3.575 MeV

The data suggests that at least two levels contribute to the cross section in the E_p = 3.4 to 3.6 MeV region. The deep dip at E_p = 3.585 MeV, θ = 89° indicates that one of these levels must have ℓ = o or 2, since these are the only possible assignments of ℓ which result in a dip at 89° (see fig. 4.2). The ℓ = 2 possibility is ruled out since this would also require a dip at ∿ 3.6 MeV, θ = 165°. Combinations of $J^\pi = 1/2^+$ for resonance 10 with $J^\pi = 1/2^-$ or $3/2^-$ for resonance 9 were tested and it was found that the combination of $J^\pi = 1/2^+$ and $3/2^-$ for the two levels together with the respective widths and energies given in table 6.1 gave a reasonable fit to the data at all angles.

It was however not possible to obtain satisfactory fits to the data in the region on the high energy side of these resonances. It is thought that this might be a consequence of the fact that no account was taken of the energy dependence of the total width in eq. 4.20. Although no quantitative estimate was made of the effect of the assumption of the energy independence of the widths, it is likely that this might lead to a discrepancy in fitting broad levels (Me 63).

Resonance 1. E_λ = 2.810 MeV.

The shape of this resonance at all angles is inconsistent with any of the single level shapes in fig. 4.2. This suggests that interference effects due to resonance 2 should be taken into account. When doing this it is found that $J^\pi = 3/2^-$ gives a good fit to the resonance shapes at all angles. No other assignment gives even a qualitative fit to the resonance shapes.

No inelastic scattering has been observed for this resonance in the present work. However Olness et al. (Ol 58) report an inelastic scattering width $\Gamma'_p \sim 0.0015$ keV.

Resonance 3. E_λ = 2.904 MeV.

Since no inelastically scattered protons were observed in the pulse height spectra at the resonance energy, it was assumed that $\Gamma_p/\Gamma = 1$. The resonance is not observed at $\theta = 89^\circ$ or 123° but is quite strong at $\theta = 165^\circ$. This can be explained (see fig. 4.2) by assigning $J^\pi = 5/2^-$ or $7/2^-$ (i.e. $\ell = 3$). If $\Gamma_p/\Gamma = 1$, then $R_l = 1$ and $\sigma_{R\lambda}/\sigma_{T\lambda}$ is thus independent of θ. We would thus expect that the ratio $\sigma_{o\lambda}/\sigma_{T\lambda}$ measured experimentally will be equal at the two angles at which the resonance was observed.

The measured values are given in table 6.2.

TABLE 6.2 Observed values of $\sigma_{o\lambda}/\sigma_{T\lambda}$ for resonance 3.

J^π	$\sigma_{o\lambda}/\sigma_{T\lambda}$	
	$\theta = 139^\circ$	$\theta = 165^\circ$
$5/2^-$	0.07 ± 0.02	0.07 ± 0.03
$7/2^-$	0.17 ± 0.07	0.05 ± 0.02

Thus an assignment of $J^\pi = 5/2^-$ is strongly indicated. However, since this resonance is very close to the broad resonance 2, and the cross section could only be measured at two angles, this assignment is accepted only as tentative. The width Γ, given in table 6.1, is calculated assuming $\Gamma_p/\Gamma = 1$, and $J^\pi = 5/2^-$.

Resonance 4. $E_\lambda = 2.920$ MeV.

In this case again no inelastic scattering was observed, hence Γ_p/Γ was assumed equal to unity. The dip in the cross section at $\theta = 89^\circ$ suggests that the orbital angular momentum involved is $\ell = 2$ although the same effect could be produced by interference with resonance 2. Resonances were generated at this energy for all possible spins and parities, with the interference from resonance 2 taken into account.

It was found that only a $3/2^+$ assignment gave a reasonable qualitative fit at all angles. The analysis then proceeded as for resonance 12 (see section 4.3.2(a)) and it was confirmed that the only possible spin-parity was $J^\pi = 3/2^+$.

Resonance 5. $E_\lambda = 3.099$ MeV.

A comparison with the single level shapes in fig. 4.2 shows that no single level shape can explain the cross section at all angles; the effects of interference with resonance 2 must thus be taken into consideration. All spins and parities for $\ell = 2$ and 3 were tried. The only assignment which reproduces the experimental shape at all four angles is $J^\pi = 5/2^-$. The widths were again assigned using method A described in section 4.3.2(a). Assignments were also made using method B and although the errors were large, the results were in fair agreement with those of method A.

The angular distribution of the inelastic protons on resonance is shown in fig. 5.2(a). The Legendre polynomial fit to this distribution is well matched by the theoretical expression (eq. 5.12) with $J^\pi = 5/2^-$. If there is no interference from other inelastic scattering resonances in the vicinity, which appears to be the case, then this assignment is unique since no other spin-parity assignment will give a distribution that matches the Legendre polynomial fit. The assignment of J^π from the elastic scattering analysis is thus

confirmed. The channel spin mixture necessary to match the Legendre polynomial fit is $M_{3/2} = 0.76$, $M_{5/2} = 0.24$.

Resonance 6. $E_\lambda = 3.200$ MeV.

The analysis was carried out by method A only (section 4.3.2(a)). The spin-parity and partial width assignments are given in table 6.1. The inelastic scattering cross section was small and consequently no angular distribution was carried out.

Resonance 7. $E_\lambda = 3.273$ MeV.

From the shape at all angles we confidently assign the spin parity of this level $J^\pi = 1/2^+$.

Resonance 8. $E_\lambda = 3.385$ MeV.

Interference with the broad levels in the vicinity helped in assigning the spin-parity of this level as $7/2^-$. This was the only assignment which would fit the data even qualitatively at all four angles. Widths were assigned by method A.

The inelastic scattering angular distribution measured is compatible with $5/2^-$ or $7/2^-$ assignments. For $7/2^-$ the channel spin mixture needed to match the Legendre polynomial fit to the distribution is $M_{3/2} = 0$, $M_{5/2} = 1$. The lowest ℓ' value for each channel is: $\ell' = 3$ for the $s' = 3/2$ channel

and $\ell' = 1$ for the $s' = 5/2$ channel. Thus the channel spin mixture given above is in agreement with the assumption that only the lowest ℓ' value is involved in the decay of a level in this energy region.

Resonances 9 and 10. $E_\lambda = 3.500$ and 3.575 MeV.

These resonances were discussed prior to Resonance 1.

Resonance 11. $E_\lambda = 3.723$ MeV.

This resonance was analysed in a similar way to the other narrow resonances. A good fit to the shape is found for $J^\pi = 5/2^-$, and because of interference with the broad levels 9 and 10, this is again found to be unique. The inelastic scattering angular distribution is compatible with either $J^\pi = 3/2^-$ or $5/2^-$. The $3/2^-$ possibility can however definitely be ruled out on the basis of the elastic scattering results. The channel spin mixture required to match the Legendre polynomial fit to the angular distribution for $J^\pi = 5/2^-$ is $M_{3/2} = 0.11$, $M_{5/2} = 0.89$.

Resonance 12. $E_\lambda = 4.002$ MeV.

The analysis of this resonance was discussed in detail in section 4.3.2. This analysis led to an assignment of $J^\pi = 3/2^+$.

The angular distribution of the inelastically scattered

Resonances 14, 15, 16 and 17. E_λ = 4.079, 4.100, 4.106 and 4.112 MeV.

The region E_p = 4.07 to 4.12 is difficult to analyse because of the fact that the level density is high. Since shapes of both resonances 14 and 15 indicate ℓ = 3 assignments the single level assumption is probably not a good approximation in this region.

Resonance 17 (E_p = 4.112) is narrow and would probably best be analysed by the methods used in section 4.3.2. However, since the "background" cross section was somewhat uncertain, this was not attempted. From the shape at all angles it is clear that only a $1/2^+$ spin-parity would give even a qualitative fit at all four angles.

Resonance 16 was not immediately apparent from the data. The dip between resonances 14 and 15 could not be understood by assignments to these two resonances only. Also the flat region on the low energy side of 17 could not be explained by interference between 15 and 17. The only way of explaining these features was by assuming a resonance with ℓ = 1 at 4.106 MeV. Both spin possibilities were attempted but it was found that for $1/2^-$ a deep interference dip resulted on the low energy side of 17. In addition, the region near resonance 15 was not well reproduced. With a $3/2^-$ assignment a good fit resulted at 165°.

In the case of resonance 14 there is no preference for

either a $5/2^-$ or a $7/2^-$ assignment. Resonance 15 on the other hand is better fit at 165° by assuming a $5/2^-$ assignment. However due to the uncertainty in the assumptions of the formalism already mentioned, the assignment is considered as tentative.

The inelastic cross section data in this region show two resonances one corresponding to resonance 14 and the other to resonance 15 and 16. The angular distribution taken on resonance 14 is compatible with either a $5/2^-$ or $7/2^-$ spin-parity assignment. The other shows strong interference effects. An attempt to match the least squares fit proved unsuccessful. This was again thought to be due to the fact that the single level assumption in the formalism was not valid in this region.

Resonance 18. $E_\lambda = 4.145$ MeV.

The symmetric peak at 89° and the large cross section at 165° strongly indicate that the orbital angular momentum involved is $\ell = 3$. Although the large peak cross section at first indicated a $J^\pi = 7/2^-$ assignment, other considerations established the spin-parity as $5/2^-$. The inelastic scattering angular distribution was found to have a small $P_2(\cos\theta)$ component and this could not be explained by $J^\pi = 7/2^-$ even after taking into account the interference from nearby levels. A $J^\pi = 5/2^-$ assignment on the other hand gives a better match

to the least squares fit to the data. With this assignment it was also found that a better fit to the data at the other angles resulted. Furthermore, attempts to fit resonance 19 proved to be impossible for a $J^{\pi} = 7/2^{-}$ assignment to resonance 18 whereas with $J^{\pi} = 5/2^{-}$ a good fit was possible. This assignment is thus unambiguous.

Resonance 19. $E_{\lambda} = 4.167$ MeV.

This resonance is strong in the inelastic cross section curve but is only observed as a "shoulder" in the elastic scattering data at 165°, and not at all at the other angles. The negative $P_2(\cos\theta)$ component in the Legendre polynomial fit to the inelastic angular distribution can be matched by a $3/2^{+}$, $3/2^{-}$ or $5/2^{-}$ assignment. Attempts to fit the elastic data in this region, using the energy and widths indicated by the inelastic data, showed that only the $3/2^{+}$ possibility gives a qualitative correct result. This assignment was thus tentatively adopted.

Resonance 20. $E_{\lambda} = 4.259 \pm 0.010$ MeV.

The deep dip at $\theta = 165^{\circ}$ and $E_p = 4.250$ MeV and subsequent plateau region indicate a broad $\ell = 1$ resonance. Although $J^{\pi} = 1/2^{-}$ gives a slightly better fit, $J^{\pi} = 3/2^{-}$ cannot be ruled out. Thus a tentative $1/2^{-}$ assignment is made.

Resonance 21. E_λ = 4.285 MeV.

This resonance is observed only at 165° in the elastic scattering data. The fact that it is not observed at the other angles indicates that the relative magnitude of the resonance at 165° is much greater than at the other angles. This would be compatible with $\ell = 3$. The inelastic scattering angular distribution has a $P_3(\cos\theta)$ component which indicates interference, possibly with the broad resonance 20. It was not possible however to match this distribution. Thus no assignment could be made in this case.

Resonance 22. E_λ = 4.440 MeV.

This resonance is too weak to be subjected to any form of analysis.

Resonance 23, 24. E_λ = 4.495, 4.496 MeV.

There are a number of indications that this is in fact a doublet. Firstly, the large width at 165° compared with that at 89°. Secondly, the shape at all angles cannot be reproduced by a single level shape, and thirdly, the inelastic cross section on resonance is too high to be explained by a single level. An investigation of the shapes at 165° and 89° limits the possible ℓ assignments to $\ell = 2$ and $\ell = 3$. All combinations of the corresponding spin-parity assignments were tried and it was found that the only combination that did not

give a large interference dip at 165° was $3/2^+$, $7/2^-$. The final shape at all angles was found to be sensitive to both the energy separation and the widths of these resonances. The parameters which give the best fit to the 165° data are found to give a reasonable fit at 139° and 89° as well but a rather poor fit at 123°. (A systematic least squares analysis using a fast computer would be required to vary all the parameters until a good fit was achieved at all angles. The present method of analysis proved to be too time consuming to improve the fits any further).

The angular distribution of the inelastically scattered protons can be matched by the above assignments for $\theta_{cm} > 90°$. The assignments are thus probably correct but they are assumed tentative owing to the poor fit at 123°.

Resonances 25, 26. E_λ = 4.570, 4.738 MeV.

For both these resonances the shapes at all angles indicate $\ell = 2$. In both cases $J^\pi = 5/2^+$ gives a slightly better fit than $J^\pi = 3/2^+$, but the latter cannot be ruled out. The $J^\pi = 5/2^+$ assignments are thus only tentatively adopted.

In the case of resonance 26 the inelastic scattering angular distribution is almost isotropic. The slight deviation from isotropy can be explained by interference from res. 27. Thus J^π $3/2^+$ as well as $5/2^+$ are possible.

Resonance 27. E_λ = 4.805 MeV.

This resonance is observed in the inelastic data as well as the elastic data at 165°. From the inelastic data an estimate of the energy and width of the resonance is obtained. An ℓ = 3 assignment gives a qualitative fit at 165°. Although there is a slight preference for $J^\pi = 7/2^-$ this can only be considered very tentative. The unsymmetric shape observed in the inelastic scattering angular distribution can be attributed to interference with levels 26, 28 and 29. The distribution for $\theta_{cm} > 90^\circ$ can be matched for either a $5/2^-$ or a $7/2^-$ assignment.

Resonances 28 and 29. E_λ = 4.865, 4.879 MeV.

From the elastic scattering data at $\theta = 165^\circ$ and the inelastic data it is clear that this anomaly is due to two resonances. The dip at 89° indicates that 28 is formed by protons with ℓ = 2 or 0. The deep interference dip at 165° however can only be explained by the ℓ = 2 assignment. The shape of resonance 29 indicates ℓ = 3. All combinations of the corresponding spins and parities were tried and it was found that only a $5/2^+$ assignment to 28 would reproduce the data at 165°. The peak following this dip could be explained by either a $5/2^-$ or a $7/2^-$ with a slight preference for the latter. The good fit at all angles confirms the assignments to these two resonances. Angular distributions

of the inelastic scattering show strong interference effects and it was not possible to match them with any of the assignments attempted. This was thought to be due, firstly, to the high density of levels in this region and secondly to the fact that in this energy range the assumption that only the lowest possible ℓ' value is involved in the decay of the level, is probably not valid. This will be shown in the discussion of resonance 30.

Resonance 30. $E_\lambda = 4.980$ MeV.

The elastic scattering data limits the spin parity assignments to $3/2^+$ and $5/2^+$. The inelastic scattering angular distribution is fit by a $5/2^+$ assignment with channel spin mixture $M_{3/2} = 0.6$ and $M_{5/2} = 0.4$. For the channel with $s' = 3/2$ the lowest allowed orbital momentum of the inelastic proton is $\ell' = 2$, whilst for the channel with $s' = 5/2$, it is $\ell' = 0$. Thus according to our assumption that only the lowest possible ℓ' value is allowed, we expect $M_{5/2} = 1$ and $M_{3/2} = 0$. That this is not so indicates that the assumption, although probably valid in the lower energy region is not valid at these higher energies. A $3/2^+$ assignment is incompatible with the inelastic scattering data.

Resonance 31. E_λ = 5.077 MeV.

The symmetric shape at 165° and relative magnitude leaves little doubt that the orbital angular momentum involved is $\ell = 3$. The inelastic scattering angular distribution contains a large negative $P_2(\cos\theta)$ term. This is easily matched for $J^\pi = 5/2^-$ and this assignment is thus unambiguous.

Resonance 32. E_λ = 5.104 MeV.

This resonance has the familiar $\ell = 2$ shape at all angles. It is found that $J^\pi = 3/2^+$ gives a better fit than $J^\pi = 5/2^+$ to the magnitudes of the resonances at all angles and this assignment is thus tentatively adopted. The inelastic scattering angular distribution is again almost isotropic so that no further evidence for either of the two J^π values could be obtained from it.

Resonances 33 and 34. E_λ = approx. 5.175 MeV.

This region contains at least two resonances. One of these must have ℓ = o or 2 to explain the dip in the cross section at $\theta = 89°$. A broad $\ell = 2$ resonance which would fit the data at $\theta = 89°$ is completely incompatible with the $\theta = 165°$ data. A possible assignment is indicated in table 6.1 and is used to generate the curve shown in fig. 3.2.

The fits at $\theta = 123^{\circ}$ and 139° are very poor. The possibility of a third resonance being present in this region is not ruled out. No other combination of two resonances gave even a qualitative fit to the data at $\theta = 165^{\circ}$.

Resonance 35. $E_{\lambda} = 5.201$ MeV.

The shape at $\theta = 89^{\circ}$ immediately suggests an $\ell = 4$ assignment. With $J^{\pi} = 7/2^{+}$ the fit at this angle is qualitatively correct but displaced along the energy axis with respect to the fit at $\theta = 165^{\circ}$. A $J^{\pi} = 9/2^{+}$ assignment on the other hand, gives a reasonable fit to the data at 89° and also predicts the correct relative magnitudes at the other angles.

The inelastic scattering angular distribution also favours an $\ell = 4$ assignment but both spin values would match the least squares fit to the distribtuions.

Resonance 36. $E_{\lambda} = 5.224$ MeV.

The inelastic scattering cross section is again useful in this case in estimating the width and energy of this resonance. All possible spin values for $\ell = 2$ and 3 were tried and the best fit to the data at 165° was obtained for $J^{\pi} = 3/2^{+}$. However, due to the close proximity of possible other $\ell = 2$ resonances in the $E_{p} = 5.16$ to 5.19 region, this assignment must be considered tentative.

Resonance 37. E_λ = 5.304 MeV.

The shape is again obviously $\ell = 2$. No inleastic scattering angular distribution was measured. Although the height of the resonance at 165° can only be explained by a $J^\pi = 5/2^+$ assignment, the $J^\pi = 3/2^+$ possibility cannot be ruled out since the background in the region of this resonance is not very well understood.

Resonances 38, 39 and 40. E_λ = 5.367, 5.376 and 5.390 MeV.

It is clear from the structure in the E_p = 5.35 to 5.40 MeV region that three levels contribute to the cross section in this region. Resonance 40 has a dip at $\theta = 89^\circ$ and decreases slowly at $\theta = 165^\circ$, indicating a spin-parity of $1/2^+$. Resonance 39 has all the required characteristics for an $\ell = 4$ assignment. It is found that the double dip at $\theta = 89^\circ$ can only be explained if the spin-parity of the level is $9/2^+$. In the case of resonance 38 the only assignment which gave even a quantitative fit to the data was $3/2^-$. The fit to this region is reasonable considering the small spacing between the levels and the fact that the possible interference effects from higher lying resonances was not taken into account.

In comparing the calculated elastic scattering cross sections with the data it should be remembered that the

fitting was carried out at $\theta = 165^{\circ}$. It is seen in fig. 3.2 that the agreement between the calculated curve and the data at $\theta = 89^{\circ}$, 123° and 139° is good at low energies but poor at high energies. The poor agreement at high energies (i.e. $E_p > 4$ MeV) is thought to be due to the limited validity of some of the assumptions made in the analysis particularly the assumption that Γ is independent of energy. Another factor that could influence the slowly varying component of the cross section is the choice of interaction radius in the calculation of the potential scattering phase shift ϕ.

Notwithstanding the poor fit to the cross section in the high energy region, it is seen that the variation of the cross section in the vicinity of individual resonances is in general in good qualitative agreement with the data. Thus even though the "background" is not well understood, the assignments of resonance parameters can be made with confidence. This applied particularly to the assignment of spins and parities since these are to a large extent based on the shapes of the resonance cross sections.

6.2 Reduced Widths

Reduced partial widths for elastic and inelastic scattering were calculated using eq. 1.1; i.e.

$$\gamma_p^2 = \Gamma_p / 2P_\ell$$

$$\gamma_{p'}^2 = \Gamma_p / 2P_\ell$$

The penetrability factor P_ℓ is related to the regular and irregular Coulomb functions F_ℓ and G_ℓ respectively through the equation

$$P_\ell = \frac{\rho_\lambda}{A_{\ell\lambda}}$$

where $A_{\ell\lambda} = F_{\ell\lambda}^2 + G_{\ell\lambda}^2$

and $\rho_\lambda = R_o / \lambda$

The factor $\frac{1}{2P_\ell}$ was obtained from graphs of $\frac{A_\ell^2}{2\rho}$ as a function of incident proton energy given by Gove (Go 58). These were calculated assuming an interaction radius $R_o = 1.4(A^{1/3} + 1)$ fm. (The assumption of a constant interaction radius is not strictly true since in general R_o need not be the same for different channels and it may also vary with λ and ℓ).

Finally, the reduced widths are given (see table 6.1) in units of the Wigner single particle limit (eq. 1.2):

$$\theta_s^2 = \gamma_s^2 / \gamma_W^2$$

where γ_w^2 is given by: (Te 52) $\gamma_w^2 = \frac{\hbar^2}{\mu R_o^2}$ †

and μ is the reduced mass.

The reduced widths for elastic scattering are not very sensitive functions of the interaction radius. The reduced inelastic widths on the other hand are in general more sensitive to R_o. This comes about because of the fact that P_ℓ becomes an increasingly sensitive function of energy and radius for low channel energies.

The method used here for determining the reduced width assumes a square well potential. This allows the partial width for a given channel to be completely separated into external and internal effects. However there is increasing evidence indicating that the nuclear surface is diffuse so that this complete separation is only approximately valid. Schiffer (Sc 63) calculated widths for resonant scattering of protons by a Woods-Saxon potential and found them to be 25% to 50% of γ_w^2. This would mean reduced widths $\theta_p^2 \sim 2$ to 4-times greater than those given in the present work. No explicit calculation of the widths using a diffuse well have been made for levels in the ^{33}Cl nucleus.

---

† The R-Matrix formalism in fact gives $\frac{3\hbar^2}{2\mu R_o}$ but the 3/2 is omitted by most authors. (Te 52, La 60).

6.3 Accuracy of Assignments

The preceding analysis led to the unambiguous assignment of orbital angular momenta for 35 of the 40 resonances observed. It has also led to unambiguous spin assignments for 21 levels and tentative assignments for 16 levels. The tentative assignments are indicated by brackets in table 6.1.

For the narrow levels the accuracy of the level energy assignments depend largely on the experimental accuracy of the incident beam energy measurement which is believed to be ~2 to 3 keV. For broad levels the errors in the level energies depend mainly on the analysis; the neglect of the level shift parameter for inelastic scattering and various other assumptions contribute to this error. Estimates of accuracy of level energies are given in table 6.1.

Estimates of errors in the total widths are also given in table 6.1. Except for the narrow levels the errors are generally between 10% and 25%.

The error in Γ_p/Γ is difficult to estimate in this type of analysis particularly for the broader levels. However, considering the agreement of better than 20% in the values determined from the elastic and inelastic data (Section 5.3) the uncertainty in Γ_p/Γ is indicated in general to be less than 20%.

Finally the errors in reduced widths θ_p^2 are believed to be less than 30%; this error being due mainly to errors

in the partial widths Γ_p and Γ'_p. There is a much greater uncertainty however for the inelastic scattering reduced width $\theta_{p'}^2$ in the region E_p = 2.8 to 3.5 MeV, due to the large penetrability factors which include a large uncertainty.

CHAPTER 7

DISCUSSION AND CONCLUSIONS

7.1 Comparison with other data

A comparison of the results of this experiment with previously reported work is only possible in the case of levels between excitation energies 5 and 6 MeV, since the level structure of ^{33}Cl at higher energies has not previously been studied. The levels in the E_x = 5 to 6 MeV region have been investigated by means of proton scattering by Olness et al. (Ol 58). The level parameters of these levels as well as those of the corresponding levels in the present work are presented in table 7.1.

From this table it is seen that the spin and parity assignments are the same for all the levels. In the case of the level at E_p = 2.904 MeV a preference is indicated for a $5/2^-$ assignment in the present work. The energies of the levels agree to within $\sim$ 5 keV except in those cases where the widths are large. The widths of the narrow resonances are generally lower than those reported by Olness et al. This could be due to the fact that the energy resolution in the present experiment was better by a factor 4 than that of Olness et al.

TABLE 7.1

Comparison of Results

THIS EXPERIMENT				OLNESS et al. (01 58)			
E_λ MeV	J^π	Γ keV	Γ_p/Γ	E_λ MeV	J^π	Γ keV	Γ_p/Γ
2.811	$3/2^-$	6	1	2.810	$3/2^-$	6	$\sim$1
2.910	$1/2^-$	400	1	2.895	$1/2^-$	360±60	1
2.904	$(5/2^-)$	$\lesssim$0.1	1	2.902	$(5/2^-, 7/2^-)$	< 0.5	$\sim$1
2.920	$3/2^+$	0.25	1	2.917	$3/2^+$	1.5±.5	$\sim$1
3.099	$5/2^-$	0.32	0.48	3.094	$5/2^-$	0.34±0.06	0.85
3.200	$5/2^+$	0.20	0.75	3.195	$5/2^+$	0.44±0.08	0.98
3.273	$1/2^+$	25	1	3.273	$1/2^+$	32±4	$\sim$1
3.385	$7/2^-$	1.5	0.25	3.374	$7/2^-$	1.0±0.2	0.4
3.500	$3/2^-$	125	1	3.480	$3/2^-$	100±15	$\sim$1
3.575	$1/2^+$	20	1	3.570	$1/2^+$	40±5	$\sim$1
3.723	$5/2^-$	1.4	0.35	3.716	$5/2^-$	1.5±.03	0.56

7.2 Level scheme and reduced widths

The energy levels of ^{33}Cl, studied in the present work are presented in fig. 7.1. In addition the reduced widths θ_p^2 for the corresponding levels, separated into the respective spin states, are shown. The length of the horizontal lines is proportional to θ_p^2. The dashed lines indicate levels for which the spin assignments are tentative. A general feature of the results in fig. 7.1 is that in the 5-6 MeV excitation region negative parity states predominate whilst in the 6.5 to 7.5 MeV region, positive parity states are stronger. An interesting aspect of the results is the systematic tendency noted for states with relatively large reduced widths. For the negative parity states the strongest elastic scattering levels (i.e. with largest θ_p^2), for the spin states $1/2^-$, $3/2^-$ and $5/2^-$ are found to be at 5.112, 5.684 and 6.309 MeV respectively. They thus occur at increasing energies with an approximate spacing of 600 keV. A $7/2^-$ level is also observed at 6.949 MeV, i.e. ~600 keV higher than the strong $5/2^-$ level. Approximately the same spacing is observed in the case of positive parity states with spins $1/2^+$, $3/2^+$ and $5/2^+$ at 5.757, 6.331 and 6.884 MeV respectively.

A diagram similar to fig. 7.1 but showing the inelastic reduced widths is presented in fig. 7.2. In this case states with large reduced widths θ_p^2 are those with spin $3/2^-$, $5/2^-$ and $7/2^-$ at 5.016, 5.295 and 5.572 MeV respectively.

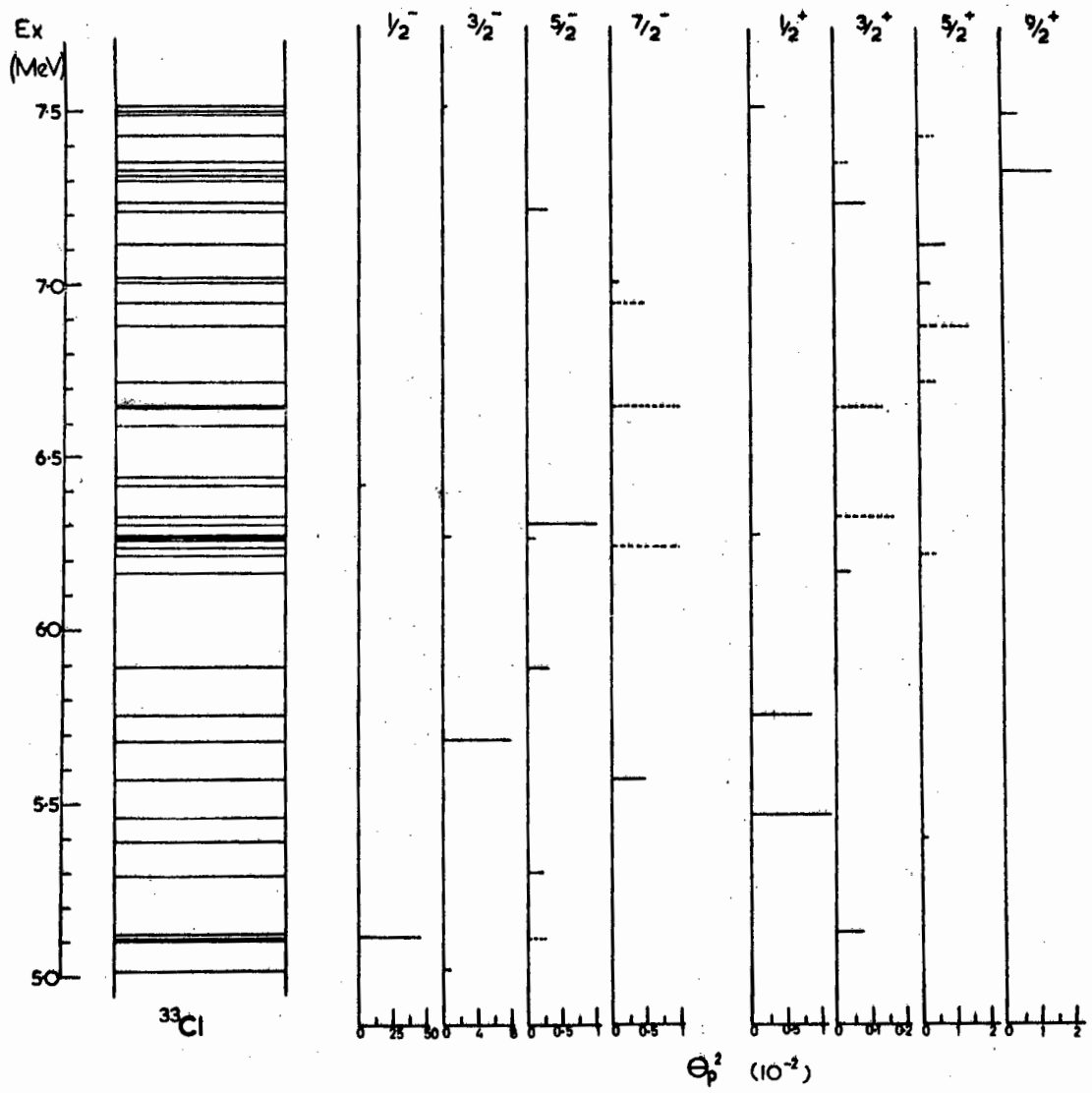

Figure 7.1 Energy levels of ^{33}Cl in the 5.0 to 7.5 MeV excitation region showing all data obtained in the present experiment. Reduced widths θ_p^2 for elastic scattering are shown classified according to spin and parity

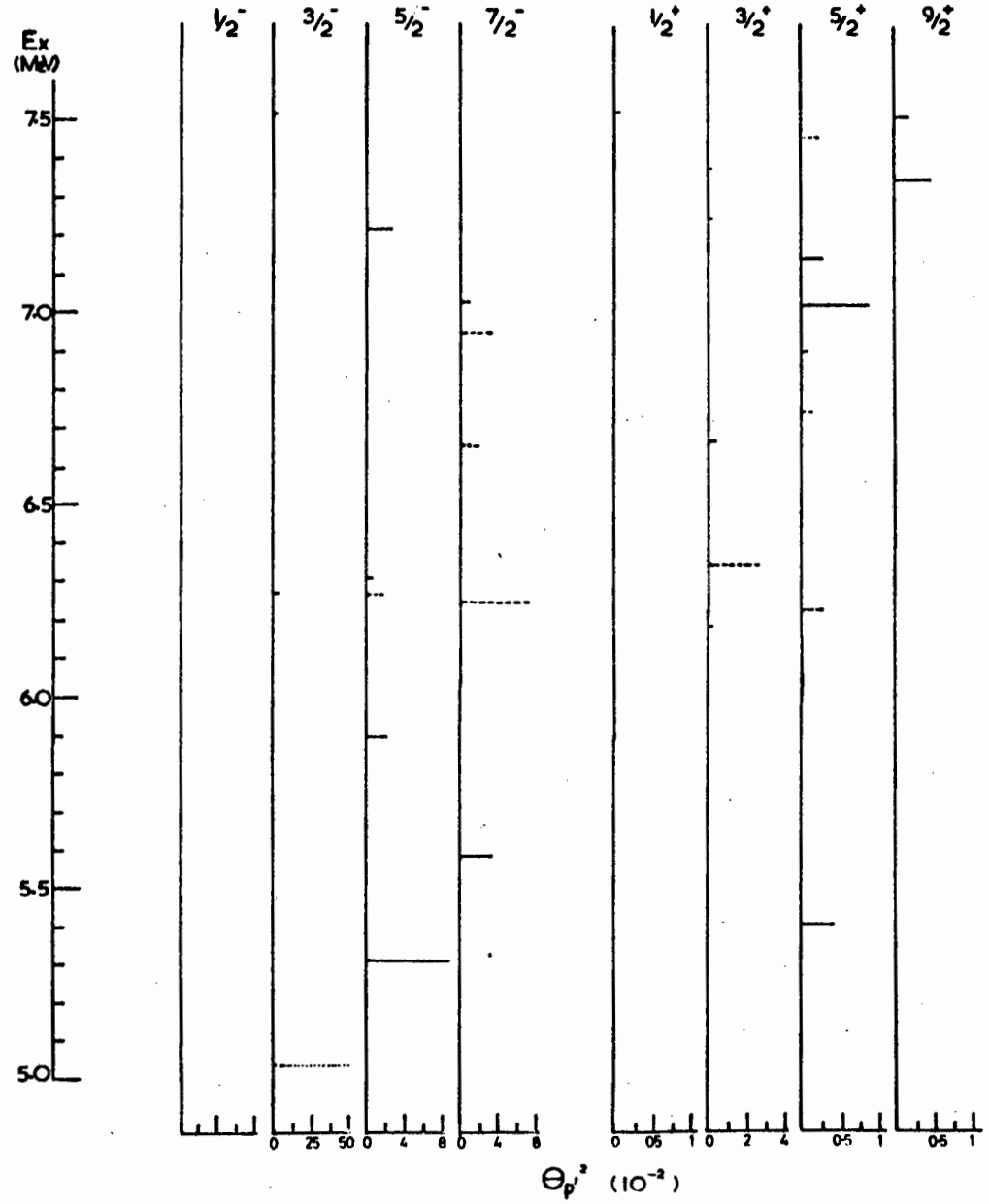

Figure 7.2 Reduced widths θ_p^2 for inelastic scattering as a function of energy for levels of ^{33}Cl classified according to spin and parity

The spacings between these levels are 279 and 277 keV respectively. A similar spacing is observed for positive parity levels with spins $3/2^+$ and $5/2^+$ at 5.122 and 5.393 MeV respectively.

The significance of these level systematics is not clearly understood. A possible interpretation in terms of the Nilsson model is discussed in section 7.4.

7.3 Limitations of the proton scattering method

Proton scattering experiments yield a considerable amount of spectroscopic information regarding the level structure of the compound nucleus. However, the potential of this method is restricted to some extent by the effect of the Coulomb barrier. This has the effect of reducing the widths of levels which are excited by protons of high orbital angular momentum ℓ. These levels are therefore difficult to observe particularly at low proton energies. The lower limit of observation of narrow levels is determined largely by the available energy resolution. It is useful to calculate the lower limit of the reduced widths θ_p^2 of levels that can be observed for a given ℓ and given beam energy and resolution. Based on a beam energy resolution of 1 keV at 3 MeV we assume that the width of a level must be greater than 100 eV in order to be observed in the present experiment. In fig. 7.3 the

value of θ_p^2 corresponding to this width is shown as a function of energy for various ℓ-values. A level with θ_p^2 and E_p such that it would lie to the right of the respective ℓ-value curve is thus assumed to be observable with the energy resolution available.

From these curves it is seen that all levels with $\ell = 0$, 1 or 2 and $\theta_p^2 > 0.001$ should be observable in the proton energy region 2.8 to 5.5 MeV. However weak levels with $\ell = 3$ or 4 will probably not be observed at low proton energies. Thus this experiment contains an intrinsic bias against weak levels of $\ell = 3$ or higher. This bias can constitute a serious disadvantage in some studies, particularly those of a statistical nature which are sensitive to the total number and distributions of levels. However in other studies, such as the present one, the failure to observe weak levels is not serious since the levels of interest to theoretical interpretation are generally those with large reduced widths.

7.4 Interpretation of level structure of ^{33}Cl

The low lying energy states of nuclei in the 2s-1d shell have been interpreted in terms of various nuclear models. Extensive shell model calculations have for example been done for nuclei ranging from ^{29}Si to ^{40}Ca (Gl 64). In these calculations it was assumed that the outer shells, $2s_{1/2}$

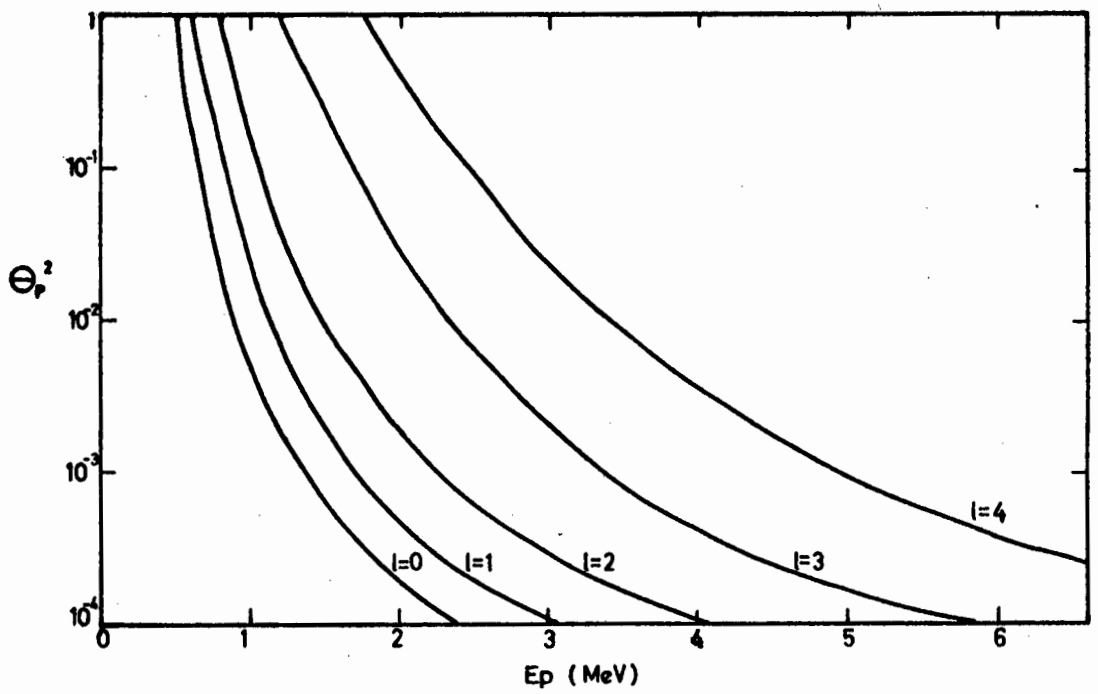

Figure 7.3 The reduced widths θ_p^2 for a given width Γ = 1 keV, plotted as a function of proton energy for different values of ℓ

and $1d_{3/2}$ are in a central field provided by the inert central core of ^{28}Si.

Another model which has frequently been applied to levels in the 2s—1d shell is the unified model of Nilsson. A review by Bhatt (Ph 62) discusses the application of this model to a number of nuclei. With ^{33}Cl in mind we restrict our interest to nuclei with Z or N = 17. Of these, ^{33}S has been discussed by Bishop (Bi 60), ^{35}Cl by Taras (Ta 66) and very recently ^{31}Si by Webb et al. (We 68). However, the model does not as yet appear to have been applied to the level structure of ^{33}Cl. It is thus of interest to do so since the model has been rather successful in accounting for the low energy spectra of the neighbouring nuclei.

In the unified model, energy levels are interpreted as members of rotational bands which are based on intrinsic single particle states associated with a deformed nuclear potential. The interaction Hamiltonian for a single particle in a deformed potential is given by Nilsson (Ni 55) as

$$H = H_o + C\underset{\sim}{l}.\underset{\sim}{s} + D\,\underset{\sim}{l}.\underset{\sim}{l} \qquad 7.1$$

where H_o is the non spherical oscillator potential, $C\underset{\sim}{l}.\underset{\sim}{s}$ is the usual spin-orbit term, and $D\underset{\sim}{l}.\underset{\sim}{l}$ serves to depress the high angular momentum states. C and D are coefficients.

The energy eigenvalue of the total Hamiltonian given by Nilsson is

$$E = (N + 3/2)\hbar\omega_o(\delta) + \kappa\omega_o(o)r^{N\Omega} \qquad 7.2$$

where N represent the total number of oscillator quanta; $\hbar\omega_o(\delta)$ is the oscillator frequency of the deformed potential; $\hbar\omega_o(o)$ is the level spacing for the harmonic oscillator and is given by $\hbar\omega_o(o) \approx 41\ A^{-1/3}$ MeV; $\kappa = -\frac{1}{2}C/\hbar\omega_o(o)$ 7.3 and $r^{N\Omega}$ is the eigenvalue of the assymetric part of the Nilsson Hamiltonian.

The eigenvalues $r^{N\Omega}$ depend on the "square well parameter", $\mu = \frac{2D}{C}$ and the core deformation parameter η. The latter is related to the nuclear distortion parameter δ by the following:

$$\eta = \frac{\delta}{\kappa}\,\frac{\omega_o(\delta)}{\omega_o(o)} \qquad 7.4$$

where $\delta = \frac{\Delta R}{R}$

and R and ΔR are the mean nuclear radius and the difference between the semi-major and semi-minor axes of the spheroidal nucleus respectively.

$\frac{\omega_o(\delta)}{\omega_o(o)}$ is assumed to be equal to unity.

By suitable choice of the parameters μ, κ and η, the intrinsic eigenstates are thus determined for an odd nucleon moving in a spherical potential due to the core nucleons in the nucleus.

In the unified model rotational energy can be coupled to each intrinsic state thus giving rotational bands based on each intrinsic state. The energy of the substates of each band based on these intrinsic states can be calculated from the following expression given by Bohr and Mottelson (Bo 53):

$$\Delta E_{JK} = \frac{\hbar^2}{2I}\left[J(J+1) - K(K+1) + a\{(-)^{J+1/2}(J+1/2) - (-)^{K+1/2}(K+1/2)\}\delta_{K,1/2}\right] \qquad 7.5$$

where J and K are the angular momenta of an excited level in a rotational band and that of its intrinsic state, respectively. ΔE_{JK} is the energy difference between the excited level with spin J and the intrinsic state with spin K in a rotational band. $\delta_{K,1/2}$ is a Kronecker delta symbol,
I is the moment of inertia of the rotational band,
and "a" is the "decoupling parameter".

The value of "a" may be calculated from

$$a = (-)^{\ell} \sum_{\ell}\left[a^2_{\ell_o} + 2\sqrt{\ell(\ell+1)}\; a_{\ell_o}\, a_{\ell_1}\right] \qquad 7.6$$

where a_{ℓ_o} and a_{ℓ_1} are coefficients which depend on μ and η. The final energy levels are given by adding ΔE to E, the energy of the intrinsic state. The value of ΔE can be negative in certain cases where "a" is large and negative.

To determine the energy of rotational substates in ^{33}Cl

it is therefore necessary to determine values for the parameters μ, κ, η and $\frac{\hbar^2}{2I}$. This has been done by comparison with the values used for other N or Z = 17 nuclei in this region (see table 7.2) and consideration of the low lying level structure of ^{33}Cl.

The value of κ used by Nilsson was 0.05. This value was chosen since it gives the correct ordering of levels for zero deformation over the whole range of nuclei. It was found (e.g. Li 58, Bi 60) that in the 2s-1d shell higher values were needed to explain the level structure. In the present case we have chosen the values $\kappa = 0.07$ for the 2s-1d shell states and $\kappa = 0.08$ for the $1f_{7/2}$ states. The values of μ are chosen as 0.167 and 0.33 for 2s-1d and $1f_{7/2}$ states respectively.

To obtain a value of the deformation parameter η we consider the systematics of neighbouring nuclei and the low lying states in ^{33}Cl in more detail: If the ground state of ^{33}Cl is considered as a single proton associated with a $2s_{1/2}$ core, then this proton must be in Nilsson orbit 8 with $K = 3/2$ if the deformation is oblate (η negative) or in orbit 9 $(K = 1/2)$ if the deformation is prolate (see fig. 7.4). In the latter case the ground state spin of $3/2^+$ can be explained as the second member of the band based on orbit 9 (if the decoupling parameter is negative and $\Delta E_{3/2,1/2}$ is negative). However quadrupole and dipole moments measured for neighbouring nuclei suggest that the deformation is oblate.

TABLE 7.2 Parameters used in Nilsson model calculations for N or Z = 17 nuclei

Nucleus	κ	μ	η	$\hbar^2/2I$ (keV)	Ref.
$^{33}_{17}S_{16}$	0.085	0.33	-2	370	Bi 60
$^{31}_{17}Si_{14}$	0.05-0.12	0.125-0.280	-2	320	We 68
$^{35}_{18}Cl_{17}$	0.10	0.167	-2	104 (#8)	
			-3(#11)	244 (#9)	Ta 66
				352 (#10)	

TABLE 7.3 Parameters used in Nilsson model calculation for ^{33}Cl

N	κ	μ	η	$h^2/2I$ (MeV)	ORBIT	K	a
					5	$5/2^+$	
					6	$1/2^+$	2.5
					7	$3/2^+$	
2	0.07	0.167	-2	0.3	8	$3/2^+$	
					9	$1/2^+$	0.95
					11	$1/2^+$	-1.5
					10	$7/2^-$	
					12	$5/2^-$	
3	0.08	0.33	-2	0.3	13	$3/2^-$	
					14	$1/2^-$	-3.8

The value of η used for most of the neighbouring nuclei is $\eta = -2.0$. This value is also used in the present case.

A diagram showing the Nilsson orbits for the values μ and κ in table 7.3 is given in fig. 7.4.

Values of $\hbar^2/2I$ were chosen to give a reasonable correspondence to the low lying energy levels. These values are also given in table 7.3.

The rotational bands predicted using these parameters are shown in fig. 7.5 together with the experimental levels of ^{33}Cl. Rotational bands based on orbits 8 and 9show good agreement with the ground state and first four excited states of ^{33}Cl predicting a spin of $3/2^+$ for the state at 2.50MeV. This spin is consistent with a $3/2^+$ state at 2.313 MeV in the mirror nucleus ^{33}S (see fig. 7.5). In addition these bands predict $9/2^+$ states at 6.9 and 8.2 MeV. Experimentally observed states are found at 7.33 and 7.5 MeV. Considering the high excitation energy, this correspondence, if it is not fortuitous, is surprisingly good.

The rotational band based on orbit 11 cannot be related to any experimental levels for the values of the parameters given in table 7.3. From fig. 7.4 it is seen that the intrinsic state energy varies rapidly as a function of η. If a value of $\eta = -5$ is used the intrinsic state energy is

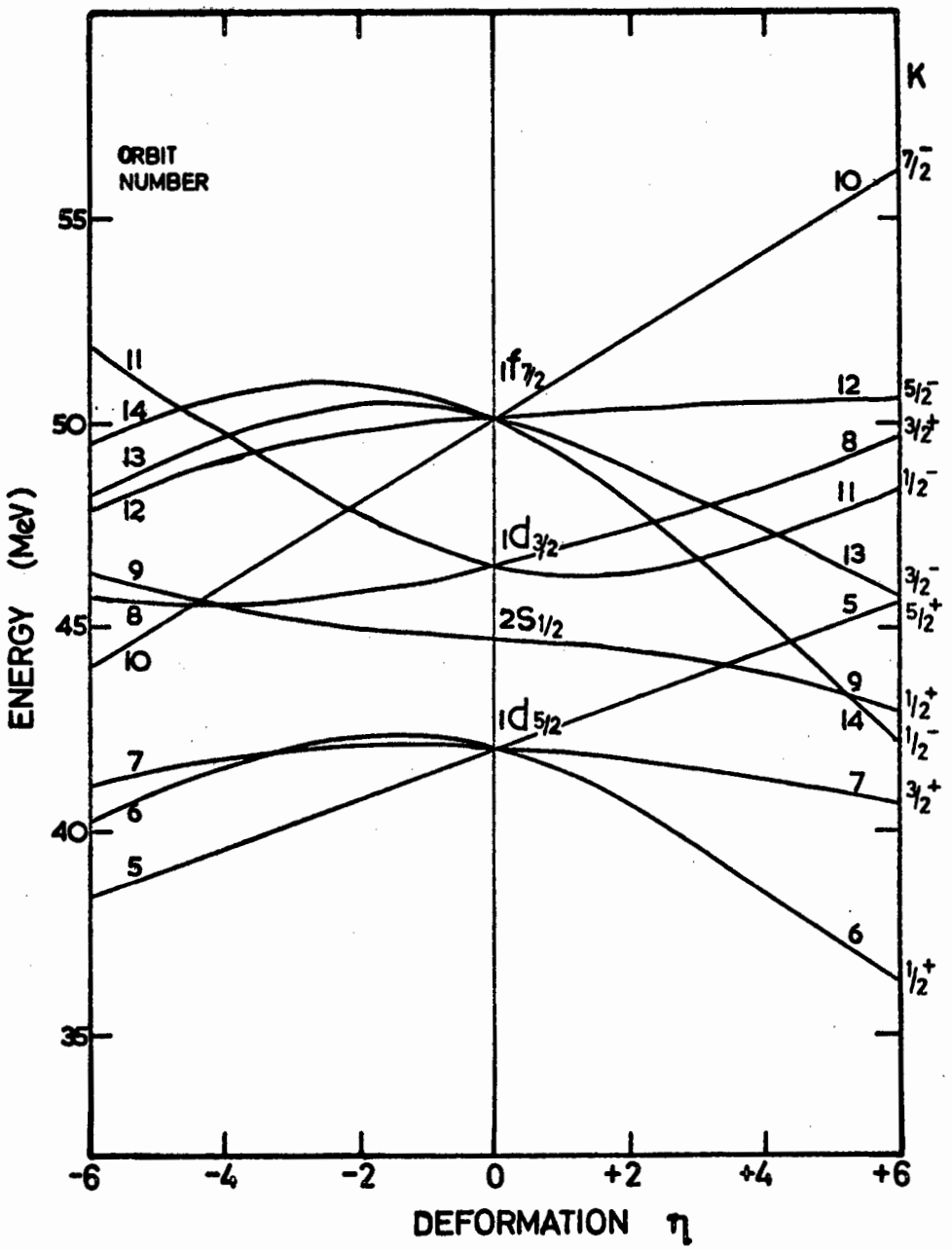

Figure 7.4 Nilsson energy levels plotted as a function of deformation parameter η. The energy scale is for a mass 33 nucleus and the energy levels are calculated for values of the parameters given in table 7.3

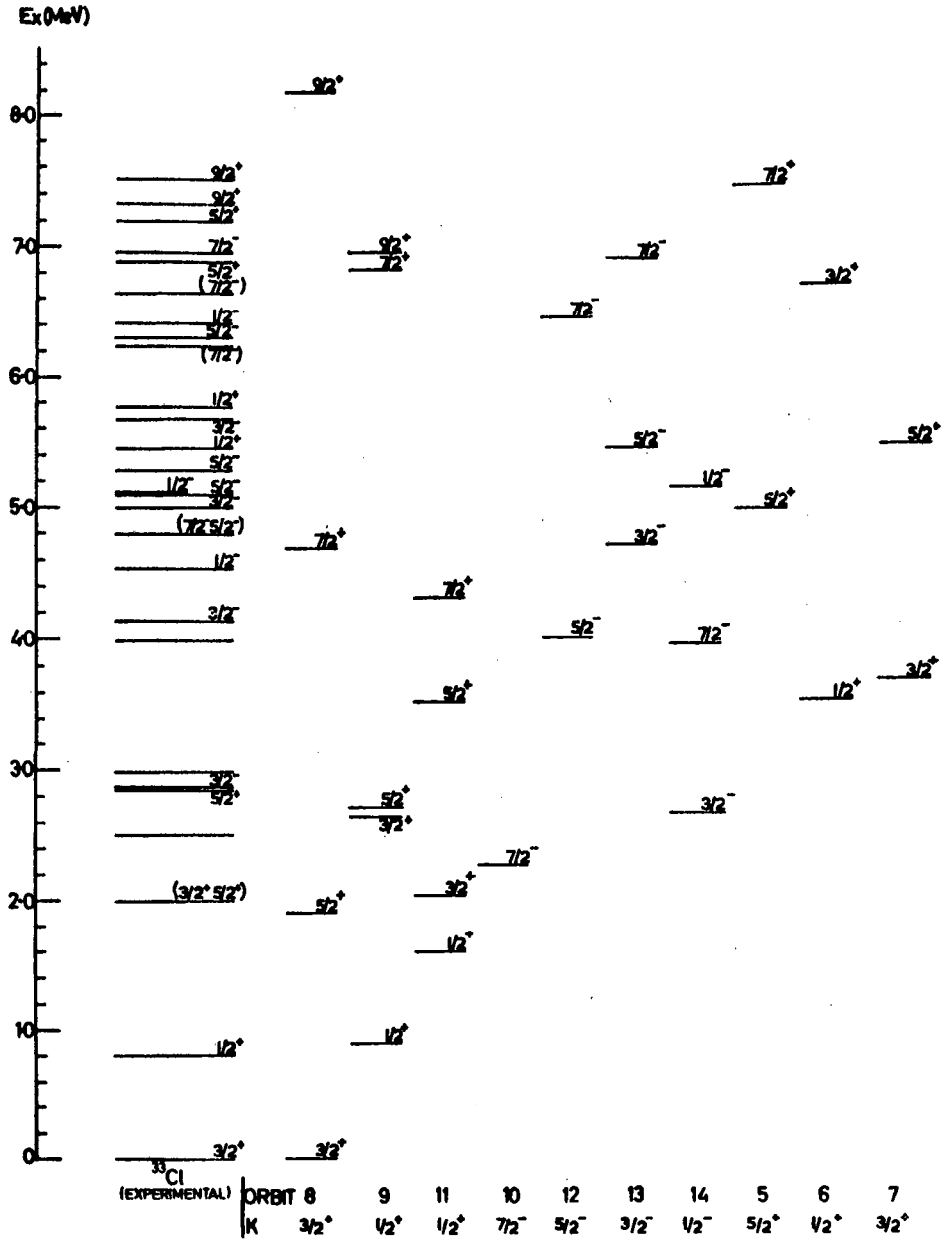

Figure 7.5 Experimental level scheme for ^{33}Cl shown together with predictions of the Nilsson model based on parameters given in table 7.3

at 5.1 MeV. It may then correspond to the experimental state at 5.46 MeV. On the other hand one of the unassigned states at 2.50 and 3.99 might have spin $1/2^+$ in which case that state would probably correspond to the predicted $1/2^+$ state. This is merely speculative but it should be noted that there is no a priori reason why η should be constant for each rotational band. In fact a variation in η might imply that neglected effects such as rotation-particle coupling (R.P.C.) are significant (Li 58).

In the case of the rotational band based on orbit 14, a reasonable correspondence with levels is found. In particular the $3/2^-$ level at the rather low excitation energy of 2.8 MeV is well explained as the second member of the band which is predicted at this low energy due to a large negative decoupling parameter.

The rotational bands based on orbits 12 and 13 can again be roughly associated with observed levels. The intrinsic states may correspond to the unassigned levels at 2.98 and 3.99 MeV or other possible undetermined levels in this region. That there are other levels in this region is strongly indicated by a comparison with the mirror nucleus ^{33}S which has a significantly higher level density in this region (see section 7.5). The higher members of these bands may be associated with negative parity states determined in the present experiment.

The $7/2^-$ intrinsic state energy of orbit 10 is given as

2.27 MeV. Again this energy varies rapidly with η (see fig. 7.4) so that for a small change in η the energy could change considerably. In ^{33}S, a state at 2.94 MeV is assigned a spin-parity $7/2^-$ (Be 66). It would be interesting to search for analogue state in ^{33}Cl since it seems extremely likely that this state is the $7/2^-$ intrinsic state.

The intrinsic states based on orbits 5, 6 and 7, as in the case of orbit 9, are attributed to the excitation of a core proton from these orbits to orbit 8. This proton pairs off to zero angular momentum in orbit 8 and the properties of the band are thus determined by the remaining proton in the respective orbits. These rotational bands predict a number of $3/2^+$ and $5/2^+$ levels in the region of the present experiment. Above 6 MeV, levels with spin parity $3/2^+$ and $5/2^+$ are found experimentally to be more numerous than levels of any other spin-parity.

In general it is seen that the unified model gives a satisfactory description of the energy levels of ^{33}Cl insofar as it can explain the low-lying level structure. For a more meaningful comparison with the model it would be necessary to obtain more experimental data for these levels; e.g. gamma-ray branching ratios as well as spins and parities. This would justify comparison with more sophisticated versions of the model including, for example, effects such as rotation particle coupling (Ma 67).

The notable feature observed in the present experiment,

i.e. the order and spacing of the strong negative parity levels, remains unexplained by this model. If the deformed nucleus was prolate and $\kappa = 0.05$, then the intrinsic states of the $1f_{7/2}$ shell, would be in the order $1/2^-$, $3/2^-$, $5/2^-$ and $7/2^-$ with the energy and spacing approximately as observed (see fig. 7.4). However, it would then be impossible to explain the low lying levels, unless one assumes a negative deformation for $2s_{1/2}1d_{3/2}$ states and a positive deformation for $1f_{7/2}$ states. However, this would leave the low lying negative parity levels unexplained. Again it would be interesting to try to locate a $7/2^-$ level at a relatively low excitation energy as this would be strong evidence for the oblate deformation for $1f_{7/2}$ levels.

An additional argument against the prolate deformation is that the reduced width, θ_p^2 for the observed levels would be incorrectly predicted by the model. It would be expected on the basis of the model that the $7/2^-$ level would have a large ($\theta_p^2 \gtrsim 0.5$) reduced width and that the $1/2^-$ would have a relatively smaller reduced width (Li 58).

7.5 Analogue States

Energy levels of the mass 33 isobars ^{33}P, ^{33}S, ^{33}Cl and ^{33}A are shown in fig. 7.6.

The low lying energy levels of ^{33}Cl in general correspond

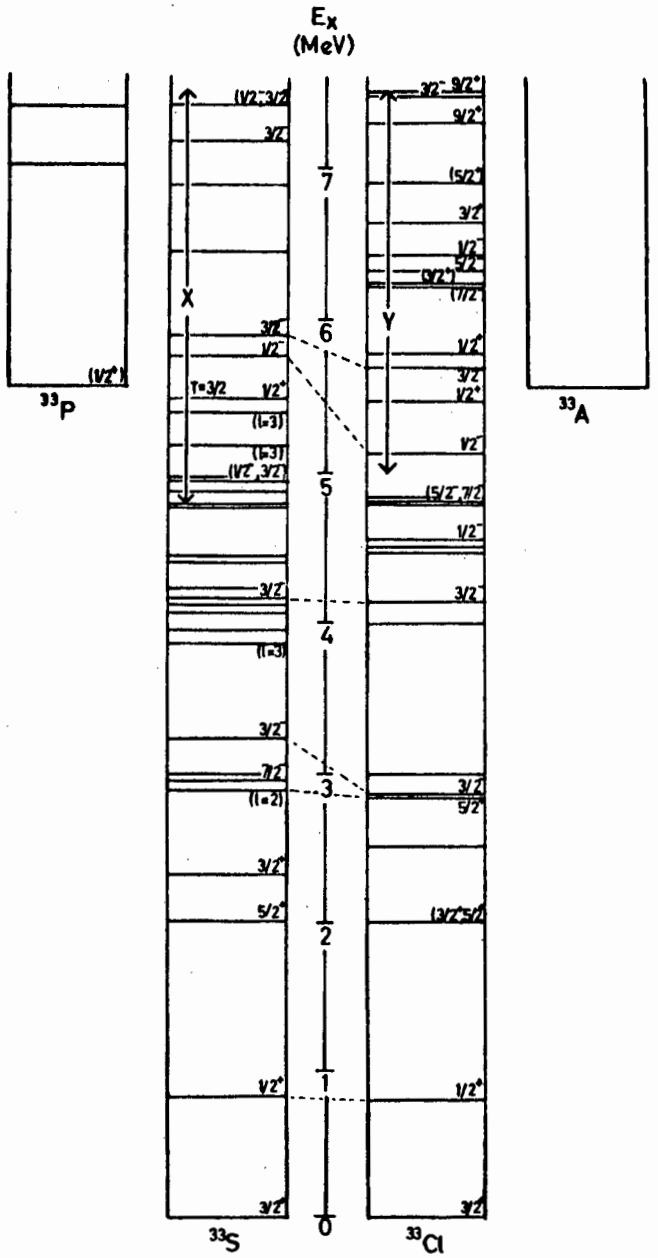

Figure 7.6 Level schemes of ^{33}P, ^{33}S, ^{33}Cl and ^{33}A. The region X in ^{33}S contains 50 levels determined by $^{32}S(d,p)^{33}S$, and region Y in ^{33}Cl contains 40 levels determined in the present experiment

to the low lying levels of the mirror nucleus ^{33}S. In the excitation region 3 to 5 MeV the number of levels in ^{33}S is twice that observed in ^{33}Cl. The reason for this discrepancy is not known but it seems likely that levels in ^{33}Cl exist that have not yet been observed. Levels in this region have been observed by means of $^{32}S(d,n)^{33}Cl$ and $^{33}S(p,\gamma)^{33}Cl$ reactions. The Q-value for the (d,n) reaction is -0.07 MeV. The most recent experiment using this reaction (Mu 67) was carried out at deuteron energy E_d = 5.0 MeV. In this experiment only those levels below 3.0 MeV excitation were investigated presumably because higher lying levels are not amenable to a D.W.B.A. analysis and were thus not of interest.

The proton experiments on the other hand are subject to a strong bias against observation of weaker levels (see section 7.3), due to the Coulomb barrier. Gamma-ray decays in the (p,γ) reaction have been observed by means of a Ge(Li) detector by Prosser et al. (Pr 67). They find no evidence for a $7/2^-$ level in this region. The proton energy range used in this experiment was 0.4 to 3.2 MeV, corresponding to the excitation energies 2.67 to 5.39 MeV. It is possible that there are levels in the energy region E_x = 3 to 5 MeV to which gamma decays from a level at 5.39 MeV would be very weak, since the transition probability for high energy gammas (i.e. to lower levels) is much greater than that for low energy gammas.

It would be of interest to carry out (p,γ) experiment at

higher proton energies to search for missing levels in this region. It might also be worthwhile to determine spins and parities of levels in this region by means of a $(p,\gamma\gamma)$ angular correlation experiment using the known spin and parity of a suitable level in the region of the present experiment.

In the excitation region 5 to 7.5 MeV 40 levels were observed in the present experiment while 50 were observed in ^{33}S. This difference can again probably be attributed to the fact that weak levels of higher spins are not observed due to the limited energy resolution of the present experiment and the Coulomb barrier. A detailed comparison of these levels is not possible since few levels in ^{33}S have been assigned spins and parities. A strong $1/2^-$ level at 5.75 and a $3/2^-$ level at 5.894 MeV are reported to have relative reduced widths $\theta_n^2 = 60$ and $\theta_n^2 = 15$ respectively (La 67). These levels probably correspond to the $1/2^-$ level at 5.11 and $3/2^-$ level at 5.68 MeV observed in the present experiment. The relative reduced proton widths for these levels are $\sim$50 and $\sim$8 respectively. The relative reduced neutron widths in the case of ^{33}S thus correspond approximately to the relative reduced proton widths in ^{33}Cl.

The first $T = 3/2$ state in ^{33}Cl (the analogue of the ^{33}A ground state) has been identified at 5.55 MeV by means of a β-delayed proton experiment (Po 66). This experiment consists of the production of ^{33}A by means of the reaction

$^{35}Cl(p,3n)^{33}A$ (threshold 39 ± 5 MeV) (Ha 66) or the reaction $^{32}S(\tau,2n)^{33}A$ (Po 66). The ground state of ^{33}A decays by β-emission to an excited state of ^{33}Cl which then decays by proton emission. The excitation of a T = 3/2 level in this way is allowed by the isospin selection rules in contrast to the excitation by means of proton scattering, which is forbidden by these selection rules. (See section 1.3). Observation of this analogue state by means of a (p,p) experiment would provide not only a more accurate measurement of the excitation energy of this state, but would yield information regarding the isospin mixing involved.

A careful search was carried out in the region 5.55 ± 0.020 MeV using optimum energy resolution and a very thin (< 1 keV) target. No narrow $1/2^+$ level was observed in this region. From considerations of barrier penetrability (see section 7.3) an approximate upper limit can be set on the reduced width θ_p^2 of the level if it exists in this region. If it is assumed that any level of width $\gtrsim$ 100 eV would be observed then the value of θ_p^2 must be less than 1×10^{-4} indicating very little isospin mixing.

On the other hand, two strong $1/2^+$ levels are observed at 5.646 and 5.757 MeV which are rather close to the analogue state energy. It is thus probable that these states contain some of the T = 3/2 strength. However they must be basically of T = $1/2^-$ character to have such large reduced widths.

No excited states are known in ^{33}A. In ^{33}P states are

observed at 1.37 MeV and 1.81 MeV. The 1.37 MeV state would be expected to have a spin-parity $3/2^+$ on the basis of the shell model predictions of Glaudemans et al. (Gl 64). A number of $3/2^+$ levels are observed in this region but no conclusions can be drawn as to which of these, if any, contain a T = 3/2 component.

7.6 Concluding Remarks

This investigation has shown that the proton scattering method is an extremely useful means of obtaining spectroscopic information about the compound nucleus level structure of ^{33}Cl. The simplicity of data collection and the relative ease with which level parameters may be extracted makes this experiment particularly attractive. This is illustrated by the fact that of the forty levels observed, energies and partial widths were determined for 38, spins and parities were assigned for 21 of the levels and parities and tentative spins were assigned for a further 16 levels.

A number of improvements in the experiment would allow a more thorough investigation to be carried out. The obvious improvement which is suggested is that of energy resolution. This would clearly allow the observation of narrow levels such as the analogue of the ground state of ^{33}A. Better computer facilities, if available, would permit a more sophisticated analysis to be undertaken. A more general

formalism could be applied and a least squares fitting of the calculated curves to the data would also be feasible.

The results of this experiment show systematic tendencies for some states with large reduced widths. The reasons for these effects are not immediately apparent and a theoretical interpretation of these states would be interesting. The Nilsson model does not provide an explanation for these states but it is found to give a useful interpretation of the low-lying levels of ^{33}Cl. Arising from the attempt to apply the Nilsson model to ^{33}Cl it would be interesting to investigate the intermediate level structure of this nucleus by means of a (p,γ) experiment. The data obtained from the present work would be very useful as a basis for such a study, for example in determining the spins of intermediate levels by means of $(p,\gamma\gamma)$ angular correlation studies.

APPENDIX A

PROTON ELASTIC SCATTERING ANALYSIS PROGRAMME

FLOW DIAGRAM
(Notation defined in eq. 4.20)

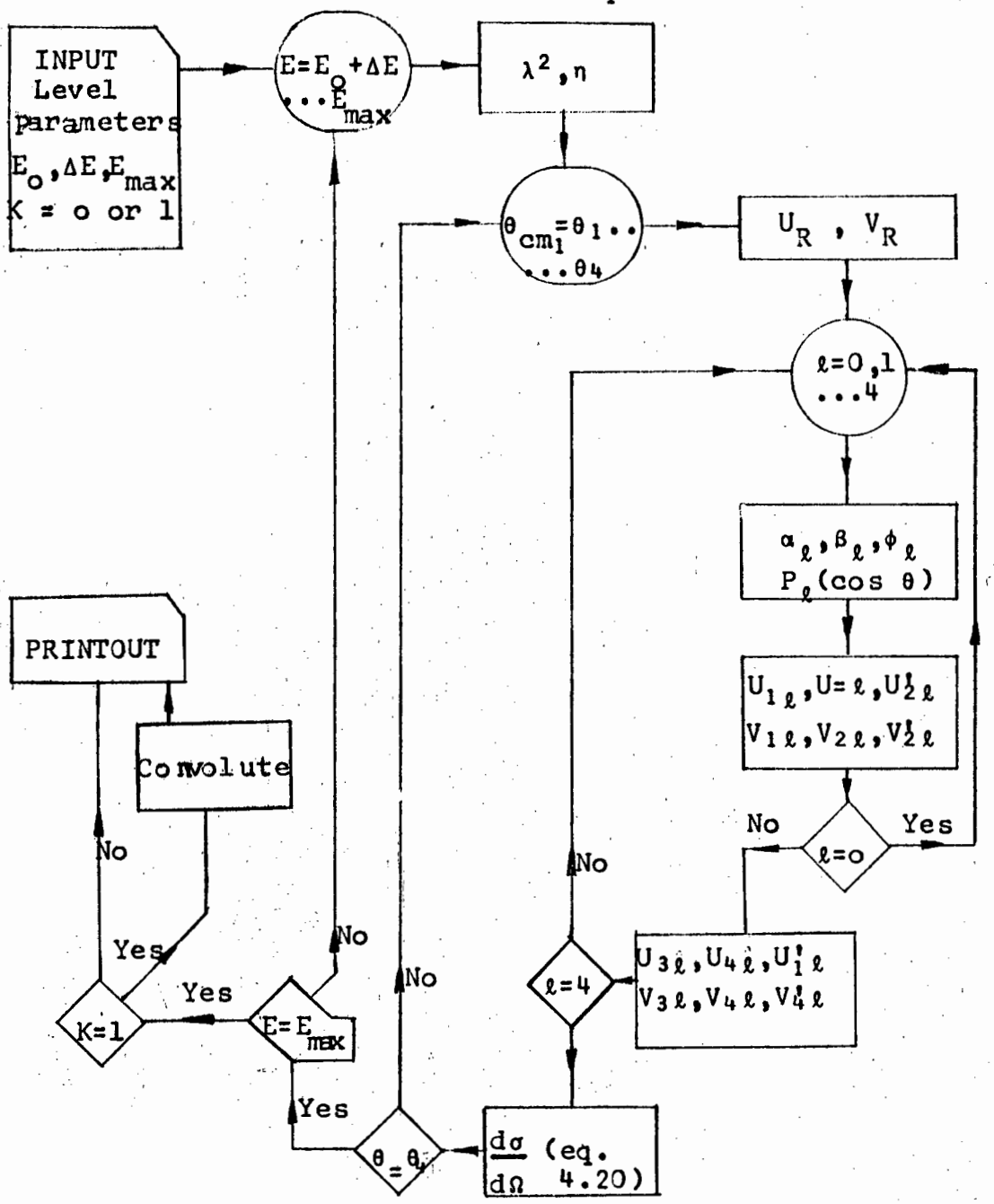

APPENDIX B

INELASTIC SCATTERING ANGULAR DISTRIBUTION ANALYSIS PROGRAMME

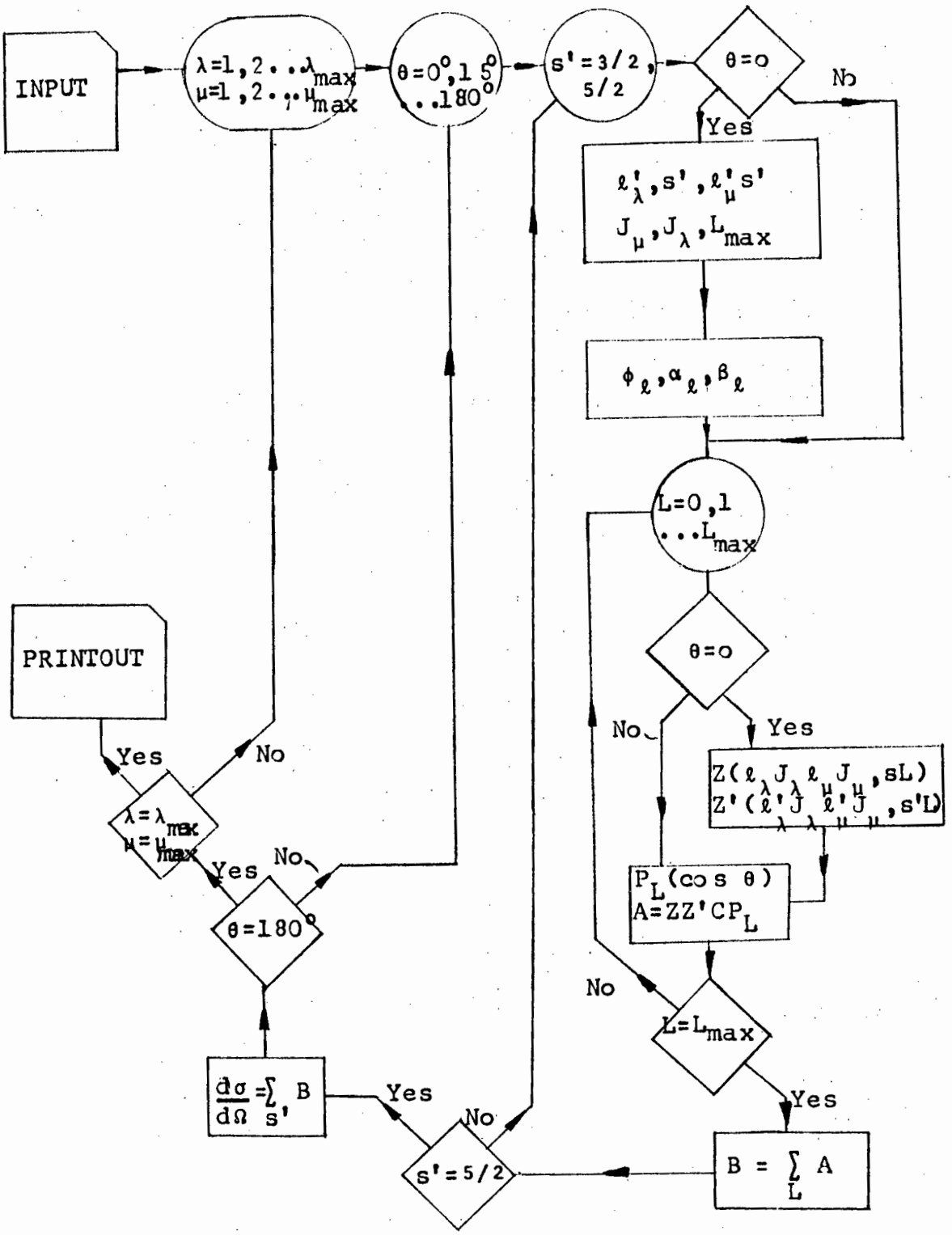

REFERENCES

Be 48 R.S. Bender, F.C. Shoemaker, S.G. Kaufman and G.M.B. Bouricius, Phys. Rev. 74 (1948) 1205

Be 61 T.A. Belote, E. Kashy and J.R. Risser, Phys. Rev. 122 (1961) 920

Be 66 J.A. Becker, L.F. Chase, O.B. Fossan and R.E. McDonald, Phys. Rev. 146 (1966) 761

Bh 62 K.H. Bhatt, Nucl. Phys. 39 (1962) 375

Bi 24 E.S. Bieler, Proc. Roy. Soc. (London) A105 (1924) 434

Bi 52 L.C. Biedenharn, J.M. Blatt and M.E. Rose, Rev. Mod. Phys 24 (1952) 249

Bi 60 G.R. Bishop, Nucl. Phys. 14 (1960) 376

Bl 51 I. Block, M.H. Hull, A.A. Broyles, W.G. Bouricius, B.E. Freeman and G. Breit, Rev. Mod. Phys. 23 (1951) 147

Bl 52 J.M. Blatt and L.C. Biedenharn, Rev. Mod. Phys. 24 (1952) 258

Bo 53 A. Bohr and B.R. Mottelson, Kgl. Danske Videnskab. Selskab. Mat.-Fys. Medd. 27 (1953) No 16; and Phys. Rev. 90 (1953) 717

Cr 49 C.L. Critchfield and D.C. Dodder, Phys. Rev. 76 (1949) 602

De 63 G. Dearnaley and D.C. Northrop, in Semiconductor Counters for Nuclear Radiations (E. and F.N. Spon Ltd., London, 1964) and Nucl. Instr. & Methods 25 (1964) 237

En 67 P.M. Endt, in Nuclear Structure, ed. Hossain et al. (North Holland Publ. Co., Amsterdam, 1967)

En 67(a) P.M. Endt and C. van der Leun, Nucl. Phys. A105 (1967) 1

Fo 49 W.A. Fowler, C.C. Lauritsen and S. Rubin, Phys. Rev. 75 (1949) 1463

Ge 13 H. Geiger and E. Marsden, Phil. Mag. 25 (1913) 604

Gl 64 P.W.M. Glaudemans, G. Wiechers and P.J. Brusaard, Nucl. Phys. 56 (1964) 529 and 548

Go 58 H.E. Gové, in Nuclear Reactions, ed. P.M. Endt and M. Demeur (North Holland Publ. Co., Amsterdam, 1959) p.259

Ha 38 O. Halpen and M.H. Johnson, Phys. Rev. 53 (1938) 939

Ha 49 O. Haxel, J.H.D. Jensen and H.E. Suess , Phys. Rev. 75 (1949) 1766

Ha 65 J.C. Hardy and R.I. Verrall, Can. J. Phys. 43 (1965) 418

Ha 66 J.C. Hardy, R.LVerrall and R.E. Bell, Nucl. Phys. 81 (1966) 113

He 66 E.M. Henley, in Isobaric Spin in Nuclear Physics , ed. J.D. Fox and D. Robson (Academic Press, New York, 1966) p.3

Ja 66 J.W. Jänecke, in Isobaric Spin in Nuclear Physics ed. J.D. Fox and D. Robson (Academic Press, New York, 1966) p.60

Ka 60 E. Kashy, R.R. Perry and J.R. Risser, Phys. Rev. 117 (1960) 1289

La 51 R.H. Laubenstein and M.J.W. Laubenstein, Phys. Rev. 84 (1951) 18

La 60 A.M. Lane, Rev. Mod. Phys 32 (1960) 519

La 67 B. Lawergren, Phys. Letters 24B (1967) 395

Li 58 A.E. Litherland, H. McManus, E.B. Paul, D.A. Bromley and H.E. Gove, Can. J. Phys. 36 (1958) 378

Ma 49 M.G. Mayer, Phys. Rev. 75 (1949) 1969

Ma 60 J.B. Marion, 1960 Nuclear Data Tables, Part 3. (Washington 1960)

Ma 63 J.B. Marion, in Progress in Fast Neutron Physics (The University of Chicago Press, 1963) p. 23

Ma 67 F.B. Malik and W. Scholz, in Nuclear Structure ed. Hossain et al. (North-Holland Publ. Co., Amsterdam, 1967) p.34

Me 61 A. Messiah, Quantum Mechanics Vol I (North-Holland Publ. Co., Amsterdam 1961)

Me 63 M.C. Mertz, Ph.D. Thesis, Illinois Institute of Technology, Chicago, June 1965

Mo 67 G.C. Morrison, in Nuclear Research with Low Energy Accelerators, ed. J.B. Marion and D.M van Patter (Academic Press, New York 1967)

Mu 67 S. Mubarakmand& B.E.F. Macefield, Nucl. Phys A98 (1967) 82

Ni 55 S.G. Nilsson, Kgl. Danske Videnskab. Selskab, Mat.-fys Medd. 29 (1955) No. 16

Ol 58 J.W. Olness, W. Haeberli and H.W. Lewis, Phys. Rev. 112 (1958) 1702

Po 66 A.M. Poskanzer, R. McPherson, R.A. Esterlund and P.L. Reeder, Phys. Rev. 152 (1966) 995

Pr 67 F.W. Prosser Jr. and J.W. Gordon, Bull. Am. Phys. Soc. 12 (1967) 572

Ra 50 J. Rainwater, Phys. Rev. 79 (1950) 432

Ro 67 R.R. Roy and B.P. Nigam, Nuclear Physics (John Wiley and Sons, New York, 1967)

Ru 06 E. Rutherford, Phil. Mag. 11 (1906) 166

Ru 11 E. Rutherford, Phil. Mag. 21 (1911) 669

Sc 63 J.P. Schiffer, Nucl. Phys. 46 (1963) 246

Su 59 M. Suffert, P.M. Endt and A.M. Hoogenboom, Physica 25 (1959) 659

Ta 66 P. Taras, Can. J. Phys. 44 (1966) 1563

Te 52 T. Teichmann and E. Wigner, Phys. Rev. 87 (1952) 123

Te 67 G.M. Temmer, Bull. Am. Phys. Soc. 12 (1967) 461

Va 58 C. Van der Leun and P.M. Endt, Physica 24 (1958) 1095

Va 59 Valter, Goncharov, Lvov and Tsytko, Izvest. Akad. Nauk, Ser. Fiz. 23 (1959) 835

We 68 V.H. Webb, N.R. Roberson and D.R. Tilley, Phys. Rev. 170 (1968) 989

Wi 47 E.P. Wigner and L. Eisenbud, Phys. Rev. 72 (1947) 29

Wi 67 G. Wiechers. Private communication